Universiteit Gent
Faculteit Ingenieurswetenschappen en
Architectuur
Vakgroep Informatietechnologie

Promotoren:

Prof. Dr. Ir. Roel Baets
Prof. Dr. Ir. Zeger Hens

Examencommissie:

Prof. Dr. Ir. Luc Taerwe(Voorzitter)	Universiteit Gent
Prof. Dr. Ir. Roel Baets (promotor)	Universiteit Gent
Prof. Dr. Ir. Zeger Hens(promotor)	Universiteit Gent
Prof. Dr. Ir. Johan Martens	KU Leuven
Prof. Dr. Christophe Detavernier	Universiteit Gent
Prof. Dr. Ir. Peter Bienstman	Universiteit Gent
Prof. Dr. Ir. Filip Beunis	Universiteit Gent
Prof. Dr. Ir. Patrice Mégret	Université de Mons
Prof. Dr. Norman Ratcliffe	University of the West of England

Universiteit Gent
Faculteit Ingenieurswetenschappen en
Architectuur

Vakgroep Informatietechnologie
Sint-Pietersnieuwstraat 41, B-9000 Gent, België

Tel.: +32-9-264.99.59
Fax.: +32-9-331.35.93

Proefschrift tot het bekomen van de graad van
Doctor in de Ingenieurswetenschappen:
Fotonica
Academiejaar 2012-2013

Dankwoord

This PhD would not have been a success without the support from colleagues, friends, and all my family. First of all, my deepest gratitude goes to professor Roel Baets for the countless advice, opportunities, freedom and kind help you have offered to me since the beginning of this PhD. Thank you for your profound as well as fatherly mentorship. So am I deeply indebted to professor Zeger Hens whose bright ideas and critical comments have always brought this work to the right track. Thank you for your critical and, at the same time, friendly guidance.

I would like to express my gratitude to professor Johan Martens and Dr. Sree for the very fruitful collaborations we have had. Sree, thank you for a number of valuable discussions and joint efforts. Professor Johan, thank you for your expert advice. I would like to extend my special thanks to professor Christophe Detavernier and Elisabeth Levrau for an excellent collaboration. Special thanks to Professor Wim Bogaerts for the invaluable insights and discussions on the design and fabrication of integrated photonic structures. Steven, my measurements and daily activities in the cleanroom would not have been smooth without your countless help. Your tirelessness and willingness to help everyone amazes me. Thank you a lot! Dr. Danae, thank you for translating the summary of this thesis into Dutch. Thank you Bart for helping me in translating my abstracts. I would like to thank Ghent University for funding this PhD through the Methusalem Smart Photonics project. I would also like to acknowledge the Flemish Research Foundation (FWO) and the European Research Commission(ERC) for supporting this work. My acknowledgement also goes to EpixFab for the fabrication of my designs on silicon photonic chips.

Above all, thank you my dearest wife, Bitiye, for being by my side and making life purposeful and amazing throughout this journey. Thank you for all the encouragements and smiles. Thank you my little daughter, Sina, for bringing extra energy, inspiration and love to the family. Lucky to have you both whom I consider a gift from above, and so are you truly! Words are too short to express my gratitude to my parents whose immense care, love and aspirations have always accompanied me. My deepest appreciations to all you have paid to us,

your children. Abiye, Aubye, thank you so much, I am very much indebted to you! My dearest sister, Tigi, I would not have known much about purpose and passion for life if not for you. You are very precious! Dear brother and sister, Sol, Mekdi, you are my inspirations, thank you a lot! Gashe, Bogish, Tsehay, Mamo, Girmiye, all my relatives, I am so grateful to all the care and love you have always given me. Dear Tsege, I owe you so much for being with us during a very crucial time. It was unthinkable to finalize my writing without your help taking care of the family. Thank you for the very great time we had together.

Dear present and past office mates, karel, Marie, Bart, Yanick, Martin, and all my colleagues, thank you for making all these years beautiful.

All good people I have met, all good things I have received, how then I forget to mention of the creator of all this beauty and of his unbound providence? Though minds are too bound and words too short to attempt this, I would not let it go without citing a verse:

O LORD, how manifold are thy works! in wisdom hast thou made them all: the earth is full of thy riches.

Psalms 104:24

Gent, December 2012
Nebiyu Adello Yebo

Table of Contents

Dankwoord **i**

Nederlandse samenvatting **xix**

English Summary **xxv**

1 Introduction **1**
1.1 Silicon Photonics . . . 1
1.2 Silicon photonic chips for sensing applications . . . 2
1.3 Review of state of the art gas detection technologies . . . 5
1.3.1 Non-optical gas sensors . . . 5
1.3.2 Fiber Optic and spectroscopic gas sensing technologies . . . 7
1.3.3 Integrated optical gas sensors . . . 9
1.4 Overview of this work . . . 14
References . . . 21

2 Light-environment interaction: the sensor perspective **27**
2.1 Introduction . . . 27
2.2 Background theory: light propagation in dielectric medium . . . 28
2.3 Refractive index sensing . . . 29
2.4 Optical absorption based sensing . . . 30
2.4.1 Basic principles . . . 30
2.4.2 Light absorption in a gas medium . . . 31
2.5 Free-space and guided wave interaction . . . 33
References . . . 36

3 Silicon photonic gas sensing **39**
3.1 Waveguide Absorption Spectroscopy . . . 39
3.2 Refractive index sensing with silicon microring resonators . . . 41
3.2.1 Microring resonator basics . . . 41
3.2.2 Ring resonator parameters . . . 44
3.2.3 Microring resonator sensor design considerations . . . 45
3.3 Chemically functionalized silicon photonic chips for gas sensing . 49

3.3.1 Gas sensitive materials 49
3.3.2 Sensitivity estimations for nanoporous coatings on silicon photonic chips 53
3.3.3 Adsorption isotherm 56
3.3.4 Gas selectivity 58
3.3.5 Response time and reversibility 59
3.4 Summary 59
References 61

4 Experimental settings **65**
4.1 Vapor generation and gas handling setup 65
4.2 Optical setup for gas sensor characterization 67
4.2.1 Fiber-to-infrared camera optical setup 67
4.3 Fiber-to-fiber optical setup 67
4.4 Measurement instruments 69
4.5 Sensor characterization procedure 69
References 71

5 Experimental study of metal oxide and polymer film coated silicon microring resonators for gas sensing **73**
5.1 Ethanol vapor detection with a porous ZnO film coated silicon - on- insulator microring resonator 74
5.1.1 Introduction 74
5.1.2 Sensor structure and sensitivity estimates 75
5.1.3 Sample Fabrication and Preparation 76
5.1.4 Experimental results 78
5.2 Sensitivity of ZnO functionalized microring resonators for carbon monoxide gas 81
5.2.1 Sensor fabrication 81
5.2.2 Experimental results 81
5.3 Reversibility and selectivity of ZnO based sensors 82
5.4 Volatile organic compound sensitivity of PDMS and ZnO films . . 83
5.4.1 Introduction 83
5.4.2 Sensor fabrication and experimental settings 83
5.4.3 Experimental results and discussions 84
5.5 Summary 88
References 89

6 Selective and reversible ammonia gas detection with nanoporous film functionalized silicon photonic micro-ring resonator **93**
6.1 Introduction 93
6.2 Sensor basics 95

6.3 Sensor design and fabrication 96
6.3.1 Design and fabrication of SOI MRRs 96
6.3.2 Mesoporous silica film deposition 96
6.3.3 Microporous aluminosilicate film preparation 97
6.3.4 Aluminum deposition on walls of mesoporous silica films using ALD 98
6.4 Sensing experiments 99
6.5 Summary 104
References 105

7 On chip interrogation of microring resonator gas sensors 109
7.1 Introduction 109
7.2 State of the art on chip spectrometers 110
7.3 Sensor interrogation with on-chip spectrometers 113
7.4 AWG basics and design for wavelength interrogation 115
7.4.1 Basics 115
7.4.2 Basic performance measures 117
7.5 A microring resonator gas sensor interrogation with an on chip arrayed waveguide grating 118
7.5.1 Sensor interrogation basics 119
7.5.2 Design and fabrication 120
7.5.3 Experiments 121
7.6 Summary 125

8 Conclusions 129

9 Future perspectives 133
9.1 Silicon photonics for on-chip gas spectroscopy 133
9.1.1 Gas absorption tests on SOI waveguides 134
9.2 Gas sensing with chemically functionalized SOI structures 138
References 140

List of Figures

1 Illustratie van de brekingsindexdetectietechniek met gefunctionaliseerde microringresonatoren. xxi

2 a) respons van een met microporeuze, zuurrijke film gecoate MRR (a) resonantieverschuiving met betrekking tot NH_3 en CO_2 concentraties (b) respons en herstel in tijd bij NH_3 concentraties van 50, 100, 200 en 400 ppm, geïntroduceerd gedurende twee minuten. xxiii

3 Illustration of a refractive index sensing apprach with surface functionalized microring resonators. xxvii

4 a) response from a microporous acidic film coated MRR (a) resonance shift with respect to NH_3 and CO_2 concentrations (b) response and recovery with time at NH_3 concentrations of 50,100,200 and 400 ppm introduced for two minutes. xxviii

2.1 Schematic representation of an OPA. 33

2.2 Schematic representation of a free space beam of light ineracting with its surrounding. 34

2.3 Schematic representation of an evanescent wave interaction of a guided wave with the surrounding above it. n_s, $n_w g$, and n_c represent the refractive index of the surrounding, the waveguide core and the bottom cladding , respectively. 34

3.1 A schematic reprsentation of a microring resonator coupled to two access waveguides. 42

3.2 A microring resonator model with a single access waveguide. . . . 42

3.3 Through and drop port transmission spectrum of a symmetrically coupled 10μm radius microring resonator 44

3.4 Illustration of a refractive index sensing apprach with surface functionalized microring resonators. 45

3.5 About 110nm thick spin coated ZnO nanoparticle film on Si MRR 52

3.6 simulated effective index sensitivity of a 450nm wide silicon waveguide as function of the thickness of a coating material for a refractive index change of 10^{-3} 53
3.7 Types of adsorption isotherms (International Union of Pure and Applied Chemistry (IUPAC) 1985, [36]) 57
3.8 A Langmuir isotherm fit to experimental CO sensitivity of a ZnO functionlized MRR 58

4.1 Schematic layout of the overall gas sensing setup. 66
4.2 Vertical gas sensing setup with an IR camera readout. 67
4.3 Vertical gas sensing setup directly coupled to input and output fibers. 68

5.1 (a) A scanning electron microscope (SEM) image of an SOI MRR of 5μm radius. (b) Cross section view of the SOI ethanol sensor structure. (c) TE mode electric field profile of a 450nm wide and 220nm high SOI waveguide with ZnO cladding , simulated with COMSOL Multiphysics. 75
5.2 (a) SEM cross section view of a drop casted ZnO film on an SOI sample. (b) SEM image showing the top view of the ZnO film. (c) Optical microscope image of a ZnO nanparticle coating on SOI ring resonators 77
5.3 (a). Measured transmission spectrum of the sensor as a function of ethanol vapor concentration. (b). The corresponding measured resonance shift at different vapor concentrations; the solid curve represents the theoretical fit based on Langmuir isotherm. 78
5.4 (Sensor response with time for one on-off cycle at 300 ppm ethanol vapor concentration. The solid lines are exponential fits at the rising (ON) and falling (OFF) edges of the response. The dotted line shows the switching between 0 (ON) and 300 ppm (OFF) ethanol. 80
5.5 Measured resonance shift of ZnO coated MRR as a function of CO concentration 81
5.6 Measured resonance shift of PDMS coated MRR as a function of xylene vapor concentration 85
5.7 Response and recovery of a PDMS coated MRR as a function of time for 0.1-1 % xylene vapor 85
5.8 Sensitivity of ZnO nanparticle film coated MRR for xylene vapor in 50 -400ppm concentration range 86
5.9 Response and recovery with time of ZnO coated MRR at ~ 380ppm xylene 86

6.1 a) schematic representation of an SOI microring resonator cross section coated with a porous gas sensitive film (not drawn to scale) (b) Scanning Electron Micrograph of a 5 μm radius MRR coated by a mesoporous silica film (thickness ~ 100 nm);Inset:magnified view of the coated MRR. 95
6.2 Toluene adsorption-desorption isotherms measured by Ellipsometric Porosimetry (EP) and mesopore size distribution (inset) of a calcined silica film which is representative of the mesoporous silica coating over the MRR prepared for further functionalization with Al ALD 97
6.3 Toluene adsorption-desorption isotherms measured by Ellipsometric Porosimetry (EP) and (inset)mesopore size distribution of a calcined silica film which is representative of the mesoporous silica coating over the MRR prepared for further functionalization with Al ALD 98
6.4 a) response from a microporous acidic film coated MRR (a) resonance shift with respect to NH_3 and CO_2 concentrations (b) response and recovery with time at NH_3 concentrations of 50,100,200 and 400 ppm introduced for two minutes. 100
6.5 a) measured response from ALD modified mesoporous silica coated MRR upon saturation with NH_3 and CO_2 gases, (b) comparison of NH_3 sensitivity of microporous aluminosilicate film, and mesoporous silica film with and without Al-ALD. 101
6.6 Response and recovery with time of a microporous aluminosilicate film after heating at 100 °C for 20min and cooling to room temperature in N_2 environment. 102
6.7 NH_3 sensitivity and recovery with time of a microporous aluminosilicate film coated sensor after thermal desorption followed by a short pre-humidification step with 1% RH. 103

7.1 A microsope image of an SOI Arrayed waveguide grating. 111
7.2 An SEM image of an SOI planar concave grating. The colorful art portrays the wavelength spiliting property of the device. 111
7.3 A schematic representaiton of an AWG structure.The inset shows a Rowland mounting configuration of the array and input/output waveguides 115
7.4 A depiction of a microring resonance of 0.05nm FWHM centered half way between two adjacent AWG channels with Gaussian response of 2.5nm FWHM (left),1.5nm FWHM(right). 118
7.5 Relative intensities at adjacent channels when the resonance is red shifted by 0.8nm for Gaussian AWG response of 2.5nmFWHM. 118

7.6 Relative intensities at adjacent channels when the resonance is red shifted by 0.8nm for Gaussian AWG response of 2.5nmFWHM. 119
7.7 Given three neighboring AWG channels centered at 1550nm, 1551.6nm and 1553.2nm, theoretical estimates of intensity ratios between adjacent channels as a function of the MRR resonance wavelength for Gaussian profiles of 1.5nm FWHM (dotted lines), and 2nm FWHM (solid lines) 120
7.8 An optical microscope image of the AWG interrogated ethanol vapor sensor with ZnO porous film on the MRR. The AWG used for the spectral response characterization is partially shown in the image. 121
7.9 Normalized transmission spectrum of an AWG with 4μm wide input waveguide 122
7.10 Illustrations of intensity changes measured from three neighboring channels at 0ppm(pure nitrogen), 120ppm and 960ppm ethanol vapor concentrations. 123
7.11 Average intensities measured from three channels at different ethanol vapor concentrations 124
7.12 calculated intensity ratios as a function of resonance shifts corresponding to vapor concentrations shown in fig 7.11 with an exponential fit to ch2:ch3 (solid line) 125

9.1 (top)Two consecutive transmission spectrum measured from 1.5cm long SOI spiral waveguide . (bottom) the ratio of the two measurements in natural log scale 135
9.2 (top)Two consecutive transmission spectrum measured from 50μm long straight SOI waveguide on 12mm layout. (bottom) ratio of the two measurements in natural log scale 136
9.3 Fourier transform of the transmission spectrum shown in figure 9.2 plotted on length scale 137
9.4 Transmission spectra measured from 150nm thick ZnO coated 1cm long spiral waveguide before and after to NH_3 137

List of Acronyms

A

ALD	Atomic Layer Deposition
AWG	Arrayed Waveguide Grating

B

BCP	Bromocresol purple
BUN	Blood Urea Nitrogen

C

CMOS	Complementary Metal Oxide Semiconductor
CNT	Carbon Nanotube

D

DUV	Deep Ultra Violet

E

EP	Ellipsometric Porosimetry
EFA	European Federation of Allergy and Airway Diseases Patients Association
ESRD	End Stage Renal Disease

F

FSR	Free Spectral Range
FBG	Fiber Bragg Grating
FWHM	Full Width at Half Maximum

G

GINA	Global Initiative for Asthma

H

HIC	High Index Contrast

I

IR	Infra Red

L

LAN	Local Area Network

LED	Light Emitting Diode

M

MEMS	Micro Electro-Mechanical System
MOF	Metal Organic Framework
MOS	Metal Oxide Semiconductor
MRR	Microring Resonator
MZI	Mach-Zehnder Interferometer

N

NIR	Near Infrared

P

PANI	Polyaniline
PCG	Planar Concave Grating
PDMS	Polydimethylsiloxane
PEL	Permissible Exposure Limit
PhC	Photonic Crystal
PMMA	Polymethylmethacrylate

Q

Q factor	Quality factor

R

RH	Relative Humidity

RIU	Refractive Index Unit

S

SAWS	Surface Acoustic Wave Sensor
SEM	Scanning Electron Microscope
SERS	Surface Enhanced Raman Scattering
SOI	Silicon-On-Insulator
SPR	Surface Plasmon Resonance
SPME	Solid Phase Micro Extraction

T

TFBG	Tilted Fiber Bragg Grating
TMA	Trimethylaluminium
TPAOH	Tetrapropylammonium Hydroxide

U

UV	Ultra Violet

V

VIS	Visible
VOA	Variable Optical Attenuator
VOC	Volatile Organic Compound

W

WDM	Wavelength Division Multiplexing

Nederlandse samenvatting –Summary in Dutch–

Er is in het recente verleden aanzienlijke vooruitgang geboekt op het vlak van siliciumfotonica. Uit deze ontwikkelingen zijn nieuwe toestellen en toepassingen voortgevloeid die aantrekkelijke alternatieven vormen voor een aantal bestaande technologieën. Een van de onmisbare toepassingen waarin de interactie van licht met haar omgeving een heel belangrijke rol speelt is optische sensing (detectie met behulp van sensoren). Zo zijn compacte en niet dure sensoren van groot belang voor mobiele, kostenefficiënte en real-time detectiemethoden voor milieutechnische, biomedische en industriële toepassingen. Op dit vlak zijn geïntegreerde optische sensoren op basis van silicium veelbelovend. Een belangrijke stuwende kracht achter siliciumfotonica is het potentieel om voort te bouwen op de alomtegenwoordige, vele miljarden vertegenwoordigende micro-elektronische productie-infrastructuur, die in de voorbije decennia een ware revolutie heeft teweeggebracht binnen de elektronica-industrie. Door gebruik te maken van de compatibiliteit met deze infrastructuur, belooft ook siliciumfotonica kostenefficiënt te zijn.

Siliciumfotonica voor biomedische en milieutechnische detectietoepassingen situeert zich grotendeels binnen de enorme markt voor gezondheidszorg-, milieu- en industriesensoren, die door de in massa geproduceerde, lage kost fotonische detectiechips kan worden bediend. Dit potentieel wordt nog vergroot door de hoge brekingsindexgevoeligheden die kunnen worden bereikt door het hoge brekingsindexcontrast van de fotonische silicium-op-isolator (SOI) structuren. Het rechtstreeks multiplexen van sensoren op siliciumchips betekent ook dat de parallelle detectie van meervoudige analieten vlot kan worden gerealiseerd op een enkelvoudige chip. Dit biedt mogelijkheden voor 'lab-op-chip' toepassingen waarbij in vergelijking met de traditionele instrumenten de volumes van de benodigde monsters en de kosten voor de laboratoriumprocessen significant kunnen worden verminderd.

Naast de detectie van biomoleculen in de vloeibare fase, worden fotonische sensoren op siliciumbasis sinds kort ook onderzocht voor gasdetectietoepassingen. Een aantal domeinen waarin geïntegreerde gassensoren een belang-

rijke impact kunnen hebben, zijn: 'point-of-care diagnostica' in de gezondheidszorg, controle en monitoring van milieuvervuiling, energie-efficiënte en real-time kwaliteits- en procescontrole in de industrie en detectie van mogelijke bedreigingen. Verder kan worden verwacht dat innovaties via state-of-the-art microproductie en de hieruit voortvloeiende dalende prijzen voor hoogperformante sensoren een belangrijke rol zullen gaan spelen in het promoten van de markt van biochemische sensoren en gassensoren in het algemeen.

Er bestaan vandaag verschillende gasdetectietechnologieën. De meeste van deze technologieën missen echter de capaciteiten die de meeste medische en milieutechnische toepassingen nodig hebben. Zo vereisen de globale noden op het vlak van gezondheidszorg dat de detectie-instrumenten toegankelijk zijn voor het grote publiek, los van economische of geografische grenzen. Daarom moeten deze instrumenten betaalbaar, energie-efficiënt, robuust en mobiel zijn en ook direct resultaat opleveren. De sensoren voor de gezondheidszorg die vandaag frequent worden gebruikt, zijn echter over het algemeen duur en weinig mobiel en dus minder geschikt voor gebruik op de plaats van de medische zorg ('point-of-care'). De traditionele bulkgassensoren zijn vaak volumineus, complex en duur. Anderzijds worden goedkope en compacte sensoren zoals diegene gebaseerd op metaaloxidehalfgeleiders doorgaans gekenmerkt door een gebrekkige selectiviteit. In massa geproduceerde fotonische gassensoren op basis van silicium en ter grootte van een chip kunnen in vergelijking met de conventionele technologieën enorme voordelen opleveren op het vlak van kostprijs, omvang en selectiviteit en zijn dus veelbelovend.

In dit onderzoek zijn fundamentele studies uitgevoerd inzake fotonische gasdetectie op basis van silicium en er zijn ook experimentele demonstraties gegeven van sensorprototypes met specificaties relevant voor praktische toepassingen. Deze specificaties richten zich vooral op de gebruikelijke prestatiemaatstaven zoals gevoeligheid, gasspecificiteit, responstijd en sensorregeneratie. Andere kenmerken zoals de sensorgrootte en -kost worden beschouwd als potentiële voordelen die inherent zijn aan de siliciumfotonicatechnologie. Voor de detectie met deze sensoren worden gasconcentraties van een aantal honderden ppb (delen per miljard) of een aantal tientallen ppm (delen per miljoen) vooropgesteld. Compacte en draagbare sensoren die binnen dit detectiebereik werken, bieden een aanzienlijk potentieel voor een aantal biomedische of industriële toepassingen zoals medische ademanalyse en industriële procescontrole. Een gasselectieve en snelle sensorrespons zijn andere cruciale prestatietargets die in het onderzoek aan bod komen. De technieken 'brekingsindexdetectie' en 'absorptiespectroscopie' worden in dit onderzoek aangeduid als zijnde interessant voor implementatie op fotonische siliciumchips. De beide technieken kunnen eventueel een aanvullende rol spelen voor een meer universeel en ruimer gamma van gasdetectie op chips. Alhoewel elke techniek op

zichzelf een significant wetenschappelijk en technologisch belang heeft, werd in dit onderzoek toch vooral nader ingegaan op gasdetectie op basis van de brekingsindextechniek. Microringresonatoren (MRR) werden hoofdzakelijk gebruikt als elementaire optische bouwelementen voor de gassensorprototypes. Een hoge brekingsindexgevoeligheid, sensormultiplexing en ultracompactheid zijn een aantal interessante kenmerken van MRR. De brekingsindexdetectietechniek gebruikt chemische omzettingsmechanismen voor een selectieve en gevoelige gasdetectie. Bijgevolg gaat het hier om een multidisciplinair onderzoek waarbij zowel vanuit optische als chemische perspectieven wordt gewerkt. Figuur 1 toont de algemene gasdetectiebenadering met een gefunctionaliseerde MRR. Vooral nanoporeuze materialen zijn van cruciaal belang in dit onderzoek. Door gebruik te maken van de door deze materialen aangeboden vrij grote oppervlakte kunnen verbeterde gasgevoeligheden worden gerealiseerd. Het nanoporeuze oppervlak leent zich verder ook tot de integratie van functionele groepen voor selectieve gasdetectie. De door de poreuze structuren bevorderde efficiënte diffusie van gasmoleculen is een ander waardevol voordeel van deze materialen voor een snelle sensorrespons. In dit verband werden met nanoporeuze ZnO-, siliciumdioxide- en polymeerfilms gefunctionaliseerde MRR onderzocht op hun efficiëntie voor gasdetectie.

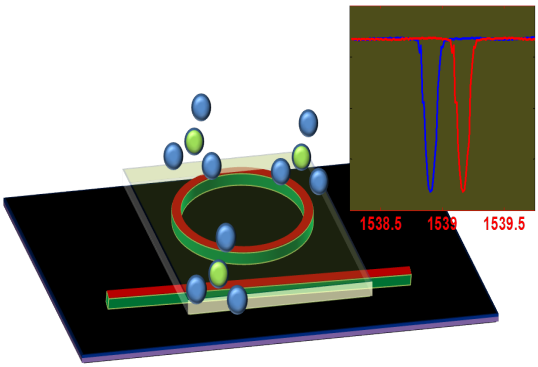

Figuur 1: Illustratie van de brekingsindexdetectietechniek met gefunctionaliseerde microringresonatoren.

Hoge gevoeligheden voor volatiele organische verbindingen, namelijk ethanol en xyleen, en voor gasvormige CO werden via experimenteel onderzoek aangetoond voor met nanokristallijne ZnO gefunctionaliseerde MRR. Daarbij werden gevoeligheden tot gasconcentraties onder ppm (delen per miljoen) bereikt.

De doorsnee responstijden voor deze sensoren schommelen tussen de 20 en 40 seconden. Anderzijds heeft deze studie tot het inzicht geleid dat metaaloxide-films, zoals ZnO, sterk kunnen reageren op een aantal gasverbindingen en dus minder geschikt zijn voor selectieve gasdetectie. Een ander typisch waargenomen kenmerk van ZnO films is dat het sensorherstel slechts partieel is. Bijgevolg zijn dergelijke toestellen beter geschikt voor eenmalige detectieapplicaties.

Polymeermaterialen zoals PDMS worden dan weer gekenmerkt door een sterke affiniteit voor organische dampen (Volatile Organic Compounds of VOC). Op basis van experimentele gegevens verkregen met een ~ 150nm dikke PDMS coating, tonen we een detectielimiet van ongeveer ~ 500 ppm voor xyleendampen aan. Bovendien wordt met deze sensor een opmerkelijke reversibiliteit en een snelle respons waargenomen. De respons- en hersteltijden bedragen respectievelijk ongeveer 20 en 40 seconden. Dit resultaat toont de mogelijke rol aan van met polymeren gefunctionaliseerde silicium-MRR als herbruikbare, goedkope en real-time VOC-detectie-instrumenten. Deze sensoren kunnen worden gebruikt voor de detectie van een bepaalde categorie van VOC's, bijvoorbeeld voor een vroege waarschuwing in industriÃńle werkplaatsen.

Nog interessanter is dat werd aangetoond dat specifiek op maat gemaakte materialen kunnen leiden tot een selectieve gasdetectie op fotonische siliciumchips. Aluminosilicaatfilms verkregen via een synthesetechniek enerzijds en via atomaire laagdepositie (ALD) anderzijds worden op de silicium-MRR gedeponeerd. Door de in het siliciumdioxidekader ingebrachte Al atomen vertonen deze films zuurrijke oppervlakken die geschikt zijn voor de preferentiële adsorptie van gasvormige basen zoals NH_3. Figuur 2 toont de experimentele resultaten. Een gevoelige, reversibele en snelle respons op NH_3 en een hoge selectiviteit met betrekking tot CO_2 worden verkregen met deze sensoren. De evenwichtsrespons wordt verkregen in minder dan 30 seconden en een herstel van 95% wordt bereikt binnen 90 seconden. Een detectielimiet van ongeveer 5ppm voor microporeuze zuurrijke films verkregen via synthese werd experimenteel gerealiseerd. Een verdere verbetering van de gevoeligheid zou kunnen worden verkregen door het optimaliseren van de porositeit en van de oppervlakte-eigenschappen van de poreuze aluminosilicaatfilms. Een mogelijke toepassing voor een dergelijke selectieve NH_3 sensor is een instrument voor medische ademanalyses voor het diagnosticeren en permanent opvolgen van nierpatiënten.

Het uitlezen van SOI MMR sensoren door het meten van de verandering van de resonantiegolflengte maakt multiplexing van sensormatrixen mogelijk en leidt tot een hogere signaal-tot-ruis-verhouding in vergelijking met het meten van intensiteitsvariaties. De huidige detectiesystemen op basis van golflengteinterrogatie worden echter meestal gekenmerkt door omvangrijke en dure instrumentatie. Doorgaans wordt gebruik gemaakt van een externe, afstembare

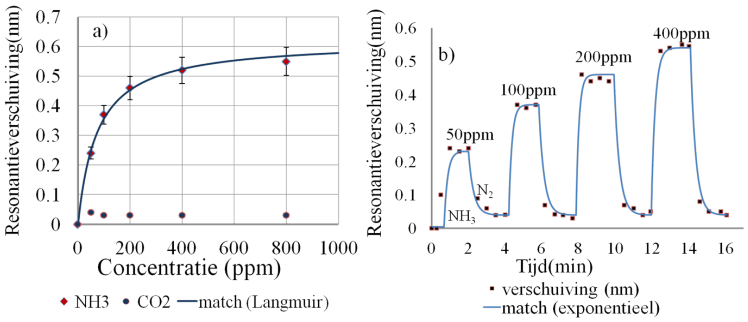

Figuur 2: a) respons van een met microporeuze, zuurrijke film gecoate MRR (a) resonantieverschuiving met betrekking tot NH3 en CO2 concentraties (b) respons en herstel in tijd bij NH_3 concentraties van 50, 100, 200 en 400 ppm, geïntroduceerd gedurende twee minuten.

laserbron of van de combinatie van een breedbandbron met een hogeresolutiespectrometer. Bijgevolg worden de voordelen van chipsensoren op het vlak van afmetingen en kosten tenietgedaan door deze externe accessoires. Ondanks een aantal inspanningen op dit vlak zijn verdere vooruitgang en nieuwe oplossingen nodig om kostenefficiënte en draagbare ringresonatorsensoren te realiseren. In dit verband wordt in dit werk geëxperimenteerd met een potentieel goedkope en compacte MRR-sensor interrogatiemethode op basis van een AWG-spectrometer op de chip. Het gebruik van deze spectrometer met goedkope breedbandlichtbronnen, zoals superluminiscente LED's, kan de grootte en de kostprijs van de huidige sensorsystemen op basis van MRR aanzienlijk terugdringen. Een SOI MMR ethanoldampsensor wordt uitgelezen aan de hand van een 200 GHz AWG ontworpen met het oog op sterk overlappende uitgangskanalen. Daarbij is aangetoond dat resonantieverschuivingen gaande van 50pm tot 800pm vlot kunnen worden gedetecteerd door het meten van de verhouding tussen twee overlappende, nabije AWG kanalen.

Algemeen wordt in dit werk aangetoond dat optische gassensoren op chips een aanzienlijk potentieel bieden voor mobiele, goedkope en real-time gasdetectiemethoden voor een brede waaier van toepassingen met inbegrip van medische ademanalyses. Met de huidige ontwikkelingen inzake gasselectieve films en efficiënte sensorspottingtechnieken kunnen verschillende, gemultiplexte sensormatrixen worden geÃŕmplementeerd op fotonische siliciumchips voor de detectie van meerdere gassen. Deze sensoren kunnen een aanzienlijke meerwaarde bieden voor toepassingen waarvoor een complexe gasanalyse nodig is zoals geurmonitoring en de detectie van kanker.

English Summary
–English Summary–

A considerable progress in the field of silicon photonics has been witnessed in the recent past. Accompanying these developments, various new devices and applications have emerged as attractive alternatives to existing technologies. One of the indispensable applications where the interaction of light with its environment plays a substantial role is optical sensing. More particularly, compact and inexpensive sensors are of a high interest for portable, cost effective, and real time sensing in a number of environmental, biomedical and industrial applications. In this regard, silicon based integrated optical sensors promise a high potential . A major driving force behind silicon photonics has been the potential to exploit the well established billions of capital microelectronic fabrication infrastructures witnessed to have revolutionized the electronic industry in the last few decades. Taking advantage of its compatibility with these infrastructures, silicon photonics promises to be cost effective with respect to materials, components and energy consumption. Moreover, characterized by the rich properties of light, the silicon photonics platform potentially offers a cost effective increase in the communications bandwidth as well as opens opportunities for various multiplexed applications.

Silicon photonics for bio-medical and environmental sensing is largely motivated by the vast health care, environmental and industrial sensing market which can well be addressed by mass-fabricated photonic sensing chips. This potential is further augmented by the high refractive index sensitivities achievable with the high index contrast silicon-on-insulator photonic structures. Straightforward multiplexing of sensors on silicon chips also means that parallel detection of multiple analytes is readily achievable on a single chip. This provides opportunities for lab-on-chip applications whereby significantly minimizing the sample volumes and the cost of laboratory processes as compared to traditional tools.

Apart from biomolecule detection in the liquid phase, silicon photonic sensors for medical, environmental and industrial gas sensing applications are being explored recently. Some of the areas integrated gas sensors can have a major

impact are: point-of-care diagnostics in health care sector, control and monitoring of environmental pollution, energy efficient and real-time quality and process control in industries, and threat detection. Moreover, dissolved gas sensors are of a high demand for water resource conservation and quality control. In addition, innovation through cutting edge microfabrication and the accompanying falling price of high-performance sensors are expected to play an important role in raising the bio-chemical and gas sensors market in general.

Various gas detection technologies exist today. Nonetheless, most of these technologies in one way or another lack the capabilities most medical and environmental applications necessitate. For instance, ensuring global health care demands that the detection tools are accessible to the general public irrespective of economic or geographic boundaries. This would require these tools to be affordable, energy efficient, robust, prompt and portable. However, the widely used sensors for health care are typically expensive and far less portable, hence, becoming less suitable for point-of-care deployment. Traditional bulk gas sensors typically suffer from large size, complexity and high cost. On the other hand, cheap and compact sensors such as those based on metal oxide semiconductors are typically characterized by limitations such as poor selectivity. Mass produced chip-scale silicon photonic gas sensors can immensely take advantage of cost, size and energy related befits over the traditional technologies, hence, promising a rapid contribution to the field.

In this research, fundamental studies on viable silicon photonic gas detection as well as experimental demonstrations of sensor prototypes of practically relevant specifications have been carried out. These specifications mainly focus on common performance measures such as sensitivity, gas-specificity, response time and sensor regeneration. Other features such as sensor size and cost are considered as potential benefits inherently offered by the silicon photonics technology. 100's of ppb - 10's of ppm gas concentrations are targeted for the detection with these sensors. Compact and portable sensors operating in this detection range exhibit a significant potential for a number of bio-medical and industrial applications such as medical breath analysis and industrial process control. Gas selective and rapid sensor response are other critical performance targets addressed in this research. The refractive index sensing and absorption spectroscopic techniques are primarily identified in this research as attractive for implementation on silicon photonic chips. Both approaches can potentially play a complementary role for more universal and broad-range on-chip gas detection. While each technique draws a significant scientific and technological interest on its own right, gas detection with the refractive index based approach has been dealt in a more detail in this research. Microring resonators(MRRs) are primarily used as basic optical building blocks for the gas sensor prototypes. High refractive index sensitivity, sensor multiplexing and

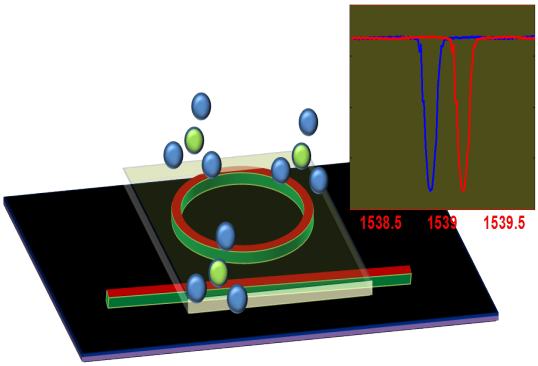

Figure 3: Illustration of a refractive index sensing apprach with surface functionalized microring resonators.

ultra-compactness are some of the attractive features of MRRs. The refractive index sensing technique typically involves chemical transduction mechanisms for selective and sensitive gas detection. Consequently, multidisciplinary efforts from both optical and chemical perspectives have been involved in this research. Figure 3 depicts the general gas sensing approach with functionalized MRRs. Nanoporous materials, in particular, have been of a central research interest in this work. Exploiting a considerably high surface area offered by these materials, enhanced gas sensitivities have been demonstrated. The nanoporous surface further lends itself for the incorporation of functional groups for selective gas detection. Efficient diffusion of gas molecules facilitated with the porous structures is another valuable feature offered by these materials for rapid sensor response. In this respect, MRRs functionalized with nanoprous ZnO, silica and polymer films have been studied for efficient gas detection.

High sensitivities for volatile organic compounds, namely ethanol and xylene, as well as for gaseous CO have been experimentally demonstrated from nanocrystalline ZnO functionalized MRRs. Sensitivities down to sub ppm gas concentrations are achieved. Typical response times for these sensors are in the range of 20-40 seconds. On the other hand, this study has provided an insight that metal oxide films, such as ZnO, as demonstrated here can be strongly responsive to a range of gaseous compounds, hence, being less suited for selective gas detection. Partial sensor recovery is another point typically observed for ZnO films. Consequently, such devices can be more suited for disposable sensing applications.

On the other hand, Polymer materials, such as PDMS, are characterized by high affinities towards industrially and environmentally relevant organic vapors. PDMS coated MRRs have also demonstrated attractive performance features for potential VOC sensing. Based on the experimental data obtained for ~ 150nm thick PDMS coating, a detection limit of ~ 500ppm is estimated for xylene vapor. Moreover, a remarkable reversibility and a fast response is measured from this sensor. The response and recovery times are approximately 20 and 40 seconds, respectively. This result demonstrates the potential role of polymer functionalized silicon MRRs as re-usable, low cost and real time VOC detection tools. Such sensors can be used to detect a given class of VOCs for early warning, for instance, in industrial workplaces.

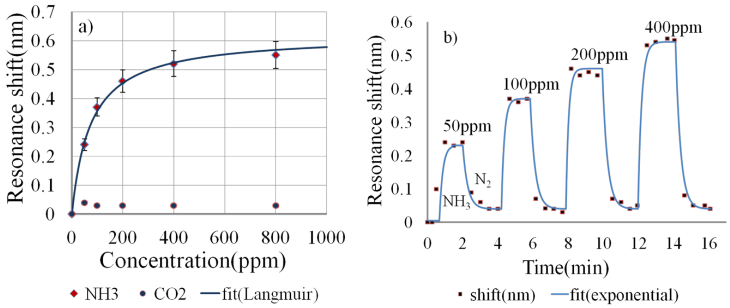

Figure 4: a) response from a microporous acidic film coated MRR (a) resonance shift with respect to NH_3 and CO_2 concentrations (b) response and recovery with time at NH_3 concentrations of 50,100,200 and 400 ppm introduced for two minutes.

More interestingly, it is demonstrated that specifically tailored materials can lead to selective gas detection on silicon photonic chips . Alumino-silicate films obtained through a synthesis based technique as well as atomic layer deposition(ALD) are incorporated on silicon MRRs. Owing to Al atoms introduced into the silica framework, these films exhibit acidic surfaces suitable for preferential adsorption of gaseous bases such as NH_3. Figure 4 shows the experimental results. Sensitive, reversible and fast response to NH_3 and high selectivity with respect to CO_2 is achieved with these sensors. Equilibrium response is attained in less than 30 sec and over 95% recovery is reached within 90 sec. A detection limit of 5ppm is estimated for microporous acidic films obtained via synthesis. A further improvement of the sensitivity could be achieved by optimizing the porosity and surface properties of the porous alumino-silicate films. Such a selective NH_3 sensor can have a future application as medical breath analysis tool for diagnosis and continuous monitoring of renal patients.

On the other hand, wavelength interrogated SOI MRR sensors offer supe-

rior sensitivities to the surrounding, allow multiplexing of sensor arrays , and provide immunity to noise with respect to the intensity interrogation schemes. However, current wavelength interrogation based sensing systems are typically characterized by bulky and costly instrumentation. An external tunable laser source or the combination of a broadband source and a high-resolution spectrometer are usually employed. As a result, the size and cost benefits of on chip sensors are overshadowed by these external accessories. Despite a few efforts made so far, more progress and novel solutions are highly required to realize cost effective and portable ring resonator sensors. In this regard, a potentially low cost and compact MRR sensor interrogation approach based on an on-chip AWG spectrometer is experimentally demonstrated in this work. This spectrometer employed with cheap broadband light sources, such as superluminescent LEDs, can significantly cut down the size and cost of the current microring resonator based sensors. An SOI MRR ethanol vapor sensor is interrogated by a 200 GHz AWG designed to have strongly overlapping output channels. It is demonstrated that resonance shifts ranging from 50pm- 800pm can readily be interrogated by measuring the ratio between two overlapping adjacent AWG channels.

In general, it is demonstrated in this work that on-chip optical gas sensors promise a considerable potential for ultra portable, low cost and real time gas detection in a wide range of applications including medical breath analysis. With ongoing developments on gas selective films and efficient sensor spotting techniques, several multiplexed sensor arrays can be implemented for multi-gas detection on silicon photonic chips. These sensors can have a significant contribution for applications involving complex gas analysis such as odor monitoring and cancer detection.

1 Introduction

1.1 Silicon Photonics

Since the pioneering works in late 1980's, growing interests and advancements in silicon photonics devices and applications have been recorded [1-4]. Silicon photonics is a subset of a general discipline of photonic integration which covers a range of material systems including III-V semiconductors, silica and silicon. Silicon photonics comprises silicon as the main constituent material for opto-electronic applications. This emerging technology targets to embed light based components in silicon chips whereby replacing discrete optical components as well as opening new opportunities for new devices and applications. A major driving force behind silicon photonics has been the potential to exploit the well established billions of capital microelectronic fabrication infrastructures witnessed to have revolutionized the electronic industry in the last few decades[2,3]. Taking advantage of its compatibility with these infrastructures, silicon photonics promises to be cost effective with respect to materials, components and energy consumption. Moreover, characterized by the rich properties of light, silicon photonics potentially offers a cost effective increase in communications bandwidth as well as opens opportunities for various multiplexed applications.

Significant expansion and diversification in the field of silicon photonics has been witnessed in the recent past. Accompanying this progress, various

new devices and applications have emerged as attractive alternatives to existing technologies[1-5]. Inspired by the huge bandwidth promised by photonic devices, the research and development has been largely focused towards data communication applications. Continually growing computer processor power has consequently imposed the demand for paralleled increase in input-output (I/O) bandwidth of the aggregate computing and communication systems. Hence, an interconnect technology which can offer performance features such as low power, low latency and high bandwidth becomes of high prospect. In this respect, integrated silicon photonic data links are highly envisioned for the near future telecommunications and computing market. Silicon photonic interconnects are being considered for on-chip communications within computers, inter-chip communications, backplane connections within servers and switches, communications between servers and switches, and for access and metro network communications[2-5].

Utilizing mature microelectronic infrastructures, significant fabrication advancements have been made demonstrating the potential for large scale and low cost production of silicon photonic devices. Silicon photonics components such as modulators and detectors capable of operating upto 40Gb/s speed for interconnects have been reported by various research groups and companies [5-7].Currently several silicon photonic components and devices for telecom applications have been developed and some of the first commercial products have been introduced to the market place[8,9]. These include, silicon based Wavelength Division Multiplexing (WDM) filters and transceivers for access metro and long haul networks, ultra variable optical attenuator(VOA) arrays, demultiplexers and multiplexers for high speed LAN and high performance computing. While silicon photonic links for chip-to-chip and longer links are making their ways into the market, integration with the cutting edge 29nm or lower CMOS line at acceptable power budget per bit is the next milestone the silicon photonics community is pushing for the realization of on-chip interconnects[3].

In addition to the aforementioned data communication areas, a broad range of novel silicon photonic applications are being explored and developed more recently. Bio-medical and environmental sensing, light detection and ranging, and microwave photonics are among these developments[10-14].

1.2 Silicon photonic chips for sensing applications

In the past five years, the silicon photonics platform for on-chip integrated biomedical and environmental sensing has increasingly become attractive[12-14]. In this respect, integrated silicon photonics components based on various device physics and architecture have been of a significant research interest

for enhanced environmental sensitivity as well as other important features such as simplicity, multiplexing and device footprint[12-15]. Silicon photonics for bio-medical and environmental sensing is largely motivated by the vast health care, environmental and industrial sensing market which can well be addressed by mass-fabricated photonic sensing chips. This potential is further augmented by high refractive index sensitivities achievable with high index contrast silicon-on-insulator photonic structures [15]. Straightforward multiplexing of sensors on silicon chips also means that parallel detection of multiple analytes is readily achievable on a single chip. This opens opportunities for lab-on-chip applications whereby significantly minimizing the sample volumes and the cost of laboratory processes as compared to traditional tools. Label-free or non-destructive detection is another key capability offered by silicon photonic bio-sensors[13].

Apart from biomolecule detection in the liquid phase, silicon photonic sensors for medical, environmental and industrial gas sensing applications are being explored recently[14,16]. Some of the areas integrated gas sensors can have a major impact are: point-of-care diagnostics in health care sector, control and monitoring of environmental pollution, energy efficient and real-time quality and process control in industrial applications, and threat detection and security. Recent projections indicate that the general chemical sensors market will reach $17.28 billion by the year 2015[17]. Developments in the medical test market and the growing demand in large-scale industrial and environmental applications are expected to drive the market for chemical sensors including gas sensors and bio-sensors. In addition, dissolved gas sensors are of a high demand for water resource conservation and quality control. Moreover, innovation through cutting edge microfabrication and the accompanying falling price of high-performance sensors are expected to play an important role in raising the chemical sensors market. Accordingly, integrated optical gas sensors exhibit a high potential for generating revenue for mass volume application in the medical, environmental, industrial, and motor vehicle sectors. The food industry is another major drive for gas sensors. For instance, carbon dioxide (CO_2) sensors in bulk food storage industry are of a considerable demand owing to their capability to indicate incipient spoilage as well as for monitoring modified atmosphere packaging[18].

The bio-medical sensing market, in particular, is expected to rise due to the increasingly aging population, more spending in the heath care, growing shift towards point-of-care diagnostics and monitoring, and increasing incidents of chronic diseases[19]. The detection of exhaled gaseous compounds is believed to have a key role in patient diagnosis and continual health monitoring. A human breath consists over 400 volatile compounds of which some have been recognized as biological indicators to specific health conditions. Nitric oxide (NO),

ammonia (NH_3), and acetone are examples of some compounds recognized to have correlations with medical cases such as asthma, renal failure and oral diseases[20-22]. Breath related health problems such as asthma have shown a dramatic rise worldwide. An earlier report released by the Global Initiative for Asthma (GINA) indicated that over 300 million patients worldwide suffer from asthma[23]. Another report from the European Federation of Allergy and Airway Diseases Patients Association (EFA), showed an estimate that the number of people with asthma could grow to 400-450 million worldwide by 2025 [24]. According to the same report, the total cost of asthma in Europe is 17.7bn Euros per year, and productivity lost to poor asthma control is estimated at 9.8bn Euros per annum [24,25].Renal failure is another serious health issue worldwide. According to a recent corporate report, the number of end-stage renal disease (ESRD) patients undergoing dialysis treatment had reached 1.77 million worldwide by the end of 2008[26].

On the other hand, some breathe gases such as NO and NH_3 have demonstrated a high promise for monitoring asthmatic and kidney patients, respectively[20,21]. NO is produced naturally in the body, and can signal the beginning of inflammation in the bronchial tubes. If not spotted in time, the inflammation will constrict the airways and trigger an asthma attack. Breath NH_3, on the other hand, has demonstrated the potential to aid the follow up of dialysis treatments on kidney patients. Furthermore, recent developments have indicated that parallel detection of some volatile compounds in human breath can be used for the diagnosis of lung cancer [63].

Various gas detection technologies exist today. Nonetheless, most of these technologies in one way or another lack the capabilities most medical and environmental applications necessitate. For instance, ensuring global health care demands that detection tools are accessible to the general public irrespective of economic or geographic boundaries. This would require these tools to be affordable, energy efficient, robust, prompt and portable. However unfortunately, widely used sensors for health care are typically expensive and far less portable for point-of-care deployment[27]. Traditional bulk gas sensors such as electrochemical sensors, gas chromatographs, mass spectrometers, and spectrophotometers, typically suffer from large size, complexity and high cost. On the other hand, as it is the case with the telecom and computing, existing electronics faces limitations for sensing applications as well. One of the issues is that there is a limited choice of gas sensitive materials which lend themselves for direct electrical/electronic interrogation. Hence, achieving practically relevant performances such as sensitivity and selectivity from electrical sensors becomes a challenge[28,29]. Mass produced chip-scale silicon photonic gas sensors can immensely enjoy cost, size and energy related befits over the traditional technologies, hence, promising a rapid penetration into the market.

Besides size and cost, other features such as adequate sensitivity, selectivity, and reliability to operate in real sensing environments are equally relevant in the development of on-chip sensors. Integrating all these performance features on silicon chips requires a combined input from a multi-disciplinary research community. Development of refined surface chemistry and efficient coating(spotting) techniques are the two major areas multidisciplinary efforts are of high importance. A valuable progress has been made in this regard leading to highly specific and multiplexed biomolecule sensors on photonic chips[12]. However, major advancements are yet to be made for efficient gas detection on integrated optical platforms.

1.3 Review of state of the art gas detection technologies

In this section a review of state of the art gas sensors both in optical and non-optical domain is briefly presented. A wide variety of gas sensing technologies are available currently at the research and commercial levels. In this review, a main focus is given to a few widely used competitive technologies.

1.3.1 Non-optical gas sensors

Conventional non-optical gas sensors may fall under the general categories of chromatographic & spectrometric sensors, electrochemical sensors and mass sensors. Each of these techniques are discussed below with regard to the respective advantages and limitations.

Gas chromatography and spectrometry

Gas chromatography is basically a technique involving a highly efficient separation of a complex mixture into individual components. When a mixture of compounds is injected into a chromatographic column, each component travels at different rates, and hence, arrives at the end of the column at different times. A chromatographic column typically consists of an adsorbent material which is characterized by different desorption(elution) rates for different compounds. A detector at the end of the column is used to quantify the concentration of each of the components. Various types of chromatographic detection systems exist with different level of complexity and size. Some of the examples are ion mobility spectrometers, mass spectrometers, and microfabricated chromatographic systems [30]. Chromatographic gas detectors are known for high reliability, precision, sensitivity, ruggedness, and capability to detect a wide range of compounds. However, these devices are mainly limited by very large size and high

cost. Hand held forms of these sensors have also been developed, and more recently research efforts towards microfabricated systems have been made [31]. However, currently commercialized reliable chromatographic sensors still remain to be large in size and highly expensive. Device costs in the range of 10's of thousands of dollars are typical for these sensors [30].

Electrical gas sensors

The basic principle of electrical sensors is based on measuring electrical quantities of a sensing unit upon interaction with a compound of interest. Widely used examples of electrical gas sensors include metal oxide semiconductors, conducting polymers and electrolytic/electrochemical detectors. Metal oxide semiconductor sensors for a wide range of toxic, polluting, combustible and medically relevant gases such as NO, NO_2, NH_3, H_2S, CH_4, H_2 have been developed[28,29]. Some of the extensively used metal oxide materials include ZnO, TiO_5, SnO_2, WO_3[32]. Moreover, electrical gas sensors employing conducting polymers have also been demonstrated. A conducting polymer, Polyaniline(PANI), is one of the frequently used polymers for detecting gaseous compounds such as NH_3 and NO_2[33]. More recently, the integration of carbon nanotube (CNT) based sensor on CMOS chip to detect hydrogen gas has been demonstrated[34]. This sensor chip is shown to detect 10ppm hydrogen concentration in air.

Non-electrolytic electrical sensors on semiconductor or polymer materials are typically small, low cost and show high sensitivities to various chemicals. Moreover, as compared to the standard electrolytic sensors, they do not require liquid electrolytes for functioning. Nonetheless, these sensors commonly suffer from issues such as inability to discriminate among unknown gas mixtures and heating requirements for a proper operation[29,32]. One of the reasons for the typically poor selectivity of conductometric gas sensors stems from the fact that there is a narrow range of materials simultaneously satisfying gas specificity and sensitivity as well as electrically compatible properties. In this respect, integrated sensing platforms with a relaxed constraint on the gas sensitive materials are of a major advantage over electrochemical sensors.

Mass sensors

Mass sensors monitor an increase in mass of a sensing unit upon adsorption of volatile compounds. Surface Acoustic Wave Sensors (SAWS) are a typical example of such sensors. In a SAW device, an electrical signal is transduced into a mechanical wave on a piezoelectric substrate which is coated with an adsorbing film. A subsequent modulation of the amplitude, phase or frequency of the acoustic wave due to vapor adsorption is converted back to electrical signal and analysed with a read-out unit. SAW devices run at very high frequencies

as high as 100MHz. Currently, SAW sensors are fabricated with (micro electro mechanical systems) MEMs technologies. Surface acoustic wave (SAW) sensors coated with polymers have been demonstrated for vapor discrimination [35]. However, an electromagnetic interference between neighboring sensors is one of the main challenges with SAW sensors for simultaneous gas detection[36].

1.3.2 Fiber Optic and spectroscopic gas sensing technologies

In the past couple of decades, a number of optical sensing technologies have been developed. Widely used optical sensing technologies can be classified into three main categories namely free-space spectroscopic, fiber optic and integrated waveguide sensors.

Optical fiber sensors

Optical fibers are one of the optical technologies with long established use in sensing applications. The interest in optical fiber sensors is mainly driven by the widely mentioned benefits such as robustness to operate in harsh environment, immunity to electromagnetic interference, remote sensing and multiplexing. From these perspectives, fiber optic sensors have been used for a remote detection of explosive gases and distributed gas detection.

Different types of configurations have been used for gas sensing with optical fibers. In general, most of these implementations can be categorized as absorption and refractive index sensors. Absorption spectroscopic sensors based on speciality fibers such as air-guiding and hollow core photonic band gap(FBF) fibers have been demonstrated[37]. In these structures, spectral absorption features of some gases are monitored through a direct interaction between the gas and the light being guided through the fibers. An air-guided PBF plays the role of a compact and inline gas cell as compared to conventional free space setups. Small sample volume and direct interaction over long distance are the benefits gained with such configurations. While hollow core structures can significantly reduce the sample volume, they are typically limited by poor gas diffusion into these structures[38]. With respect to the conventional gas cell based spectroscopic techniques, sensitivity to temperature and fringe related noise are other limiting factors in fiber optic absorption sensors.

Another class of fiber optic sensors detects gas induced complex refractive index variations at the fiber surface. Typically, a gas sensitive transducer film is deposited on an exposed area of the fiber core. A change in the optical and structural characteristic of the chemical film due to the presence of a gas leads to a change in the effective index of the optical fiber through evanescent wave interaction. Evanescent wave gas sensors based on fiber Bragg gratings, nanotapers, and uncladded regions have been demonstrated[39-42]. Refractive index,

or intensity variations are monitored in these sensors. Hydrogen concentrations as low as 1% are detected using coated fiber Bragg gratings[41]. Volatile organic compounds have also been detected with intensity measurements on optical fibers that are functionalized with color changing films[42].

However, fiber optic sensors remain less suited for an integrated implementation, thus, lacking a key feature attractive for highly portable and low cost applications. Another challenge with fiber optic evanescent wave sensors is that inconvenient fabrication processes are needed to remove the claddings before depositing chemically sensitive films. The relatively broad reflection peaks in fiber bragg gratings (typically > 0.5nm) can also have impact on the detection limit[65].

Free-space spectroscopic gas sensors

Absorption spectroscopy is a powerful and versatile chemical analysis tool for the identification and quantification of gaseous constituents in the atmosphere [43]. Gas spectroscopy is one of the mature optical techniques that have been successfully used in a wide range of applications. This technique gains its popularity owing to its capability to detect unique gas absorption fingerprints where by allowing highly selective gas detection.

Trace gas concentrations ranging from ppm - ppt levels have been detected using various forms of optical spectroscopic techniques[43]. Such low detection limits have been achievable employing a variety of noise suppression techniques as well by increasing the interaction length. Dual beam spectroscopy, wavelength modulation spectroscopy and cavity enhanced spectroscopy are some of the technique demonstrated to be powerful in further pushing down the trace gas detection limits[44]. Enhanced gas detection in recent years has also been augmented by developments in the light sources such as NIR tunable lasers and Quantum cascade lasers in the Mid Infrared regions[44,45]. A number of gaseous species that are of importance in environmental, industrial and environmental applications have been detected using these techniques[43].

However, most practical spectroscopic sensors are implemented on free-space bulk configurations. As a result, these devices are typically characterized by large physical size. Moreover, complex source and read-out instruments are usually employed, especially, when very low gas concentrations are required to be detected. Because of these issues, spectroscopic sensors have been mainly used for laboratory applications. Consequently, sensor portability and high instrumentation cost are the current limitations in spectroscopic sensors for various applications.

Another form of spectrophotometric technique attractive for molecular detection is Raman spectroscopy[66]. This technique is based on the so called the Raman process in which an incident photon may gain energy from or do-

nate energy to a vibrational or rotational energy level of a molecule. As a result, the incident light is scattered at wavelengths red(Stokes) or blue(Anti-Stokes) shifted from the excitation wavelength. This shift provides a unique information about the target molecules. This method has the capability to explore molecular energy levels in the mid and far-infrared while using visible light for the excitation and detection. Moreover, some gases having insignificant IR absorption bands can be measured with the Raman technique. Because of this reason, this technique is often considered to be complementary to the IR spectroscopy. However, typically, Raman signals are extremely weak even for dense samples such as solids and liquids. Consequently, the application of this technique becomes more challenging for molecules in gas phase. Recently, the enhancement of the Raman signal with novel approaches such as Surface Enhanced Raman Scattering (SERS) are being explored[67]. Such approaches, if implemented on planar optical platforms, can be attractive future candidates for portable multi-gas analysis.

1.3.3 Integrated optical gas sensors

With recent advancements in the wafer-scale microfabrication, it has become possible to incorporate hundreds of integrated waveguide structures into a single sensor chip[46]. Significant progress has also been made on the integration of light sources and detectors onto chip-based analytical platforms[46]. Such intrinsically scalable platforms offer a high level of sensor multiplexing within small sample volumes. Particularly, an increasing interest in integrated biosensors has been noticed in the past few years owing to the label-free detection capabilities. More recently, the research on chip-scale bio-chemical sensors is being extended to gaseous analytes as well. Highly compact and inexpensively fabricated gas sensors can overtake the role of current sensing technologies in the medical, industrial and environmental applications where weight, cost, portability and power consumption are relevant.

However, in general, the research in the field of integrated optical gas sensing has been very limited until recently. A few compact optical gas detection schemes have been proposed and demonstrated on different platforms. Guided wave plasmonic and evanescent wave optical sensors can be considered as the two main category of such sensors.

Plasmonic gas sensors

Plasmonic gas sensors employ optically excitable surface charge density oscillations at the interface between two media with dielectric constants of opposite sign, typically a metal and a dielectric. This surface wave oscillation is termed as surface plasmon resonance. The charge density wave is associated with an

electromagnetic wave whose field vectors reach maximum at the interface and evanescently decay into both media. This surface waves are excited at specific angles or wavelengths of the input light. Refractive index changes near the surface of the plasmonic waveguide structures is detected through a shift in the SPR wavelength or angle. The detection of some polluting and biological gases such as NO_2 and NH_3 using SPR has been demonstrated[47,48]. In an SPR based NH_3 sensor, refractive index variations of a sensitive polymer film on the top metal surface is monitored and a detection limit of 32ppm was demonstrated[47]. In another demonstration, by incorporating NO_2 sensitive functional groups in a porous silica matrix and coating it on the top gold layer of an SPR sensor, a detection limit down to 10's of ppb has been demonstrated[48]. Despite the fact that SPR sensors can be highly sensitive, their waveguide based implementations are often accompanied by bulky or moving components [49]. In majority of SPR sensor layouts such as the Kretschmann configuration, bulky prism coupling is used. This makes it difficult to realize SPR sensors on purely planar platforms as integrated sensors. On the other hand, phase-matching issues between the dielectric waveguide and SPR modes impose challenges for an implementation on high index contrast platforms such as SOI[64].

Integrated evanescent wave gas sensors

Another family of waveguide based sensors which have become increasingly popular in biomolecule detection applications are evanescent field sensors[46,50]. More recently, progress in these sensors for the detection of gaseous molecules has been made[14,51]. Various planar waveguide configurations have been employed for evanescent wave sensing. Interferometric techniques, resonant structures and grating based schemes are among the extensively used evanescent wave sensing techniques on planar waveguides. Basically, evanescent wave sensors rely on the interaction of an analytes with a portion of waveguide mode field extending outside the waveguide boundaries. Despite a small fraction of the field reaching out the surface, significantly high sensitivities to the surface perturbations are proven to be achievable with these sensors [15]. While evanescent waveguide sensors are typically small in size, more compact and highly sensitive configurations have been demonstrated recently[12].

Evanescent wave sensors employing planar Mach-Zehnder interferometers(MZI), microring resonators(MRRs), and photonic crystals often used in biochemical applications lend themselves for straightforward use in gas sensing. Depending on a chosen configuration, an intensity or a wavelength based interrogations can be employed[52].

Machzehnder interferometer(MZI) on different waveguide platforms is one of the well known configurations used for bulk and surface refractive index sensing. An MZI based non-selective gas detection has been demonstrated on Si_3N_4

waveguide. Zaricona and TiO_2 films were deposited on the sensing arm of the Si_3N_4 rib waveguide for sensitive detection of CO_2 gas[53]. However, this sensor was only limited to qualitative demonstration of the refractive index sensitivity and the detection limit was not indicated. While MZI waveguide sensors can be used with less complicated read out techniques, they require relatively large arm lengths hence covering larger footprints. Moreover, the MZI sensing scheme is less suited to multiplexed detection as compared to, for instance, MRRs.

Photonic crystal waveguide (PhC) structures are another class of sensing technologies which have recently gained a growing interest for biochemical and gas detection[54]. Different PhC waveguide topologies have been used for spectroscopic and refractive index sensing of gaseous compounds. High refractive index sensitivity of an air slot photonic crystal cavity has been demonstrated on SOI substrate[55]. In this sensor, a defect cavity is formed by a slot waveguide sandwiched between two other slightly narrow slot waveguide sections. A quality factor of about 26,000 is achieved and refractive index sensitivity of 520nm/RIU along with a detection limit below 1 x 10^{-5} RIU is demonstrated. However, in this demonstration, the cavity resonance shifts were measured upon exposure to gases of known refractive indices and the gas selectivity aspects were not addressed. Another important feature of PhC cavities can be the ultra small volume in the order of $0.04\mu m^3$. This can allow operations with very small sample volume as well as lead to lower detection limits.

Absorption spectroscopy of CH_4 gas on SOI photonic crystal slot waveguide has also been demonstrated[56]. This approach takes advantage of a slow light induced interaction enhancement in a narrow slot waveguide region. The authors claimed an experimental detection of 100ppm CH_4 on just $300\mu m$ long PhC slot waveguide. Moreover, theoretical estimates indicate that, over two orders interaction enhancement can be attained with slow light guiding in these waveguides. However, in this particular demonstration, experimentally claimed over 3 orders absorption enhancement appears to be less justifiable with the theoretical estimates. Hence, further studies may be required to better understand the key mechanisms behind this sensing approach. One of the limitations in PhC structures is that slow light guiding is restricted within narrow bands. This imposes high fabrication precision as well as thermally stable operation to maintain a sufficient overlap between the slow light regime and a target gas absorption band. In addition, a parallel detection of absorption peaks of one or more gases in a broadband range becomes less practical.

Despite the fact that photonic crystal waveguide structures bear a huge potential for integrated, highly compact and sensitive gas sensing applications, the progress in this discipline has been largely restrained by the current fabrication challenges. To minimize fabrication imperfections, thus far demonstrated

PhC gas sensors were fabricated using small scale electron beam lithographic techniques[54-56]. In general, progresses in the fabrication of PhCs with the standard mass fabrication technologies are yet to be made for feasible implementation of PhC based sensors.

Another attractive planar waveguide structures under extensive research recently are microring resonators (MRRs)[13,50]. Microrings are compact resonant circuits characterized by circulating waveguide modes confined in the vicinity of the waveguide surface. Due to the fact that the light undergoes a repeated circulations in the waveguide while evanescently interacting with the surface, longer interaction lengths are achievable on very small footprints. As a result, high quality factor microring resonators have become attractive for ultra-compact integrated sensing applications. Typically, refractive index sensitivities below 1 x 10^{-5} refractive index units(RIU) are feasible with currently realizable high Q microring resonators[12]. Increasingly growing interest in microrings for biochemical detection in the liquid phase has been recently noticed. However, as it is the case with other integrated waveguide architectures, more progress is still awaiting on the application of microrings for gas sensing.

An ammonia sensor using a polymer coating on SOI microring resonator has been demonstrated [51]. The polymer film of Polymethylmethacrylate (PMMA) was doped with a sensitive dye, Bromocresol Purple (BCP), for NH_3 sensing. A detection limit of 4% NH_3 was achieved with this sensing scheme. In another work, a high refractive index sensitivity of a slot waveguide MRR is demonstrated by measuring resonance shifts induced due to a gas environment in the vicinity of a bare SOI microring resonator[16]. A refractive index change on switching between N_2 and acetylene gas is detected indicating a detection capability as low as 1 x 10^{-4} RIU. A refractive index sensitivity of 490nm/RIU is estimated for this sensor. The main feature of the slot ring architecture is that a large evanescent field is available in air slot region for an enhanced interaction with the gas environment. However, due to high sensitivity to fabrication imperfections, slot structures are currently limited by high propagation losses and hence low Q values[16]. Consequently, the net gain in the sensitivity enhancement may not be as high unless with better fabrication precisions.

Inherent multiplexing feature is another interesting capability of MRR based waveguide sensors. This allows the detection of multiple analytes of small sample volumes on a single chip. Such muliti-analyte handling potential is highly attractive in gas sensing applications such as medical diagnostics and odor-monitoring.

Integrated optical sensing platforms

Waveguide based sensing architectures discussed so far, MZIs, PhCs, and MRRs have been implemented on various material platforms. The most widely used

material systems include polymers, silica on silicon, silicon nitride, and silicon on insulator substrates. Each of these platforms is characterized by its own attractive features as well as limitations. In what follows, implementations of the above mentioned sensor architectures on different material systems are briefly reviewed.

Owing to the versatile nature of the MZI and MRR sensor designs, they have been implemented on a range of material systems including silicon oxide, polymers, silicon nitride and SOI[57-59]. For PhC sensors, however, the SOI substrate appears to be a material system of choice[54-56].

MZI sensors on silicon oxide waveguides have been demonstrated. For instance, laser inscribed MZI on a fused silica substrate has been fabricated for a sensing application[58]. A detection limit of 1 x 10^{-4} RIU is estimated with this MZI sensor having a device size of nearly 20mm length. Moreover, a MRR on a glass substrate has been fabricated and demonstrated for biomolecule sensing [57]. In this demonstration, the MRR has a radius of 60μm, and ~12000 Q value. A detection limit of 1 x 10^{-5} is achieved with this sensor. A relatively large device footprint is one of the limitations of the silica based waveguide architectures.

MZI and ring resonator sensing configurations have also been demonstrated on polymer waveguide platforms. An MZI for biochemical detection was employed using SU-8 resist as a core/cladding material [59]. A porous polymer ring resonator of 60μm radius and nearly 2μm wide waveguide has been demonstrated for refractive index sensing[60]. Recent interests in polymer materials for optical applications have been driven by a low cost and simple fabrication as well as a high coupling efficiency to optical fibers. However, a relatively low refractive index(around 1.5) of these materials would also imply that larger waveguide dimensions and bending radii are necessary for efficient wave guiding. Another driving force behind the polymer based optical sensors is inspired by printed circuit processing on flexible substrates for applications such as wearable sensors[61]. However, these moves are currently at an early stage and a number of design and fabrication challenges stand ahead. In general, printed optical devices /sensors can be suitable for low-end applications requiring a minimum of performance and limited life time compared to the standard silicon technology. Some of the challenges in the printed sensors include limited line width, limited printable materials, stability over time, and reliability.

Finally, the high index contrast SOI material system is another attractive platform on which integrated sensors have been implemented[12-16]. In contrast to low index structures such as polymer and silica waveguides, SOI structures are capable of confining light in sub-micron scale. Moreover, the waveguides can be bent to very small radii (down to 3μm), hence, making the fabrication of ultracompact sensors possible. MZI based bio-sensors have been demonstrated on SOI substrate with comparable sensitivties as other competitive

technologies such SPR sensors[15]. parallel detection of analytes has also been demonstrated with MZI biosensors. A two orders higher sensitivity in contrast to similar device implementations on silica waveguides has been reported for an SOI MZI sensor of 1.5mm long sensing arm[62]. This also corresponds to 2-5 times higher sensitivity with respect to Si_3N_4 waveguides. Higher refractive index sensitivities achievable on SOI waveguides are attributable to strong electric field localized near the waveguide surface due to the high index contrast[15]. The fabrication of photonic crystals (PhCs) on the high index SOI material system offers additional opportunities for functional devices due to its rich dispersive properties and ability to strongly confine light. Biomolecule and gas sensors have been successfully demonstrated using SOI PhC waveguides and cavities[54-56].

On the other hand, microring resonators on SOI platform have gained an increasing interest for sensing applications. In contrast to sensor architectures implemented on low index contrast systems such as polymers and glass substrates, SOI microrings offer multi-fold advantages. These benefits cover aspects such as size, high sensitivity, multiplexing and potentially low cost and large scale fabrication with the standard microelectronic fabrication facilities. Moreover, the high robustness and stability of this material system offers a versatile platform for diverse applications as compared, for instance, to polymer waveguides. Owing to the high promise for a highly scalable and commercially viable microfabrication, an increasing progress in the fabrication and functionalization of MRRs on a single chip has been made[12-15]. Sensitivities down to 1 x 10^{-7} RIU and upto 32 SOI MRRs multiplexed on a single chip have been demonstrated[15]. However, despite these proven capabilities, SOI MRR sensors, apart from biochemical sensing, have barely been exploited for other highly relevant applications such as gas detection. Leveraging on the technologies already being developed for the bio-sensing applications, gas sensors on SOI platform can make a quick transformation into the sensing market. Highly portable, low power, and inexpensive gas sensors, in general, can have an immense impact in the health and environmental sector.

1.4 Overview of this work

This doctoral research is mainly inspired by a growing interest for better gas sensing solutions as well as by the technological opportunities offered by the silicon photonics platform. As discussed earlier in the introduction, there is a high demand for multi-featured and efficient gas detection tools in a range of bio-medical, industrial and environmental applications. Complementary to this demand, silicon photonics potentially offers a range of capabilities conducive for efficient and economically appealing sensing devices.

This work builds upon prior research and PhD work on silicon photonic bio-molecule detection at the Photonics Research Group, led by professor Peter Bienstman and extends them to gas sensing[13]. Particularly, previous studies on silicon microring resonators for sensing applications have been of a significant inspiration to this work. The silicon photonic structures employed in this thesis such as microring resonators and arrayed waveguide gratings have been designed by the author based on the IPKISS/PICAZZO mask design building blocks originally developed by professor Wim Boagerts of the photonics research group[68]. The fabrication of the optical chips has been done at the standard CMOS fabrication facility of imec, Leuven. Chemical aspects required for interfacing the silicon photonic sensing structures with gaseous environments have been mainly based on the expertise gained from the Physics and Chemistry of Nanostructures group of professor Zeger Hens at Ghent University. Gas sensitive metal oxide films, more specifically, zinc oxide nanoporous films used in this work have been developed using colloidal nanoparticle synthesis techniques at professor Hens' laboratory. The author of this thesis has been involved in adapting these previously established synthesis procedures in the group [69] for the application on the silicon photonic sensing chips. Colloidial ZnO suspension used for ethanol detection in this work has been prepared by the author following these procedures. Moreover, the functionalization of the silicon photonic chips with the ZnO nanoparticle films and the characterization of the gas sensor prototypes have been carried out by the author. Extending this multidisciplinary expertise, collaborations on the development of specialized gas sensitive materials have been made with the group of professor Johan Martens at the Center for Surface Science and Catalysis of the Katholieke Universiteit Leuven. Nanoporous silicate films of selective ammonia detection capabilities have been developed through this collaboration. Nanoporous silicate materials of different pore dimensions (microporous-mesoporous) with and without aluminum functionalization have been prepared by Dr. Sreeprasanth Pulinthanathu Sree of the Surface Science and Catalysis group. These materials have been functionalized on silicon chips containing microring resonators which were post-CMOS-fabrication processed by the author. The gas sensing properties of these sensor prototypes were experimentally investigated by the author. A collaboration with professor Christophe Detavernier's Coating and Contacting of Nanostructures group at Ghent University on atomic layer deposition(ALD) of functional materials has also been of a significant contribution to this research. Atomic layer deposition was used as an alternative technique for aluminium functionalization of mesoporous films prepared at professor Martens' group for selective ammonia detection. Elisabeth Levrau, a doctoral student at professor Detavernier's group was directly involved in the ALD of these films.

The scope of this research extends from fundamental studies on possible silicon photonic gas detection routes to experimental demonstrations of sensor prototypes of practically relevant specifications. These specifications mainly focus on common performance measures such as sensitivity, gas-specificity, response time and sensor regeneration. Other features such as sensor size and cost are considered as the potential benefits inherently offered by the silicon photonics technology. 100's of ppb - 10's of ppm gas concentrations are targeted for the detection with these sensors. Compact and portable sensors operating in this detection range exhibit a significant potential for a number of bio-medical and industrial applications such as medical breath analysis and industrial process control. Gas selective and rapid sensor response are other critical performance targets addressed in this research. Combining the multidisciplinary expertise involved in this work, silicon photonic gas sensor prototypes of different performance features have been demonstrated and insights on the potential near future applications are provided. Due to the multidisciplinary nature of this work, the author has been responsible for identifying feasible interdisciplinary routes in order to meet specified gas detection targets. In this regard, he has been involved in initiating collaborations, for instance, on the development of different gas sensitive materials. The overall technical aspects involved in this research include the design of silicon photonic sensing chips, the preparation of gas sensitive materials and their functionalization on silicon chips, and the characterization of the sensor prototypes. Two in-house experimental setups have been built by the author by integrating existing optical facilities with new components and configurations suitable for the characterization of the gas sensors.

Fundamental aspects of optical gas detection, more particularly, silicon photonic gas sensing are discussed in chapter 2 and 3. Chapter 4 describes the gas sensor characterization setups used in this work. Experimental studies on porous metal oxide and polymer film functionalized silicon photonic chips for gas detection are discussed in chapter 5. Chapter 6 discusses an experimental demonstration of selective ammonia gas detection with nanoporous aluminosilicate films on silicon photonic sensors. In chapter 7, an experimental study of an on-chip Arrayed Waveguide Grating based sensor interrogation approach as a low cost and compact alternative to the currently used wavelength shift interrogation techniques is presented. Concluding remarks are provided in chapter 8. Finally, preliminary experimental studies on silicon waveguide based gas absorption spectroscopy are presented and future insights on this sensing approach are provided.

In this study, the refractive index sensing and absorption spectroscopic techniques are primarily identified as attractive for an implementation on the silicon photonic chips. Both approaches can potentially play a complementary

role for more universal and broad-range on-chip gas detection. While each technique draws a significant scientific and technological interest on its own right, gas detection with the refractive index based approach has been dealt in a more detail in this research. With the current technological capabilities, the refractive index sensing route lends itself more readily for on-chip implementation because of a less stringent requirement on the system noise level and device size. Moreover, provided the considerable scientific and technological depth of each of these techniques, focus on a specific route becomes a preferred approach. Preliminary studies have also been conducted providing valuable future insights on spectroscopic gas sensing with silicon photonic chips.

Microring resonators are primarily used in this thesis as a basic optical building block for the gas sensor prototypes. High refractive index sensitivity, sensor multiplexing and ultra-compactness are some of the attractive features of MRRs. The refractive index sensing technique typically involves chemical transduction mechanisms for selective and sensitive gas detection. Accordingly, multidisciplinary efforts from both optical and chemical perspectives have been involved in this research. Nanoporous materials, in particular, have been of a central research interest in this work. Exploiting a considerably high surface area offered by these materials, enhanced gas sensitivities have been demonstrated. The nanoporous surface further lends itself for the incorporation of functional groups for selective gas detection. Efficient diffusion of gas molecules facilitated with the porous structures is another valuable feature offered by these materials for rapid sensor response. In this respect, MRRs functionalized with nanoprous ZnO, silica and polymer films have been studied for efficient gas detection. The potential and limitations of these sensor prototypes have been evaluated with respect to valuable performance measures for practical applications.

High sensitivities for volatile organic compounds, namely ethanol and xylene, as well as for gaseous CO have been experimentally demonstrated from nanocrystalline ZnO functionalized MRRs. Sensitivities down to sub ppm gas concentrations are achieved. Typical response times for these sensors are in the range of 20-40 seconds. On the other hand, this study has provided an insight that metal oxide films, such as ZnO, as demonstrated here can be strongly responsive to a range of gaseous compounds, hence, being less suited for selective gas detection. Partial sensor recovery is another point typically observed for ZnO films. Consequently, such devices can be more suited for disposable sensing applications.

On the other hand, Polymer materials, such as PDMS, are characterized by high affinity towards industrially and environmentally relevant organic vapors. In relation to this, PDMS coated MRRs prepared by the author have demon-

strated attractive performance features for potential VOC sensing. Based on an experimental data obtained for ~ 150nm thick PDMS coating, a detection limit of ~ 500ppm is estimated for xylene vapor. Moreover, a remarkable reversibility and fast response is measured from this sensor. The response and recovery times are approximately 20 and 40 seconds, respectively. This result demonstrates the potential role of polymer functionalized silicon MRRs as re-usable, low cost and real time VOC detection tools. Such sensors can be used to detect a given class of VOCs for early warning, for instance, in industrial workplaces.

More interestingly, it is demonstrated that specifically tailored materials can lead to selective gas detection on silicon photonic chips. Alumino-silicate films obtained through a synthesis based technique as well as an atomic layer deposition(ALD) technique are incorporated on silicon MRRs. Owing to the Al atoms introduced into the silica framework, these films exhibit acidic surfaces suitable for preferential adsorption of gaseous bases such as NH_3. Sensitive, reversible and fast response to NH_3 and high selectivity with respect to CO_2 is achieved with these sensors. An equilibrium response is attained in less than 30 seconds and over 95% recovery is reached within 90 seconds. A detection limit of 5ppm is estimated for microporous acidic films obtained via direct synthesis. A further improvement of the sensitivity could be achieved by optimizing the porosity and the surface properties of the porous aluminosilicate films. This work in general demonstrates the high potential of on-chip optical gas sensors for ultra portable, low cost and real time gas detection in a wide range of applications including medical breath analysis. With ongoing developments on gas selective films and efficient sensor spotting techniques, several multiplexed sensor arrays can be implemented for multi-gas detection on silicon photonic chips. These sensors can have a significant contribution for applications involving complex gas analysis such as odor monitoring and cancer detection.

On the other hand, wavelength interrogated SOI MRR sensors offer superior sensitivities to the surrounding, allow multiplexing of sensor arrays, and provide immunity to noise with respect to the intensity interrogation schemes. These devices have increasingly become appealing for trace gas and biomolecule detection. However, current wavelength interrogation based sensing systems are typically characterized by bulky and costly instrumentation. An external tunable laser source or the combination of a broadband source and a high - resolution spectrometer are usually employed. As a result, the size and cost benefits of on chip sensors are overshadowed by these external accessories. Despite a few efforts made so far, a continuing progress on novel solutions is highly required to realize cost effective and portable ring resonator sensors.

In this regard, a potentially low cost and compact MRR sensor interrogation approach based on an on-chip AWG spectrometer is experimentally demonstrated in this work. This spectrometer employed with cheap broadband light

sources, such as superluminescent LEDs, can significantly cut down the size and cost of the current microring resonator based sensors. An SOI MRR ethanol vapor sensor is interrogated by a 200GHz AWG designed to have a strongly overlapping output channels. It is demonstrated that resonance shifts ranging from 50pm- 800pm can readily be interrogated by measuring the ratio between two overlapping adjacent AWG channels.

Besides the extensive study on the refractive index sensing technique, preliminary studies on waveguide absorption spectroscopy have also been conducted in this research. It has been noted that the limited interaction length and the overall system noise on silicon photonic chips are the major issues to be addressed for spectroscopic gas detection. Practical optical spectroscopy is often characterized by noise contributed by various system components. An attractive approach to attain less stringent requirement on the system noise level can be a technique to enhance the density of gas molecules near the evanescent field region. A gas pre-concentrating layer on the waveguide surfaces can be considered for this purpose. Preliminary experimental observations with respect to noise and gas density enhancement on silicon photonic chips are presented under the future prospects chapter. Based on these observations, some insights are provided for future improvements and feasible implementation of on-chip gas spectroscopy.

Publications in international journals

1. N.A Yebo, S. P. Sree, E. Levrau, C. Detavernier, Z. Hens, J. A. martens and R. Baets. *Selective and reversible ammonia gas detection with nanoporous film functionalized silicon photonic micro-ring resonator.* Optics Express, 20(11): p.11855-11862 (2012).

2. N.A Yebo, W. Bogaerts, Z. Hens and R. Baets. *On-Chip Arrayed Waveguide Grating Interrogated Silicon-on-Insulator Microring Resonator Based Gas Sensor.* Photonics Technology Letters, 23(15), p.1505-1507 (2011).

3. N.A Yebo, P. Lommens, Z. Hens and R. Baets. *An integrated optic ethanol vapor sensor based on a silicon-on-insulator microring resonator coated with a porous ZnO film.* Optics Express, 18(11), p.11859-11866 (2010).

Publications in international conferences

4. N.A Yebo, Z. Hens and R. Baets. *Silicon microring resonators surface functionalized with organic and inorganic films for volatile organic compound (VOC) detection.* In proceedings of XI Conference on Optical Chemical Sensors and biosensors (EUROPTRODE XI), Spain, p.162 (2012).

5. N.A Yebo, W. Bogaerts, Z. Hens and R. Baets. *On-chip interrogation of a silicon-on-insulator microring resonator based ethanol vapor sensor with an arrayed waveguide grating(AWG) spectrometer.* In proceedings of the SPIE, 8264, pp. 82640P-82640P-6 (2012).

6. N.A Yebo, D. Taillaert, J. Roels, D. Lahem, M. Debliquy, Z. Hens and R. Baets. *Integrated optical gas sensors on silicon-on-insulator platform.* Integrated Photonics Research, Silicon and Nano Photonics (IPR), Photonics in Switching (PS), United States, p.JTuB.17.pdf (3 pages) (2010)

7. D. Vermeulen, K. Van Acoleyen, S. Ghosh, S. Selvaraja, W.A.D. De Cort, N.A Yebo, E. Hallynck, K. De Vos, P.P.P. Debackere, P. Dumon, W. Bogaerts, G. Roelkens, D. Van Thourhout and R. Baets *Efficient Tapering to the Fundamental Quasi-TM Mode in Asymmetrical Waveguides.* ECIO, United Kingdom, p.paper WeP16 (2 pages) (2010).

8. N.A Yebo, D. Taillaert, J. Roels, M. Debliquy, D. Lahem, P. Lommens, Z. Hens, D. Van Thourhout and R. Baets *Efficient Tapering to the Fundamental Quasi-TM Mode in Asymmetrical Waveguides.* Proceedings of the 2009 Annual Symposium of the IEEE Photonics Benelux Chapter, Belgium, p.153-156 (2009).

9. A. Casas Bedoya, M.Y. Ling, J. Brouckaert, N.A Yebo, D. Van Thourhout and R. Baets, *Biodiesel sensing using Silicon-on-Insulator technologies.* SPIE europe, Microtechnologies for the new millenium, Germany, (2009).

Publications in national conferences

10. N.A Yebo, Zege Hens and R. Baets. *An integrated optical gas sensors on silicon-on-insulator platform.* 11th FirW Doctoraatssymposium, Belgium, p.41 (2010).

References

[**1**] R. Soref and J. Larenzo . *All-silicon active and passive guided-wave components for λ = 1.3 and 1.6 μ m* . IEEE Journal of Quantum Electronics,22 ,22:873-879, 1986.

[**2**] B. Jalali and S. Fathpour *Silicon Photonics*. IEEE Journal of Lightwave Technology, 24: 4600-4615,2006.

[**3**] T. Baehr-Jones, T. Pinguet, S. Danziger, D. Prather and M. Hochberg. *Myths and rumours of silicon photonics*. Nature Photonics 6:206?208,2012.

[**4**] R. Soref. *The Impact of Silicon Photonics*. IEICE Transactions on Electronics, E91.C: 129-130, 2010.

[**5**] T. Baehr-Jones, R. Ding, A. Ayazi, T. Pinguet, M. Streshinsky, N. Harris, J. Li, L. He, M. Gould, Y. Zhang, A. E. -J. Lim, T.-Y. Liow, S. H.-G. Teo, G.-Q. Lo and M. Hochberg. *A 25 Gb/s Silicon Photonics Platform*. arXiv:1203.0767v1 [physics.optics], 2012

[**6**] M. Asghari, and A. V. Krishnamoorthy. *Silicon photonics: Energy-efficient communication*. Nature Photonics ,5: 268-270 ,2011.

[**7**] X. Zheng, F.Y. Liu, J. Lexau, D. Patil, G. Li ; Y. Luo , H.D. Thacker , I. Shubin, J. Yao , K. Raj, R. Ho , J.E. Cunningham, A.V. Krishnamoorthy . *Ultralow Power 80 Gb/s Arrayed CMOS Silicon Photonic Transceivers for WDM Optical Links* . IEEE Journal of Lightwave Technology,30:641 - 650 ,2012.

[**8**] web address: http://www.luxtera.com.

[**9**] web address: http://www.kotura.com.

[**10**] J. K. Doylend, M. J. R. Heck, J. T. Bovington, J. D. Peters, L. A. Coldren, and J. E. Bowers. *Two-dimensional free-space beam steering with an optical phased array on silicon-on-insulator*. Optics Express, 19,21595-21604 ,2011.

[**11**] J. Capmany and D. Novak. *Microwave photonics combines two worlds*. Optics Nature Photonics, 1: 319 - 330 ,2007.

[**12**] M. Iqbal, M.A. Gleeson, B. Spaugh, F. Tybor, W.G. Gunn, M. Hochberg, T. Baehr-Jones, R.C. Bailey and L.C. Gunn . *Label-Free Biosensor Arrays Based on Silicon Ring Resonators and High-Speed Optical Scanning Instrumentation*. IEEE Journal of Selected Topics in Quantum Electronics, 16:654-661,2010.

[**13**] K. De Vos, T. Claes, Y. D. Koninck, S. Popelka, E. Schacht, R. Baets, and P. Bienstman. *Multiplexed antibody detection with an array of silicon-oninsulator microring resonators.* IEEE Photonics Journal, 9: 225-235,2009.

[**14**] N. Yebo, D. Taillaert, J. Roels, D. Lahem, M. Debliquy, D. van Thourhout and R. Baets. *Silicon-on-Insulator (SOI) Ring Resonator Based Integrated Optical Hydrogen Sensor.* IEEE Photonics Technology Letters, 21:960-962, 2009.

[**15**] A. Densmore, D.-X. Xu, P. Waldron, S. Janz, P. Cheben, J. Lapointe, A. Delâge, B. Lamontagne, J. H. Schmid and E. Post. *A Silicon-on-Insulator Photonic Wire Based Evanescent Field Sensor.* IEEE Photonics Technology Letters,18(23): 2520-2522, 2006.

[**16**] J.T. Robinson, L. Chen and M. Lipson. *On-chip gas detection in silicon optical microcavities.*Optics Express 16: 14296-4301, 2008.

[**17**] web address :http://www.strategyr.com/

[**18**] P. Puligundla, J. Jung and S. Ko. *Carbon dioxide sensors for intelligent food packaging applications.*Food Control 25: 328-333, 2012.

[**19**] web address: http://www.bis.gov.uk/files/file27987.pdf

[**20**] P. Puligundla, J. Jung and S. Ko. *Exhaled nitric oxide and biomarkers in exhaled breath condensate indicate the presence, severity and control of childhood asthma.*Clinical & Experimental Allergy, 37(9):1303-11,2007.

[**21**] L. R. Narasimhan, W. Goodman and C. K. N. Patel. *Correlation of breath ammonia with blood urea nitrogen and creatinine during hemodialyis.* PNAS ,98: 4617-4621,2001.

[**22**] L. Wang, K. Kalyanasundaram, M. Stanacevic and P Gouma. *Nannosensor device for breath acetone detection.* Sensor letter, 8 :1-4, 2010

[**23**] web address: http://www.ginasthma.org/reports-global-burden-of-asthma.html

[**24**] web address: http://www.efanet.org/asthma/index.html

[**25**] web address: http://dev.ersnet.org/268-white-book.htm

[**26**] web address: http://reports.fmcag.com/reports/fmc/annual/2008/gb/english/401040/dialysis-market.html

[**27**] G. Neri . *Solid-State Gas Sensors for Clinical Diagnosis.* Biological and Medical Sensor Technologies, Krzysztof Iniewski , 201 - 226, CRC Press 2012.

[**28**] X. Wang, N. Miura and N. Yamazoe. *Study of WO3-based sensing material for NH3 and NO detection*.Sensors and Actuators B, 66:74-76,2000.

[**29**] F. Winquist, A. Spetz and I. Lundstrom. *Determination of ammonia in air and aqueous samples with a gas-sensitive semiconductor capacitor*.Analytica Chimica Acta, 164:127-138,1984.

[**30**] C. K. Ho, M . T. Itamura, M. Kelley and R. C . Hughes. *Review of chemical sensors for in-Situ monitoring of volatile contaminants*.Sandia Report, SAND2001-0643, 2001.

[**31**] W.H. Steinecker, S. Reidy, G.R. Lambertus, A.A. Astle, K. Najafi, E.T. Zellers, L.P. Bernal, P.D. Washabaugh and K.D. Wise . *A Micropump-Driven High-Speed MEMS Gas Chromatography System* . Solid-State Sensors, Actuators and Microsystems Conference, 1505 - 1508, 2007.

[**32**] G. Jiménez-Cadena , J. Riu and F. X. Rius . *Gas sensors based on nanostructured materials* .Sandia Report, Analyst, 132:1083-1099.2007.

[**33**] H. Bai and G. Shi. *Gas sensors based on conducting polymers* . Sensors:267-307, 2007.

[**34**] S. M. Seo, J. H. Cheon , S. H. Kim , T. J. Kang , J. W. Ko , I.-Y. Chung, Y. H. Kim and Y. J. Park . *Carbon Nanotube-Based CMOS Gas Sensor IC: Monolithic Integration of Pd Decorated Carbon Nanotube Network on a CMOS Chip and Its Hydrogen Sensing* .IEEE Transaction on Electron Devices, 58: 3604 - 3608, 2011.

[**35**] H.C. Haoa, K.T. Tangb,P.H. Kuc ,J.S. Chaod, C.H. Lib, C.M. Yangc and D.J. Yaoa . *Development of a portable electronic nose based on chemical surface acoustic wave array with multiplexed oscillator and readout electronics*. Sensors and Actuators B: Chemical, 146:545 - 553, 2010.

[**36**] K. Reddy, Y. Guo, J. Liu, W. Lee, M. K . K Oo and X. Fan. *GRapid, sensitive, and multiplexed on-chip optical sensors for micro-gas chromatography*. Lab chip, 12: 901-905, 2012

[**37**] T. Ritari, J. Tuominen, H. Ludvigsen, J. Petersen, T. Sørensen, T. Hansen, and H. Simonsen. *Gas sensing using air-guiding photonic bandgap fibers*. Optics Express, 12 :4080-4087, 2004.

[**38**] J. P . Parry, B. C. Griffiths, N. Gayraud, E. D. McNaghten, A.M .Parkes,W. N. MacPherson and D. P. Hand. *Towards practical gas sensing with micro-structured fibres*. Measurement Science and Technology, 20:075301(8pp), 2009.

[**39**] G. Brambilla . *Optical fiber nanotaper sensors.* Optical Fiber Technology 16:331-342, 2010.

[**40**] W. Ecke and R. Willsch. *Optical fiber Bragg grating hydrogen sensor based on evanescent-field interaction with palladium thin-film transducer* . Optics Lasers in Engineering 47: 1018-1022, 2009.

[**41**] D. Y. Wang, Y. Wang, J. Gong, and A. Wang. *Fully Distributed Fiber-Optic Hydrogen Sensing Using Acoustically Induced Long-Period Grating.* IEEE IEEE photonics technology letters 23:733-735, 2011.

[**42**] X. Tian ,S. Wu , Q. Zhang , G. Zou . *Colorimetric Sensor for Fine Differentiation of Organic Solvents Based on Only One Kind of Polydiacetylene Coated on Polymer Optical Fiber.* IEEE Sensors Journal, 12: 1946-1949, 2012.

[**43**] X. Cuia,C. Lengignona, W. Taoa, W. Zhaoa, G. Wysockid, E. Ferteina,C. Coeura, A. Casseza,L. Croizea,W. Chena, Y. Wangb, W. Zhangb, X. Gaob, W. Liub,Y. Zhangb and F. Dongb. *Photonic sensing of the atmosphere by absorption spectroscopy* . Journal of Quantitative Spectroscopy and Radiative Transfer, 113:1300-1316, 2012.

[**44**] J. Manne, O. Sukhorukov, W. Jäger and J. Tulip. *Pulsed quantum cascade laser-based cavity ring-down spectroscopy for ammonia detection in breath.*Applied Optics, 45:9230-9237, 2006.

[**45**] P. P. Vadillo. *Isotope selective analysis of CO2 with tunable diode laser (TDL) spectroscopy in the NIR.*Laser Diode Gas Spectroscopy, Semiconductor Laser Diode Technology and Applications, Dnyaneshwar Shaligram Patil (Ed.), ISBN: 978-953-51-0549-7, 2012.

[**46**] A. L. Washburn and R. C. Bailey. *Photonics-on-a-chip: recent advances in integrated waveguides as enabling detection elements for real-world, lab-on-a-chip biosensing applications* .Analyst, 136: 227-236, 2011.

[**47**] N. Menegazzo, B. Herbert, S. Banerji, K. S. Booksh. *Discourse on the utilization of polyaniline coatings for surface plasmon resonance sensing of ammonia vapor.*Talanta, 85 :1369-1375, 2011.

[**48**] A.Berrier, P. Offermans, R Cools, B. V. Megan, W. Knoben, G. Vecchi, J .G Rivas, M. C-Calama, S. H. Brongersma. *Enhancing the gas sensitivity of surface Plasmon resonance with a nanoporous silica matrix.*Sensors and Actuators B, 160:181-188, 2011.

[**49**] Raman Kashyap and Galina Nemova. *Surface Plasmon Resonance-Based Fiber and Planar Waveguide Sensors.* Sensors and Actuators B, Journal of Sensors ,Doi:10.1155/2009/645162.

[**50**] V. M. N. Passaro, F. Dell-Olio, B. Casamassima and F. De Leonardis. *Guided-Wave Optical biosensors.* Sensors, 7:508-536, 2007.

[**51**] V. M. N. Passaro , F. Dell-Olio and F. De Leonardis. *Ammonia optical sensing by microring resonators* .Sensors, 7: 2741-2749, 2007.

[**52**] X. Fan, I.M. White, S.I. Shopova, H. Zhu, J.D. Suter and Y. Sun. *Sensitive optical biosensors for unlabeled targets: A review (Review).*Analytica Chimica Acta, 620:8-26, 2008.

[**53**] D. Celo, E. Post, M. Summers, T. Smy, M. J. Brett and J. Albert. *Interferometric sensing platform with dielectric nanostructured thin films.*Optics Express, 17 :6655-6664, 2009.

[**54**] Y. Zhao, Y-N. Zhang, Q. Wang. *Research advances of photonic crystal gas and liquid sensors* .Sensors and Actuators B, 160:1288-1297, 2011

[**55**] J. Jágerská, H. Zhang, Z. Diao, N. L. Thomas and R. Houdré. *Refractive index sensing with an air-slot photonic crystal nanocavity.*Optics Letters, 35:2523-2525, 2010.

[**56**] W.-C. Lai, S. Chakravarty, X. Wang, C. Lin and Ray T. Chen. *On-chip methane sensing by near-IR absorption signatures in a photonic crystal slot waveguide.*Optics Letters, 36:984-986, 2011.

[**57**] A. Yalcin, K.C Popat, J.C. Aldridge, T.A. Desai, J. Hryniewicz, N. Chbouki, B.E. Little, O. King, V. Van, S. Chu, D. Gill, M. Anthes-Washburn, M.S. Unlu, B.B. Goldberg . *Optical sensing of biomolecules using microring resonators.*IEEE Journal of selected Topics in Quantum Electronics, 12:148-155, 2006.

[**58**] A. Crespi , Y. Gu, B. Ngamsom , H. J. Hoekstra, C. Dongre , M. Pollnau, R. Ramponi, HH. van den Vlekkert, P. Watts, G. Cerullo and R. Osellame . *Three-dimensional Mach-Zehnder interferometer in a microfluidic chip for spatially-resolved label-free detection.*Lab on a Chip, 10 :1167-1173, 2010.

[**59**] B.Y. Shew, Y.C. Cheng, Y.H. Tsai. *Monolithic SU-8 micro-interferometer for biochemical detections.*Sensors and Actuators A, 141: 299-306, 2008.

[**60**] M. Mancuso, J. M. Goddard vand D. Erickson . *Nanoporous polymer ring resonators for biosensing.*Optics Express, 20: 245-255, 2012.

[**61**] J. Courbata, D. Brianda, J. Wöllensteinb and N.F. de Rooija . *Polymeric foil optical waveguide with inkjet printed gas sensitive film for colorimetric sensing.*Sensors and Actuators B: Chemical, 160: 910-915, 2011.

[**62**] A. Densmore, M. Vachon, D.-X. Xu, S. Janz, R. Ma, Y.-H. Li, G. Lopinski, A. Delâge, J. Lapointe, C. C. Luebbert, Q. Y. Liu, P. Cheben and J. H. Schmid. *Silicon photonic wire biosensor array for multiplexed real-time and label-free molecular detection.*Optics Letters, 34:3598-3600, 2009.

[**63**] web address: http://metabolomx.com/

[**64**] P. Debackere, S.Scheerlinck, P. Bienstman and R. Baets. *Surface plasmon interferometer in silicon-on-insulator: novel concept for an integrated biosensor.*Optics Express, 14:7063-7072, 2006.

[**65**] W. Liang, Y. Huang,Y. Xu, R. K. Lee and A. Yariv. *Highly sensitive fiber Bragg grating refractive index sensors.*Applied Physics Letters,86: 151122, 2005.

[**66**] K. Kneipp,H. Kneipp, I. Itzkan, R. R. Dasari, and M. S. Feld. *Ultrasensitive Chemical Analysis by Raman Spectroscopy.*Chemical Review,99:2957-2975,1999.

[**67**] A. S. P. Chang, A. Maiti, N. Ileri, M. Bora, C. C. Larson, J. A. Britten, T. C. Bond. *Detection of volatile organic compounds by surface enhanced Raman scattering.*Advanced Environmental, Chemical, and Biological Sensing Technologies IX, in proceedings SPIE, 8366: 83660S-1, 2012.

[**68**] web address: http://photonics.intec.ugent.be/research/facilities/design/default.htm

[**69**] P. Lommens, K. Lambert, F. Loncke, D. D. Muynck, T. Balkan,F. Vanhaecke, H. Vrielinck, F. Callens, Z. Hens. *The Growth of Co:ZnO/ZnO Core/Shell Colloidal Quantum Dots: Changes in Nanocrystal Size, Concentration and Dopant Coordination.*A European Journal of Chemical Physics and Physical Chemistry, 9: 484?491, 2008.

2

Light-environment interaction: the sensor perspective

2.1 Introduction

Light - matter interaction is responsible for numerous physical phenomena in nature and has also been widely exploited for various technological applications. One of the areas where the interaction of light with its environment plays a substantial role is optical sensing. Direct or indirect interaction of light with an analyte of interest can lead to changes in the light propagation properties namely, its phase and amplitude. These variations are measured using different techniques for qualitative and quantitative analysis of the surrounding. In this chapter, basic interaction mechanisms which are specifically relevant to optical sensing applications are discussed. While, in general, light-matter interaction can be linear or nonlinear in nature, linear processes involved in most practical optical sensors are particularly viewed in this thesis.

2.2 Background theory: light propagation in dielectric medium

Light with an angular frequency of $\omega = 2\pi\nu$ passing through a physical medium can undergo a number of physical processes. Some of the light can be scattered , absorbed or propagated through the medium. In real situations, the light experiences a combination of these processes. Commonly, optical environmental sensing involves interactions with analytes whose optical properties can well be approximated by that of dielectric materials. Gaseous and liquid biochemicals and pollutants popular in the sensing world are among examples of these materials. Hence, well known electromagnetic principles associated with the interaction of light with dielectric media can serve as model for optical sensors.

Starting with Maxwell's equations listed in eq(2.1) and taking the free charge density to be zero for a dielectric medium, it can be shown that an optical wave in a dielectric media of permitivity ε satisfies the wave equation described by eq.(2.2)

$$\nabla \times \vec{E} = -\frac{\partial \vec{B}}{\partial t} \tag{2.1a}$$

$$\nabla \times \vec{B} = \mu\varepsilon \frac{\partial \vec{E}}{\partial t} \tag{2.1b}$$

$$\nabla \cdot \vec{D} = \rho \tag{2.1c}$$

$$\nabla \cdot \vec{B} = 0 \tag{2.1d}$$

where $\vec{D}$, $\vec{E}$, and $\vec{B}$ are the electric displacement, the electric field and the magnetic flux density respectively. ρ,μ,ε represent the electric charge density, the magnetic permeability and the dielectric permittivity of the medium respectively.

$$\nabla^2 \vec{E} - \mu\varepsilon \frac{\partial^2 \vec{E}}{\partial t^2} = 0 \tag{2.2}$$

Eq.(2.2) has a plane wave solution of the form

$$\vec{E}(\vec{r}, t) = \vec{E}_0 \exp[j(\vec{k} \cdot \vec{r} - \omega t)] \tag{2.3}$$

where $\vec{E}_0$,$\vec{k}$, $\vec{r}$ and ω are the initial electric field vector, the wave vector, spatial propagation direction and the angular frequency, respectively.

Following eq.(2.3), the phase velocity of light as it propagates through a dielectric medium is given by

$$\nu = \frac{\omega}{k} = \frac{c}{n} \tag{2.4}$$

where $n = \sqrt{\varepsilon}$ is called the refractive index of the medium.

This relation shows that, in a conventional dielectric medium, an electromagnetic wave propagates with a phase velocity which is slower than the velocity of light in vacuum. This is one of the key phenomena which lays the ground for optical environmental sensing.

On the other hand, in eq(2.3) it is implicitly assumed that the dielectric permittivity of the medium is real. However, in some dielectric materials ε is complex and the role of the imaginary component has to be taken into account. Hence, the wave vector $\vec{k}$ is more appropriately expressed as

$$\vec{k} = \frac{2\pi\tilde{n}}{\lambda} \tag{2.5}$$

where $\tilde{n} = n + j\kappa$ represents the complex refractive index of a medium. Consequently, eq.(2.3) can be re-written as

$$\vec{E}(\lambda) = \vec{E}_0(\lambda)\exp(-\frac{2\pi\kappa}{\lambda}z)\cdot\exp(j\frac{2\pi}{\lambda}(nz-ct)) \tag{2.6}$$

where, n and κ represent the real and imaginary components of the complex refractive index. z, λ and c are the propagation direction, the wavelength and the speed of light, respectively.

Thus, in addition to a phase change, an optical wave undergoes an attenuation or amplification as it propagates through a complex refractive index medium. Once again, this optical phenomena induced through an environmental interaction becomes a second key principle behind optical sensors. Moreover, in real situations, the complex refractive index is a wavelength dependent parameter as indicated in eq.(2.6). Hence, different frequencies of a wave experience different phase velocities while propagating through a medium. Likewise, there may exist some frequency bands which are strongly absorbed by the medium. In general, this phase or absorption wise interaction with a propagation medium plays a fundamental role in industrial, environmental, or biomedical sensing based on light. In the following sections, more detailed overviews into these two sensing mechanisms, namely refractive (phase) sensing, and optical absorption spectroscopy are presented.

2.3 Refractive index sensing

As discussed in the previous section, the real part of a complex refractive index medium determines the phase velocity of the light traveling through it. Hence, an optical phase change following a change in the refractive index of a medium can be exploited for sensing with the aid of different optical configurations. For a propagation length of L and a given refractive index change Δn, the corresponding phase change can be given by eq. (2.7)

$$\Delta\phi = \frac{2\pi}{\lambda}\Delta n_{eff}L \tag{2.7}$$

Interferometric or resonant optical sensing schemes are often used to interrogate/detect phase changes upon interaction with the surrounding medium[1-5]. Sensors in Fabry-Perot, Machzehnder or ring resonator configurations are some examples for refractrometric sensors. Either intensity variations or spectral shifts are employed as interrogation mechanisms in these sensors. Optical refractive index sensors can potentially be implemented using free space or guided wave schemes. However, for practical reasons such as size and sensitivity, these sensors are often implemented on guided wave platforms[1-5].

In gas detection application, which is the subject of this thesis, different techniques can be used to reach a required level of performance from refractive index sensors. Provided the low density of gas molecules in free space, additional transduction mechanisms and optical configurations are often employed to enhance the refractive index changes to detectable levels[6,7]. The detailed aspects of refractive index based sensing with respect to free space and planar techniques are presented in section 2.5

2.4 Optical absorption based sensing

Besides the phase interrogation technique, optical interaction with the imaginary component of the dielectric permittivity is another attractive sensing approach. This fundamental phenomenon is exploited in widely used spectroscopic gas sensors[8-10].This interaction basically represents absorption or scattering of light by the propagation medium.

2.4.1 Basic principles

In a complex refractive index medium , the basic principles governing linear absorption of light upon interaction is described by the Beer-Lambert Law. The incoming light frequency $\omega = 2\pi\nu$, and the frequency dependent complex refractive index of a medium $n(\omega)$, are the important parameters in the Beer-Lambert relation. For a light beam traveling along z direction of an absorbing medium of number density C and transverse area A, the total number of illuminated molecule for a material thickness dz is $CAdz$. Given an absorption cross section σ, the total probability of a molecule being either absorbed or scattered is given by[10,11]

$$\frac{dI_z}{I_z} = \frac{\sigma CAdz}{A} \tag{2.8}$$

which after integration gives the Beer-Lambert law for linear attenuation

$$I = I_0 \exp(-\sigma Cz) = I_0 \exp(-\mu z) \tag{2.9}$$

If scattering is neglected, the linear attenuation coefficient $\mu = \sigma C$ is equal to the linear absorption coefficient α and the Beer-Lambert relation can be rewritten in the form

$$I(\lambda) = I_0(\lambda)\exp(-\alpha(\lambda)z) \tag{2.10}$$

The absorption coefficient α is related to the imaginary component of a complex refractive index through the equation

$$\alpha(\lambda) = \frac{4\pi\kappa(\lambda)}{\lambda} \tag{2.11}$$

where $\kappa(\lambda)$ is the wavelength dependent imaginary component of the refractive index.

2.4.2 Light absorption in a gas medium

The absorption of light by gas molecules is an interesting subject in a number of scientific, industrial and environmental areas. Unique and often sharp spectral absorption signatures presented by gaseous molecules offer opportunities for unambiguous molecular identification through the technique called absorption spectroscopy. In this section, basic physical properties of gases leading to unique interaction with light and established principles of practical absorption spectroscopy are briefly discussed.

The absorption of light by a gas takes place when the energy carried by an incoming photon is resonant with the difference between two molecular energy states. In general, the electronic structure and different kinds of molecular motion determine the distribution of energy states in a gas. These transitions are commonly referred to as, rotational, vibrational and electronic. The distribution of these energy states depends on a particular symmetry of a target molecule[11]. Moreover,in some cases, molecular transitions can also interact with each other according to established selection or combination rules, giving rise to complex absorption spectra[11,12]. Electronic molecular signatures can be probed using (Ultraviolet -Visible)UV-VIS absorption spectroscopy[11,12]. Whereas, molecular absorption associated with vibrational or rotational transitions are commonly analyzed with infrared(IR) and Raman spectroscopic techniques[12]. For most industrially and environmentally interesting gases, the fundamental absorption bands are in the mid-infrared frequency range while overtones of these bands mostly exist in near infrared region as well. Fundamental or overtone absorption bands can be used for molecular sensing depending on the instrumentation convenience and the required level of detection[10].

Absorption line shape and broadening

Different physical processes affect the sharpness and shape of a gas absorption feature. In spectroscopic gas analysis, the Beer-Lambert law is commonly expressed in the form given in eq(2.12)

$$I(\bar{\nu}) = I_0 \exp(-\kappa(\bar{\nu})Cz) \tag{2.12}$$

where $\kappa(\bar{\nu})$ is the absorption coefficient at the frequency $\bar{\nu}$ which is given in inverse length units according to the relation

$$\bar{\nu}(cm^{-1}) \equiv \frac{1}{\lambda(cm)} = \frac{\nu(Hz)}{c(cms^{-1})} \tag{2.13}$$

where c is the speed of light.The absorption coefficient $\kappa(\bar{\nu})$ is given in cm^2/molecule.

since the shape of the absorption profile is interesting in gas absorption studies and applications, the absorption coefficient is rewritten to include the information about the line shape

$$\kappa(\nu) = Sg(\nu - \nu_0) \tag{2.14}$$

where the lines strength S is the integrated absorption coefficient given by

$$S = \int_{-\infty}^{+\infty} \kappa(\nu) \mathrm{d}\nu \tag{2.15}$$

while the lineshape function $\mathbf{g}(\nu - \nu_0)$ is normalized according to $\mathbf{g}(\nu - \nu_0) = C\phi(\nu - \nu_0)$, $\int_{-\infty}^{+\infty} g(\nu - \nu_0) = 1$. S is given in cm/molecule and the lineshape function $\mathbf{g}(\nu - \nu_0)$ is given in cm.

Though the ideal gas absorption lines can be of δ like function, in reality they are characterized by some finite linewidth due to a number of broadening processes. The convolution of the result of each of these broadening effects determines the final line shape function for a given absorption transition. The Full Width at Half Maximum(FWHM) of the absorption profile is usually used to express the line features[11]. Figure 2.1 illustrates a line shape profile. The two well known line broadening mechanisms are Doppler effect and molecular collisions[11]. The absorption profile associated with the Doppler broadening effect is commonly approximated by the Gaussian lineshape. The second broadening mechanism is associated with molecular collisions, and it is often represented with a Lorenzian absorption profile. In practice, the final absorption is usually the result of more than one type of broadening effect such that a purely Gaussian or Lorentzian line shape is not sufficient to describe the line profile. Hence, the convolution of the two lineshapes, termed as Voigt profile, is typically used to approximate the actual lineshape[16].

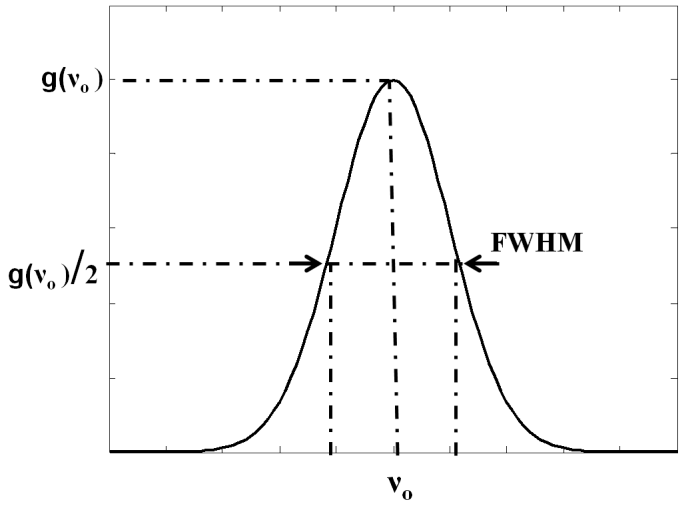

Figure 2.1: Schematic representation of an OPA.

2.5 Free-space and guided wave interaction

On one hand, optical sensors can be realized on open space setups using bulk optical components such as mirrors and beam splitters[13]. In such a configuration, the whole light beam undergoes direct interaction with its environment. In an alternative approach, light propagating through an optical waveguide structure can be allowed to interact with its surrounding. An evanescent electric field extending outside the waveguide boundaries is responsible for such waveguide based sensing. Both approaches have their own merits and limitations. In this section a brief overview of the two techniques is given with respect to the interaction efficiency and convenience for an application of interest.

Both open-space and guided wave sensor implementations can take advantage of either absorption spectroscopy or refractive index sensing. Distinctions between the two techniques are associated with parameters such as size, complexity and the proportion of electric field available for interaction with the surrounding medium.

Figure 2.2 and 2.3 show simplified graphical representations of free space and guided wave sensors, respectively. An evanescent field interaction with the region near a waveguide surface is shown in figure 2.3 . The plane wave representation of an optical field given in eq. (2.6) can be used to describe an electric field at a given coordinate on a dielectric waveguide. An important consideration, however, is that since a waveguide is a multilayer structure, an effective

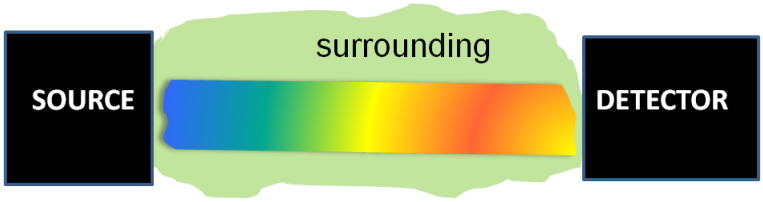

Figure 2.2: Schematic representation of a free space beam of light ineracting with its surrounding.

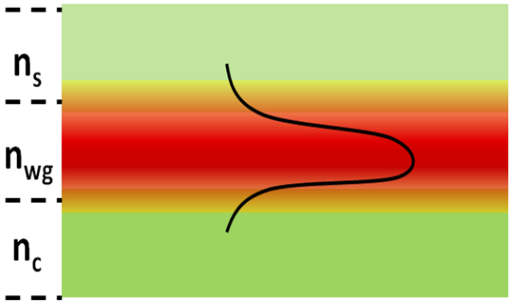

Figure 2.3: Schematic representation of an evanescent wave interaction of a guided wave with the surrounding above it. n_s, n_{wg}, and n_c represent the refractive index of the surrounding, the waveguide core and the bottom cladding, respectively.

index seen by a propagating waveguide mode has to be taken into account. Accordingly, for a mode propagating in z direction, the electric field at a point (x, y) on a waveguide cross section can be given by [14]

$$E(x,y,z) = E_0(x,y)\exp(j(\beta z - \omega t)) \tag{2.16}$$

where $\beta = n_{eff}(\frac{2\pi}{\lambda})$ is the propagation wave vector.

Through evanescent field interaction, the effective mode index is modified depending on the dielectric properties of the environment near the waveguide surface. The corresponding magnitude change in the effective index can be described by the overlap between the waveguide mode field distribution with the surrounding dielectric function perturbation $\Delta\varepsilon$ or equivalently Δn as given in eq(2.17)[14].

$$\delta n_{eff} = c\int \Delta\varepsilon EE^* dydx = 2c\varepsilon_0 \int n\Delta nEE^* dydx \tag{2.17}$$

where E^* represents the conjugate of the electric field.

A parameter, often used to measure the amount of overlap or the field extending outside is termed as the confinement factor, Γ, given by eq(2.18). Γ is

unity for free space sensors since the whole light beam is free to interact with the surrounding, and it is less than unity for guided wave sensors.

$$\Gamma = \frac{n_s c\varepsilon \iint\limits_{s} |E|^2 dxdy}{\iint\limits_{\infty} Re\{E \times H^*\} \cdot \vec{e}_z dxdy} \tag{2.18}$$

where, n_s is the surrounding refractive index, and H^* is the conjugate magnetic field

For high index contrast waveguides such as those implemented on an SOI platform, the confinement factor can be particularly high. This is could be attributed to two factors. The first is the boundary conditions imposed on the electric field displacement normal the waveguide interface. Since the normal electric displacement ($D = \epsilon E$) must be continuous across the interface,the electric field at the outside interface is enhanced by the ratio of the dielectric constant of silicon to that of the cladding material[15]. Moreover, the typically high group index of these waveguide structures contributes to further enhancement in the confinement factor[15]. Eq(2.19) relates the confinement factor with the group index and the electric field enhancement:

$$\Gamma = \frac{n_g \iint\limits_{s} \varepsilon |E|^2 dxdy}{n_s \iint\limits_{\infty} \varepsilon |E|^2 dxdy} \tag{2.19}$$

where n_g denotes the group index, and ε represents the spatial distribution of the dielectric constants in the respective regions.

In general, the confinement factor defines the amount of optical field available for absorption or refractive index related detection of an environment. Free-space spectroscopy of gases is a widely used technique taking the advantage of direct beam-wise interaction with gaseous environment. However, this approach is effective only for line-of-sight and suffers from sensitivity to misalignment and external perturbations. Typically large size and high device cost are other major limitations with these sensors. Guided wave sensing provides the advantage of more versatile and less perturbed measurements. Particularly, for refractive index sensing, waveguides provide a suitable platform for incorporating additional transduction techniques such as chemical films for enhanced gas detection. High portability and low cost fabrication are the other potential advantages planar waveguide based sensors can offer.

References

[**1**] A. Densmore, D.-X. Xu, P. Waldron, S. Janz, P. Cheben, J. Lapointe, A. Delâge, B. Lamontagne, J. H. Schmid and E. Post. *A Silicon-on-Insulator Photonic Wire Based Evanescent Field Sensor*. IEEE Photonics Technology Letters, 18(23): 2520-2522, 2006

[**2**] D. Celo, E. Post, M. Summers, T. Smy, M.J. Brett and J. Albert. *Interferometric sensing platform with dielectric nanostructured thin films*. Optics Express, 17(8):6655 - 6664, 2009.

[**3**] N.M. Jokerst, L.Luan ,S. Palit, M. Royal, S. Dhar, M. Brooke and T. Tyler . *Progress in Chip-Scale Photonic Sensing*. IEEE Transactions on Biomedical Circuits and Systems,3(4):202 - 211, 2009.

[**4**] Y. Zhao, Y-N. Zhang and Q. Wang . *Research advances of photonic crystal gas and liquid sensors*. Sensors and Actuators B, 160:1288-1297, 2011.

[**5**] D. Y. Wang, Y. Wang, J. Gong and A. Wang. *Fully Distributed Fiber-Optic Hydrogen Sensing Using Acoustically Induced Long-Period Grating*. IEEE Photonics Technology Letters, 23(11):733 - 735, 2011.

[**6**] K. Schroeder,W. Ecke and R. Willsch. *Optical fiber Bragg grating hydrogen sensor based on evanescent-field interaction with palladium thin-film transducer*. Optics and Lasers in Engineering, 47:1018-1022, 2009.

[**7**] N. A. Yebo, D. Taillaert, J. Roels, D. Lahem, M. Debliquy, D. Van Thourhout and R. Baets. *Silicon-on-insulator (SOI) ring resonator based integrated optical hydrogen sensor*.IEEE Photonics Technology Letters, 21: 960-962, 2009.

[**8**] X. Cuia, C. Lengignona, W. Taoa, W. Zhaoa, G. Wysockid, E. Ferteina, C. Coeura, A. Casseza, L. Croizea, W. Chena, Y. Wangb, W. Zhangb, X. Gaob, W. Liub, Y. Zhangb, F. Dongb. *Photonic sensing of the atmosphere by absorption spectroscopy*.Journal of Quantitative Spectroscopy and Radiative Transfer, 113:1300-1316, 2012.

[**9**] W. Jing, G. Peng, J. Zhang, Y. Wang, T. Liu, D. Jia, H. Zhang, Y. Zhang. *Wavelength Sweep of Intracavity Fiber Laser for Low Concentration Gas Detection* .IEEE Photonics Technology Letters, 20: 1515- 1517, 2008.

[**10**] G. Hörner, S. Lau, Z. Kantor and H-G. Löhmannsröben. *Isotope selective analysis of CO2 with tunable diode laser (TDL) spectroscopy in the NIR*. Analyst, 129:772-778, 2004.

[**11**] P. P. Vadillo. *Isotope selective analysis of CO2 with tunable diode laser (TDL) spectroscopy in the NIR.*Laser Diode Gas Spectroscopy, Semiconductor Laser Diode Technology and Applications, Dnyaneshwar Shaligram Patil (Ed.), ISBN: 978-953-51-0549-7, 2012.

[**12**] J. Michael Hollas. *Modern spectroscopy* .ISBN: 978-0-470-84416-8, 2003.

[**13**] Y. Her and B.J. Orr. *Rapid measurement of cavity ringdown absorption spectra with a swept-frequency laser.* Applied Physics B, 79: 941-945, 2004.

[**14**] S. Janz, A. Densmore, D.-X. Xu, P. Waldron, J. Lapointe, J. H. Schmid, T. Mischki, G. Lopinski, A. Delâge and R. McKinnon, et al. *Silicon Photonic Wire Waveguide Sensors.* Advanced Photonic Structures for Biological and Chemical Detection, Integrated Analytical Systems,II, 229-264, 2009.

[**15**] Y. Her and B.J. Orr. *Rapid measurement of cavity ringdown absorption spectra with a swept-frequency laser.* Applied Physics B 79: 941-945, 2004.

[**16**] J. T. Robinson, K. Preston, O. Painter and M. Lipson. *First-principle derivation of gain in high-index contrast waveguides.* Optics Express, 16(21):16659-16669 , 2008.

[**17**] B. Lins, F. Pflaum, R. Engelbrecht, B. Schmauss. *Absorption line strengths of* $^{15}NH_3$ *in the near infrared spectral region.* Applied Physics B: Lasers and Optics, 102(2): 293-301, 2011.

3

Silicon photonic gas sensing

In this chapter, the two optical sensing approaches discussed in the previous chapter namely, refractive index sensing and waveguide absorption spectroscopy are viewed with the relevance to the silicon photonic platform. Special emphasis is given to the refractive index based gas detection which is mainly dealt in this thesis. Both the spectroscopic and the refractive index sensing approaches on a chip scale are attractive for portable and low cost sensing applications. While each technique offers its own unique benefits, various practical requirements need to be addressed for feasible chip scale implementation. The chapter begins by providing an overview of practical system requirements for on-chip absorption spectroscopy on silicon chips. The rest of the chapter is dedicated to the refractive index sensing scheme. A brief review of the optical design aspects and performance measures for microring resonator based refractive index sensing is provided. Later on, the current state of chemically assisted optical gas sensing is reviewed. Finally, material and technological aspects of chemically functionalized silicon photonic gas sensors are thoroughly discussed.

3.1 Waveguide Absorption Spectroscopy

The principles of gas absorption spectroscopy have been discussed in the previous chapter. Highly specific gas detection using molecular absorption finger-

prints is a major advantage of this technique. Despite the fact that optical gas spectroscopy is very mature and widely used, it is typically characterized by less portable, expensive and complex instrumentation today. As a matter of fact, a working chip-scale direct gas absorption spectroscopy is currently non-existent.

Practical challenges for miniature implementations of spectroscopic sensors have to do with both the properties of the gas molecules and the instrumentation noise. Firstly, gases are the least dense form of matter. Second, though spectrally distinct, the gas absorption cross sections are very small, typically in the order of $10^{-22} - 10^{-18}$cm^2/molecule [1,2]. Recalling the Beer-Lambert relation, $I = I_0\exp(-\sigma CL)$ (where L is the physical interaction length) discussed in section 2.4, the above mentioned two issues impose a critical requirement for sufficiently long interaction length. On the other hand, noise levels present in the spectroscopic systems set lower limits on the detectable concentrations.

Propagation loss in planar silicon waveguides is one of the factors limiting the waveguide length and hence the interaction length. Typically, optimal waveguide lengths remain within a couple of centimeters. Another important factor measuring the evanescent light interacting with the surrounding gas molecules is the confinement factor. The confinement factor for silicon waveguide structures is typically in the range of 10-30%. Taking the waveguide loss(absorption), α_{wg}, and the confinement factor, Γ, into account the Beer-Lambert relation can be re-written in the form given in eq. (3.1) for waveguide based spectroscopic analysis[3].

$$I = I_0\exp(-\Gamma\sigma CL)\exp(-\alpha_{wg}L)) \tag{3.1}$$

We may express the sensitivity of this system with respect to change in the concentration as:

$$S = \frac{dI}{dC} \tag{3.2}$$

following this equation, the optimum waveguide length, l_o, at which the change in the intensity is maximum for a given concentration change can be estimated by solving the equation[3]:

$$\frac{dS}{dL} = 0 \tag{3.3}$$

This leads to:

$$l_o = \frac{1}{\sigma\Gamma C + \alpha_{wg}} \tag{3.4}$$

which is, in fact, the $1/e$ length of the waveguide.

Noise in free space absorption spectroscopy are also relevant in waveguide absorption spectroscopy. Laser and detector noise, mechanical vibrations, polarization dependent noise, and interference fringes are common in optical absorption spectroscopy[4]. Fringe related noise, however, can be more dominant in waveguide structures because of reflections at various waveguide interfaces.

A combination of counter techniques can be adopted to cope with these noise issues. One option could be the use of gas preconcentrating films on waveguides such that the number density of gas molecules is increased near the evanescent field interaction region. This would involve a thorough selection of films which will preserve the molecular fingerprints while maintaining minimal influence on the light propagation.

In this research, only a preliminary study has been carried out on gas absorption spectroscopy with silicon waveguides. The respective experimental observations and future insights are presented in chapter 9. An in depth investigation into this gas sensing approach is left for continuing future studies.

3.2 Refractive index sensing with silicon microring resonators

Owing to the high index contrast, silicon-on-insulator waveguide structures are typically characterized by strong evanescent field at the waveguide surfaces[5]. Hence, they lend themselves for refractive index based sensing approaches. The high index contrast further offers opportunities for the implementation of highly compact gas sensors. Chemical transducer films are typically integrated on the waveguide structures to achieve sensitivities to low gas concentrations on a compact interaction area[6,7]. Practically, these films are chosen so that gas-specific response is attained.

One of the integrated photonic structures which have recently gained an increasing interest for sensing applications is a microring resonator(MRR)[5-9]. A significant progress has been particularly made on MRRs for bio-sensing applications. Especially, MRRs implemented on high index contrast platforms are becoming more attractive because of high refractive index sensitivities on ultra small footprints. A wavelength interrogation scheme often employed in MRR sensors further allows multiplexing of sensor arrays on a chip.

3.2.1 Microring resonator basics

At a basic level, a microring resonator consists of an optical cavity made of a ring waveguide which is closely coupled to one or two access waveguides. A schematic representation showing a basic configuration of a microring resonator of radius r and two coupling waveguides is shown in figure 3.1. Conventionally, the four input/output ports in this configuration are labeled as input, through, add, and drop ports. At the resonance condition, light from the input port is coupled to the ring cavity and coupled out via the drop port. The extent of optical power delivered in and out of the ring cavity is determined by the

coupling ratios as well as the propagation loss. A micro ring resonator supports

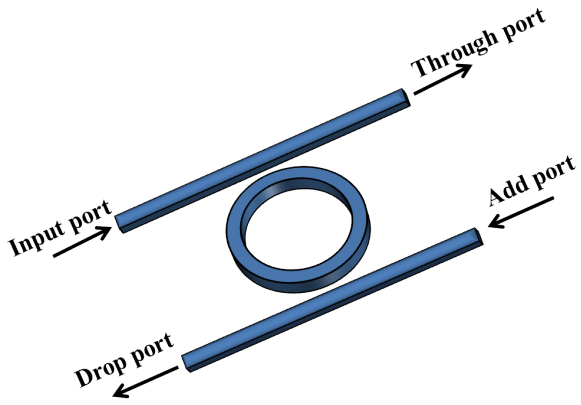

Figure 3.1: A schematic reprsentation of a microring resonator coupled to two access waveguides.

circulating waveguide modes in the ring cavity. The resonance condition for a ring resonator is given by

$$n_{eff}L = m\lambda \tag{3.5}$$

where n_{eff}, L, λ, and m represent the effective index of an optical mode in the ring cavity, the cavity length, the resonance wavelength and the resonance order number respectively.

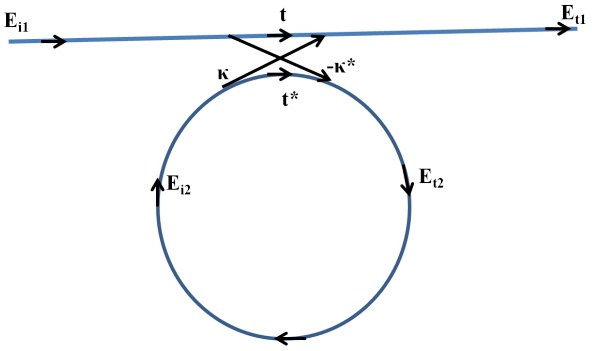

Figure 3.2: A microring resonator model with a single access waveguide.

A scattering matrix model can be used to analyze different configurations of microring resonators[10]. In its simplest layout, a microring resonator consists

of a ring coupled to a single access waveguide schematically shown in figure 3.2. With the assumption that the coupling is limited to waves traveling in one direction and if the total power entering and leaving the coupling region are equal, a unitary subset of scattering matrix with two constants κ and t relating the light in the ring and the access waveguide is given by

$$\begin{pmatrix} E_{t1} \\ E_{t2} \end{pmatrix} = \begin{pmatrix} t & \kappa \\ -k^* & t^* \end{pmatrix} \begin{pmatrix} E_{i1} \\ E_{i2} \end{pmatrix} \tag{3.6}$$

$$|\kappa^2| + |t^2| = 1 \tag{3.7}$$

where t and κ represent the transmission and coupling coefficients for the electric field respectively.
The above two equations are further supplemented by the circulation condition in the ring given by

$$E_{i2} = \alpha E_{t2} exp(j\theta) \tag{3.8}$$

α, and θ are the loss and the phase shift per round trip.

Extending this model to a microring in add - drop configuration , the through-port and drop-port mode amplitudes can be expressed by the following two equations

$$E_{t1} = \frac{t_1 - t_2^* \alpha exp(j\theta)}{1 - t_1^* t_2^* \alpha exp(j\theta)} \tag{3.9}$$

$$E_{t2} = \frac{-\kappa_1^* \kappa_2 \alpha_{1/2} exp(j\theta_{1/2})}{1 - t_1^* t_2^* \alpha exp(j\theta)} \tag{3.10}$$

where $\alpha_{1/2}$ and $\theta_{1/2}$ are half the round trip loss and phase, respectively. On a resonance, the power at the through-port becomes extinct.

For a symmetrically coupled ring resonator, it can be deduced from eq(3.9) that zero through-port mode amplitude is achieved if the ring resonator is lossless ($\alpha = 1$), which is not for purely passive waveguides. Solving eq(3.9) for zero through-port mode amplitude gives

$$\alpha = |\frac{t_1}{t_2}| \tag{3.11}$$

Consequently, matching the ratio of the coupling parameters t_1 and t_2 to the loss coefficient, α, using asymmetric couplers is a practical way to achieve high extinction ratios. However, noting the Q factor dependence on the coupling coefficients, optimization for high extinction ratio would also lead to reduced Q values[35]. High Q values are, on the other hand, required for sensing applications. Hence, design for optimal operating points with regard to both parameters is necessary. In practice, a critically coupled all-pass (single access waveguide) ring resonator configuration can provide sufficiently optimal

performance for sensing applications. Figure 3.3 illustrates a through-port and drop-port transmission spectrum for a symmetrically coupled, lossy, 10μm radius ring resonator.

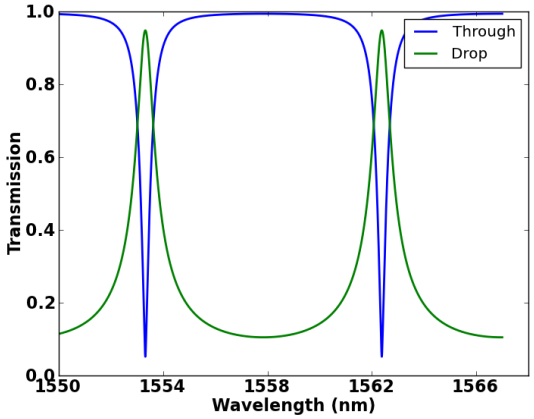

Figure 3.3: Through and drop port transmission spectrum of a symmetrically coupled 10μm radius microring resonator .

3.2.2 Ring resonator parameters

In this section, ring resonator parameters useful for practical applications are briefly reviewed.

The free spectral range

The free spectral range defines the spectral separation between two consecutive resonance orders of a ring resonator. It is given by

$$FSR = \Delta\lambda = \frac{\lambda^2}{n_g L} \tag{3.12}$$

where n_g is the group index of the guided mode. In sensing applications, the free spectral range determines the maximum possible dynamic range of detection.

Finesse and Quality factor

Finesse, F, is defined as the ratio of the FSR and the full width at half maximum (FWHM) of the resonance. For a MRR is in add-drop configuration, the FWHM is given by

$$FWHM = 2\delta\lambda = \frac{\lambda^2}{\pi n_{eff} L} \cdot \frac{1 - t^2\alpha}{t\sqrt{\alpha}} \tag{3.13}$$

The quality factor described by the ratio between the resonance walvelength and the FWHM, measures the sharpness of a microring resonance or the amount of energy stored at the resonance wavelength.

$$Q = \frac{\lambda}{2\delta\lambda} = \frac{\pi n_{eff} L}{\lambda} \cdot \frac{t\sqrt{\alpha}}{1 - t^2\alpha} \approx \left(\frac{1}{Q_{int}} + \frac{1}{Q_{ext}} \right)^{-1} \tag{3.14}$$

Where, $Q_{int} = \frac{\pi n_{eff} L}{\lambda \gamma^2}$, $Q_{ext} = \frac{\pi n_{eff} L}{\lambda \kappa^2}$, are the intrinsic and extrinsic Q values, respectively. $\kappa^2 = 1 - t^2$, and $\gamma^2 = 1 - \alpha^2$. The Q factor is a critical parameter in determining the detection limit of microring resonator based sensors.

3.2.3 Microring resonator sensor design considerations

In a microring based sensing, the resonance shift due to the surrounding refractive index change is spectrally quantified as a measure to a target analyte concentration. The schematics in figure 3.4 depicts the refractive index sensing scheme with MRRs. In this section design parameters for MRR based sensing applications are briefly discussed.

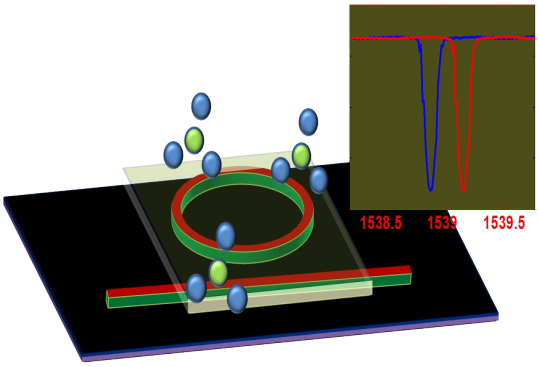

Figure 3.4: Illustration of a refractive index sensing apprach with surface functionalized microring resonators.

Sensitivity

The sensitivity of an optical waveguide structure is defined as the change in the measured optical parameter with respect to a waveguide parameter affected by the analyte to be detected. In a typical ring resonator based sensing, the shift

in resonance wavelength due to change in the surrounding refractive index is used to specify the sensitivity, which is defined as

$$S = \frac{\Delta\lambda}{\Delta n_s} \tag{3.15}$$

where λ and n_s are the resonance wavelength and the surrounding refractive index, respectively.

In practice, the sensitivity would be given by the wavelength shift per unit concentration of an analyte. The normalized sensitivity relevant to compare MRRs operating at different wavelengths is given by

$$S' = \frac{S}{\lambda} = \frac{\Delta\lambda}{\lambda}\frac{1}{\Delta n_s} \tag{3.16}$$

Starting with the resonance condition (eq. (3.5)), the wavelength shift with the surrounding refractive index change is given by

$$\frac{\Delta\lambda}{\lambda} = \frac{\Delta n_s}{n_g}\frac{\partial n_{eff}}{\partial n_s} = \frac{\Delta n_s}{n_g}\Gamma \tag{3.17}$$

where n_g , n_{eff} and Γ are the group index , effective index and the confinement factor, respectively.

Detection limit

The detection limit is one of the critical performance measures for a given sensor platform. The detection limit defines the lowest possible waveguide parameter perturbation that corresponds to the smallest analyte concentration measurable by a system. For a ring resonator the detection limit refers to the lowest refractive index change due to an analyte which leads to a measurable resonance shift. Ideally, the minimum measurable shift is solely determined by the accuracy and resolution of the measurement instrumentation. However, such a requirement on the interrogation system is relaxed for high Q ring resonators. Narrow resonance peaks allow smaller shifts to be measured with a higher accuracy. Accordingly, the detection limit of a ring resonator sensor is often expressed with respect to its quality factor or the FWHM of the resonance peak. Practically, the detection limit is a certain fraction(e.g. 20%) of the FWHM. The detection limit and the FWHM are related through the sensitivity, S, as given by eq (3.18) [11,12].

$$DL = \Delta n_{min} = \frac{K \cdot FWHM}{S} = \frac{K}{QS'} \tag{3.18}$$

where, n_{min} is the minimum detectable refractive index change, and K is a constant less than unity representing a fraction of the FWHM.

For instance, considering a Q factor of 30,000, a detection limit in the order of 10^{-5} refractive index unit(RIU) or lower can be achieved.

Dynamic range

The dynamic range of a microring resonator based sensor is the sensitivity range in which unambiguous detection of an analyte concentration can be realizable. For a given sensor, it is determined by an intrinsic ring resonator parameter, namely the FSR, as well as by the transduction mechanism employed. The FSR defines the largest detectable resonance shift which in turn corresponds to the maximum measurable analyte concentration. Thus, rings with smaller radii offer larger dynamic ranges. Sensor transduction schemes such as surface chemistry also put a limit on the practical dynamic range due to effects such as film saturation.

Noise

As any other measurement system, a ring resonator based sensing scheme is subject to the influence of noise in the system. Hence, it is necessary to take noise into account when specifying performance measures such as, the detection limit and sensitivity.

Noise in microring resonator sensors can have different origins. Part of the noise is contributed from the measurement instruments while the rest can be due to the basic characteristics of the main sensor unit[13]. Depending on the employed interrogation scheme, intensity and wavelength related noise can have impact on the sensor performance. Intensity noise due to the source power fluctuation and the low frequency (1/f) noise is more relevant when intensity interrogation is used. In commonly used wavelength shift interrogation, the spectral noise in the light source, and thermally induced resonance perturbations are more relevant.

With analogy to the photodetector Detectivity, a time-normalized sensitivity was proposed to define a figure of merit for the sensitivity of ring resonator sensor systems[13]. In this definition, the measurement equivalent bandwidth is included to account for the system noise. It is defined as

$$S^* = \sqrt{\frac{\Delta f}{N}}\frac{1}{\Delta n_{NE}} = \sqrt{\frac{\Delta f}{N}}\frac{S}{\Delta\lambda_{min}} = \sqrt{\frac{\Delta f}{N}}\frac{\Gamma}{\Delta\lambda_{min}}\frac{\lambda}{n_g} \tag{3.19}$$

where, $\frac{\Delta f}{N}$ is the equivalent bandwidth with N representing the number of discrete wavelengths at which a measurement is taken; Δn_{NE} is the noise equivalent refractive index change, and $\Delta\lambda_{min}$ is the wavelength shift corresponding to it.

While the instrumentation noise is taken care of with this expression, an additional treatment is required for the wavelength noise due to thermal effects.

Because of the high thermo-optic coefficient of the silicon waveguide structures, a large proportion of noise comes from thermal variations on the sensor chip. Commonly, compensation techniques such as temperature control and temperature insensitive designs are used to achieve thermally tolerant sensor performance. The refractive index change limited by temperature induced noise in a compensated system can be given by

$$\Delta n_T = \frac{dn}{dT} \cdot \Delta T \tag{3.20}$$

where, dn/dT is the thermoptic coefficient of the sensor device, and ΔT is the temperature fluctuation in a temperature compensated system.

3.3 Chemically functionalized silicon photonic chips for gas sensing

Gas detection with optical waveguide structures typically involves a critical choice of suitable chemical materials. Optical, chemical and morphological properties are some of the most important factors considered in the selection process of a material for a specific gas sensing application. In addition to the material properties, efficient techniques for incorporating these materials on the underlying photonic sensing structures are highly relevant. In practice, achieving a specified set of performance targets such as a detection limit and gas-specificity would require a rigorous synthesis of a sensitive material out of a combination of materials or functional compounds. While gas sensitive materials can be useful in bulk forms, the thin film versions are of a particular interest for integrated gas detection owing to their compatibility with micro fabrication technologies.

3.3.1 Gas sensitive materials

Various inorganic and polymer materials have been used as gas sensitive transducers in electrical and optical sensors [14-16]. In recent years, gas sensitive films with porous structures have attracted a strong interest in contrast to the dense film counterparts. More specifically, materials with nano dimensional pores offer attractive properties for sensing application. Nanoporous materials are typically characterized by a high surface area per unit volume, hence, allowing enhanced adsorption for a given gas concentration. Conventionally, nanoporous materials fall under three categories based on the pore dimensions. These are, microporous (< 2nm pore diameter), mesoporous (2-50nm pore diameter), macroprous (>50nm pore diameter).

Nanoporous films of a range of materials have been developed using various techniques. Nanoporous metal oxides, zeolites, metal-organic-frameworks and polymers are among materials employed for sensing and catalytic applications [14-19]. Moreover, various organic and inorganic functional molecules have been attached to nano-porous surfaces for enhanced response and specificity towards target gas molecules. With regard to material synthesis, techniques involving sol-gel or colloidal chemistry are usually used [20,21].

For optical gas sensing applications, changes in absorption and refractive index of the sensitive materials can be exploited. Adsorption of gas molecules in nanoporous films can alter the chemical properties resulting in changes in color or refractive index of these films. Other than chemical changes, the physical binding of gas molecules within the pores can modify the overall effective refractive index of the porous film.

Gas sensors using metal oxide nanopraticles have been reported. Nano composite films of NiO - Au and ZnO - Au have been reported to have optical sensitivities to CO and NO_2 gases. In these sensors, the shift in Au surface plasmon peak due to gas adsorption is monitored at 300 °C [16]. Similarly, Au doped NiO nanoparticles embedded in a sol gel SiO_2 porous matrix and coated on a silica substrate have been demonstrated to have sensitivities towards H_2 and CO concentrations as low as 0.01 %. Optical intensity variation in the surface Plasmon peak in the visible region is used as a measure for the gas concentrations [22]. However, a common issue with metal oxide based sensors becomes the lack of gas specificity and high temperature operation [23,24].

Another class of materials successfully demonstrated for optical gas detection are thin films of color changing dyes. pH indicator dyes as thin films or embedded in porous matrix have shown sensitivities to gases such as NH_3 and NO_2. Using a 20nm thick pH indicator dye, brumothyblue, film on TiO_2 slab waveguide, a detection of 1 part per trillion(ppt) NH_3 has been demonstrated by monitoring the absorbance near 630nm. This dye changes in color from yellow to blue when exposed to NH_3 with the response and recovery times of 1 and 30sec respectively [14].

Optical gas sensors using metal complexes as colorimetric sensitive films have also been demonstrated. NO_2 detection with a nanostructured Aluminum hydroxide substrate functionalized with phthalocyaninato-iron(II) has been reported with a detection limit of 20ppb[15]. The sensor responded to NO_2 without significant interference from NO, SO_2, CO_2 and humidity. Specific interaction of NO_2 with the organo metallic complex changes the optical absorption behavior of the film in the visible spectrum. Nonetheless, most gas sensitive dyes are temperature sensitive in their response characteristic and can irreversibly lose stability due to the environmental influence [25]. In addition, almost all reported gas sensitive dyes show response in the visible spectrum, thus, precluding their integration on potentially cheap and mass producible silicon photonic technology.

Metal organic frameworks (MOF) are another type of novel porous materials which have been demonstrated to have high potential for gas phase analytical applications such as catalysis, gas storage and sensing [17,18]. Preferential physical adsorption of CO_2 and H_2 gases on microporous manganese formate at room temperature has been reported[18]. High sorption capacity of MOFs relative to other nanoporous materials such as zeolite and activated carbon has also been demonstrated [17]. However, these being preliminary demonstrations, further research and progress on selective functionalilzation and thin film synthesis of MOFs is still to be made for practical sensing applications.

Nanoporous silicate materials have also gained increasing interest for sensing applications. Porous silicates are attractive as reactive surfaces as well as

supporting matrix for functional materials. Some of the interesting features of silica for optical sensing applications include, stability, relative inertness in many environments, and transparency in UV- NIR spectrum[26]. In conventional porous silicate synthesis, surfactant templates cooperatively assemble with inorganic precursors to produce an aluminosilicate or silicate matrix. The surfactants are typically removed by calcination to produce nanoporous structures. Nanoporous silicate surfaces can be functionalized with co-condensation of function groups or using post synthesis techniques[27,28].

A few demonstrations of nanoporous silicates for gas sensing have been reported. A fiber optic evanescent wave sensor utilizing microporous alumino silicate films, often termed as zeolites, has been reported for selective ammonia detection[29]. The refractive index change initiated by adsorption of gas molecules on the microporous surface is monitored by measuring the shift in the reflection peak of a long period grating on the optical fiber. The sensor demonstrated selective response to NH_3 with respect to CO_2, H_2S, H_2 and CH_4 for concentrations higher than 3%. Such alumino- silicate films exhibit high surface acidity favorable for adsorbing base gases such as NH_3. The detection potential of these materials at lower concentrations (ppm-ppb) has not been yet reported.

In addition to the microporous films, mesoporous silicate films are attractive materials for sensing applications. These films are typically characterized by spacious pores suitable for accommodating functional molecules without compromising efficient gas diffusion and adsorption capabilities. A meso - structured alumino silicate powder (Al - MCM - 41) impregnated with a bromocresol green (BG) dye was reported for colorimetric NH_3 detection[30]. In another work, an organic dye immobilized porous silica film on an optical fiber is used for trace ammonia detection in gas and water samples[31]. The corresponding detection limits for gaseous and water-dissolved ammonia traces was reported to be 13ppb and 5ppb, respectively. In this sensor, a thin Polydimethylsiloxane(PDMS) film is used to prevent interference from water in liquid samples. The absorbance change of the probe molecule upon interaction with NH_3 is measured with UV-VIS absorption spectrometry. However, the potential of functionalized nanoporous materials for gas sensing on mass producible, energy efficient and highly portable optical platforms has been barely studied.

Among a range of materials discussed so far, selecting a gas sensitive material particularly for silicon photonic sensors involves a few important considerations. In order to exploit high refractive index sensitivity, minimal sensitivity to the intensity noise, and the multiplexing capabilities of microring resonators, materials exhibiting measurable refractive index response to gas molecules become of a prior choice. High surface area nanoporous materials offer a high po-

tential in this regard. Trace gas detection in ppm - ppb range can be realizable due to the enhanced gas adsorption on these materials. In addition, gas specific detection can be achieved by tuning the nanoporous surface with various functional groups. Another consideration is that gas sensitive materials are typically chosen to be optically transparent in the NIR region so that the propagation loss in the waveguide structures is minimized.

Once an appropriate gas sensitive material has been identified, the following step involves thin film coating on the optical waveguides. The two important coating parameters are the thin film homogeneity and thickness. Coating techniques suitable for smooth film fabrication are typically used to minimize waveguide loss incurred due to surface roughness. This is critical especially for high index contrast SOI structures where the sensitivity to surface roughness is high. Uniform film coating techniques such as spin coating are the preferred techniques in this respect. Figure 3.5 shows a microscope image of a spin coated smooth ZnO nanoparticle film on a Si MRR. Typical surface roughness as low as 2-20nm are attained from these films.

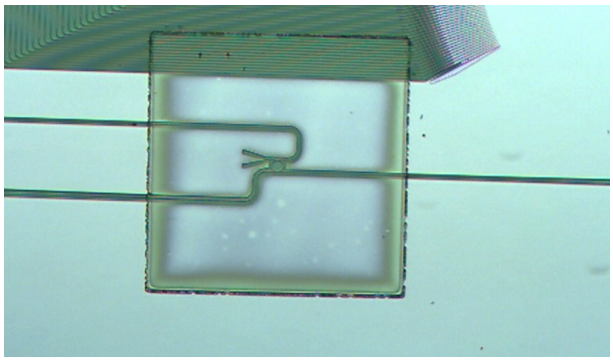

Figure 3.5: About 110nm thick spin coated ZnO nanoparticle film on Si MRR .

The film thickness , on the other hand, determines the extent of interaction with the evanescent field. Too thin films can limit the interaction to only some proportion of the evanescent light, hence limiting the sensitivity and dynamic range of the sensor. Excessively thick films can also raise the detection limit and, in addition, lead to slow sensor response. Hence an optimum film thickness has to be determined. Figure 3.6 shows a simulated effective index sensitivity of a 450 nm wide silicon waveguide as function of the thickness of a coating material for a refractive index change of 10^{-3}. In this simulation, the coating refractive index is taken to be 1.5.

While nanoporous thin films potentially provide high specific surface area for efficient gas sensing , they are at the same time expected to exhibit specificity

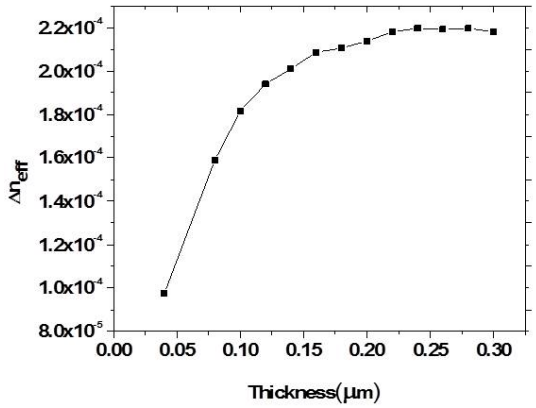

Figure 3.6: simulated effective index sensitivity of a 450nm wide silicon waveguide as function of the thickness of a coating material for a refractive index change of 10^{-3}.

towards target molecules. Different functionalilzation approaches are used to achieve selective surface properties. The direct synthesis and post synthesis functionalization routes are the two general category of techniques. In the first method, organic or inorganic functional groups are attached to the surface or introduced into the material framework during the synthesis[27]. Alternatively, functional groups can be attached by various post synthesis mechanisms. Post synthesis immobilization (impregnation) and Atomic Layer Deposition(ALD) are the two possible post synthesis functionalization techniques[28].

Atomic layer deposition is an attractive technique with capability to control thin film deposition process to a monolayer scale. This technique has recently gained interest for a specific functionalization of nanoporous surfaces. For instance, efficient incorporation of functional materials such as Ti and Al into mesoporous materials and a subsequent improvement in catalytic properties have been demonstrated[28]. In this thesis, both the direct synthesis and the ALD techniques are employed for functionalization of nanoporous silica materials for selective gas detection.

3.3.2 Sensitivity estimations for nanoporous coatings on silicon photonic chips

The adsorption of gaseous molecules on porous films can involve various mechanisms depending on the physical and chemical properties of the porous surface and the target molecules. In general, an adsorption process may involve

a chemical interaction or physical binding on the pore walls. Each of these adsorption mechanism can alter the refractive index of the porous medium through different effects. One of the possible scenarios is that, some gaseous molecules can physically adsorb on the pores via capillary condensation. This is usually the case for volatile organic compounds with boiling points above room temperature. In such a situation, some percentage of the pore volume can be assumed to be occupied by the vapor molecules and the effective refractive index can be estimated. Apart from capillary condensation, physical adsorption of some gaseous compounds can take place via weak interactions depending on the pore structure and the surface properties of the adsorbate material[17,18]. This can possibly lead to change in the refractive index.

Moreover, some porous materials have higher chemical affinity towards a specific or a broad range of gaseous compounds. In such cases, a strong chemical binding can effectively increase the density of gas molecules in the matrix, hence, modifying the overall film refractive index. However, it is worth noting that a chemical adsorption can be of a more complex effect. It may give rise to other chemical or physical changes in the film properties such as color and dimension. These changes on their own right can alter the optical constants of the film.

In a simplified scenario where other possible chemical/physical changes are neglected, the refractive index change of a porous film upon gas/vapor adsorption can be estimated with the Lorentz-Lorenz relation. The relation between the optical constants and the properties of a multi- component system as described by this relation [32] is:

$$B_{eff} = \frac{3}{4\pi} \cdot \frac{n_{eff}^2 - 1}{n_{eff}^2 + 2} = \sum N_i \alpha_i \tag{3.21}$$

where B_{eff} is the effective polarizability of a unit of volume, n_{eff} is the effective index of the composite medium, N_i and α_i are the number of molecules and molecular polarizability per unit volume of each component, respectively. If a film is composed of two components, namely a material matrix and pores in case of porous films, (3.21) can be rewritten as

$$B_{eff} = B_p \cdot P + B_m \cdot (1 - P) \tag{3.22}$$

or equivalently

$$\frac{n_{eff}^2 - 1}{n_{eff}^2 + 2} = \frac{n_p^2 - 1}{n_p^2 + 2} \cdot P + \frac{n_m^2 - 1}{n_m^2 + 2} \cdot (1 - P) \tag{3.23}$$

where P is the pore fraction, and the subscripts $_p$ and $_m$ stand for the pore and the matrix material, respectively.

In the case of volatile organic compounds, which can easily condense into the pores, the refractive index within the occupied pores can be approximated with that of the liquid phase. For instance, considering a 40% porous film with refractive index of 1.4, a rough estimate of the refractive index increase due to the adsorption of a VOC can be made with e.q. (3.23). In this estimation, adsorption of a VOC, xylene, with a refractive index of ~ 1.493 is to be considered. It is further assumed that about 15 % of the pores are occupied when the film is fully saturated at room temperature. The resulting refractive index change estimated with eq. (3.23) is in the order of $2.5 \cdot 10^{-2}$. This corresponds to a MRR resonance shift of ~ 2nm at 1550nm. The assumption that only a fraction of the pore volume is occupied at the saturation pressure is based on the fact that the adsorption-desorption equilibrium is a function of the surface temperature and the binding strength.

On the other hand, for compounds which are in the gaseous phase at room temperature, the refractive index change is largely determined by the adsorption efficiency, and hence, the density of gas molecules in the pores. The resulting modified refractive index within the pores can be taken to be a fraction of the liquid phase refractive index of the respective compound.

Despite the simplified cases considered so far, an adsorption process can be of a more complex nature and other mechanisms may also contribute to the refractive index change. For instance, chemical adsorption of gas molecules on a porous semiconductor surface can involve electron transfers; hence, variations in the carrier density of the porous media may affect the refractive index. A crude estimate of the refractive index change induced by the change in carrier concentration can be given by the Drude-Lorentz model[33].

$$\Delta n_{index} = \frac{-e^2 \lambda_o^2}{8\pi^2 c^2 \epsilon_o n_{index}} \left(\frac{\Delta n}{m_e^*} + \frac{\Delta p}{m_h^*} \right) \tag{3.24}$$

where, n_{index} is the refractive index of the material, Δn and Δp denote the excess electron and hole densities, e is the electron charge, λ_o is the free space wavelength, c is the speed of light, ϵ_o is the vacuum permittivity, m_e^* and m_h^* are the electron and hole effective masses.

From this relation, considering a material with a refractive index $n = 1.5$, it can be deduced that a change in carrier density as high as $1 \cdot 10^{19}/cm^3$ is required to have index changes in the order of $1 \cdot 10^{-3}$ at a wavelength of 1500nm. The literature on adsorption induced carrier density modulation is barely available. However such a fairly high carrier density change required for measurable effects may imply that this process may be of a less significant contribution to the sensing application considered here.

On the other hand, adsorption is in general exothermic involving heat release to the surrounding. The heat of adsorption for chemical adsorption pro-

cesses is typically high as compared to physical adsorption[34]. For materials characterized by high thermo-optic coefficients, such as silicon waveguides coated by adsorbing films, the released heat can result in instantaneous effective index changes. The instantaneous temperature rise with an adsorption process can be estimated with

$$\Delta H = mC\Delta T \tag{3.25}$$

where, ΔH is the heat of adsorption, C is the heat capacity, m is the mass of the adsorbent film, and ΔT is the change in temperature.

For instance, considering a zeolite material with typical values of $\Delta H = 70 - 100$KJ/mol, an adsorption capacity of 0.2mmol/g, and a heat capacity of $0.8\text{JK}^{-1}\text{g}^{-1}$ at room temperature, temperature increases in the order of 10-20 K are estimated. This can lead to 0.8 - 2nm shift in the resonance wavelength of a MRR. However, once an adsorption equilibrium is reached, the released heat is likely to be gradually dissipated to the surrounding, hence, resulting in no net effects. Accordingly, the thermo-optic based sensing approach becomes more relevant when the interaction with the gas environment is capable of continuous heat generation[6].

In general, the possible mechanisms discussed so far indicate that vapor condensation and increased density of gas molecules in porous films are the predominant processes contributing to refractive index sensing with functionalized silicon photonic chips.

3.3.3 Adsorption isotherm

The amount of gas molecules adsorbed or the surface coverage of a porous material is a function of the surface properties as well as the gas pressure. Different analytical approximations, often termed as adsorption isotherms, are used to estimate the relation between the gas pressure and the surface coverage of an adsorbate. In literature, physical adsorptions are commonly classified into six groups[36] as depicted in figure 3.7.

Adsorption phenomena in micro- and meso-porous materials, which are of interest in this research, may be best modeled with the so called Type-I and Type-IV adsorption isotherms, respectively[36]. The Type-I adsorption isotherm is often termed as 'pseudo-Langmuir' isotherm. The Langmuir adsorption model is limited to the formation of a monolayer, hence does not describe most real adsorption phenomena. Nonetheless, this model can successfully be applied to Type-I adsorption in purely microporous materials. It is worth noting, however, that the reason for the limiting value(plateau) in this type of adsorption is the micropore filling rather than the monolayer limit; hence, it is termed 'pseudo-Langmuir'[36]. The Langmuir isotherm is given by

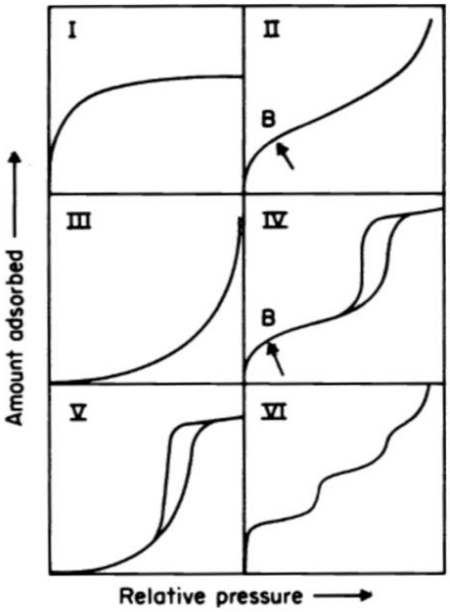

Figure 3.7: Types of adsorption isotherms (International Union of Pure and Applied Chemistry (IUPAC) 1985, [36]) .

the relation:

$$\theta = \frac{KP}{1+KP} \tag{3.26}$$

where θ is the fractional surface coverage, P is the gas pressure(concentration), and K is the Langmuir adsorption constant which is a function of temperature and binding energy.

For typically small refractive index changes($10^{-4} - 10^{-2}$) due to gas adsorption in microporous materials, the fraction of the surface coverage and the refractive index change can be approximated to be of a linear relationship. Hence, the resonance shift with gas concentration of a MRR sensor functionalized with such a film can be modeled with the Langmuir isotherm given in eq. (3.26).

A Langmuir isotherm fit to experimentally measured resonance shifts for CO adsorption on a ZnO functionalized MRR is depicted in figure 3.8

As pointed out earlier, adsorption in mesoporous materials is commonly of a Type-IV nature. The low pressure regime in this type of adsorption is attributed to a monolayer formation on the pore surface followed by a multilayer formation. Point B on the figure 3.7 indicates the stage at which the monolayer adsorption is complete. Moreover, Type-IV adsorption is characterized by hysteresis loop due to capillary condensation in the mesopores[36]. The onset of the hysteresis loop marks the beginning of the capillary condensation. However, at

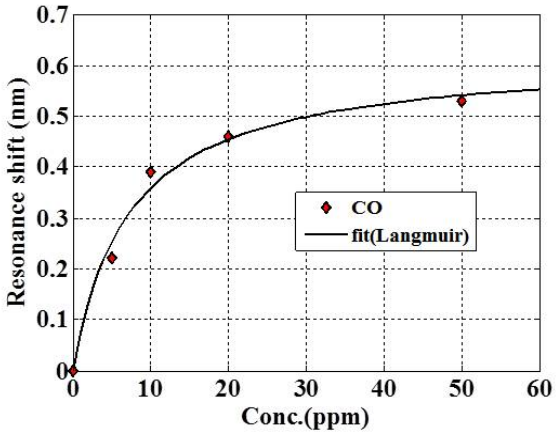

Figure 3.8: A Langmuir isotherm fit to experimental CO sensitivity of a ZnO functionlized MRR .

sufficiently low pressures, the adsorption of gas molecules on mesoporous films may still be approximated with the Langmuir model.

3.3.4 Gas selectivity

Sensor specificity towards a target gas is another critical parameter considered in the sensitive material selection process. However, in practice, attaining a material which is solely responsive to a single target gas is hardly possible. As a result, it is often a practical approach to choose a material such that it is less influenced by interfering gases within a specific application environment. Various materials involving a wide range of chemical approaches have been reported. Specific adsorption of gases on metal complexes, organic dyes, and functionalized nanoporous surfaces have been used for selective optical detection of gases such as NH_3, NO_2, and H_2 [6,15,29]. Particularly for the silicon microring based sensors, materials characterized by measurable refractive index changes in the NIR upon specific gas adsorption are required.

In this work, nanoporous metal oxide, ZnO, a polymer material-PDMS, and surface functionalized nanoporous silica materials are studied. Selective detection of NH_3 has been achieved using the functionalized nanoporous silica material, whereby demonstrating the potential of tuning these materials for selective detection of different gases. Another important aspect with various chemical sensors is interference from humidity. In this regard, tailoring the hydrophilic or hydrophobic properties of the sensitive materials can be a valuable approach to tackle humidity related issues.

3.3.5 Response time and reversibility

A rapid detection of gaseous analytes is a critical performance measure in the majority of gas sensing applications. Hence, sensitive materials with response times shorter than 1-2min are of a typical interest. Besides the chemical properties, the morphology of thin film gas sensitive materials plays a crucial role in determining the response time. In this respect, nanoporous materials allow fast gas diffusion and access to the sensitive surface providing opportunities for rapid detection.

On the other hand, in some applications, sensor reversibility can be a requirement. Reusable sensors are interesting in applications where frequent replacements are impractical or expensive. In such situations, fast and full recovery of the sensitive material is necessary. Hence, a relatively weak and still selective interaction with gas molecules is a key feature expected of such materials. Different materials including metal oxides, organic materials, and nanoporous silica materials have been reported to exhibit reversible responses to some gases[6,14]. In some other applications, however, sensor sensitivity and selectivity can be of a primary interest than reversibility. Biomedical sensing is a typical example of such applications where sample contamination is strictly unacceptable. In these cases, cheap and disposable sensors are preferred and reversibility becomes a secondary aspect.

In this work, it is demonstrated that rapid on-chip optical gas detection in a few seconds is achievable using different gas sensitive materials such as metal oxides, polymers and functionalizied nanoporous silicates. It is also indicated that the nature of interaction with gas molecules and the structure of the sensitive materials has a major impact on the sensor reversibility. For instance, ZnO nanoparticle films are observed to have relatively longer equilibrium response as well as recovery time for gases such as CO, and ethanol. This can be attributed to a strong chemical binding of the gas molecules on the highly reactive ZnO surface at room temperature. On the contrary, relatively weaker adsorptions of gases on PDMS and nanoporous alumino silicate materials have resulted in faster recovery in a few seconds time scale.

3.4 Summary

In this chapter, practical aspects for silicon photonic gas sensing application are discussed. Waveguide absorption spectroscopy and refractive index sensing are the two potential approaches for silicon photonic gas sensing. Owing to the relative ease of implementation with current technologies, the refractive index sensing approach can be of an immediate practical application. Currently,the waveguide propagation loss and the overall system noise are among the major

limiting factors for absorption spectroscopy. However, these challenges can potentially be resolved by employing novel techniques and designs as well as with fabrication improvements. Techniques for gas density enhancement near the waveguide surface can, for instance, be used to compensate for shorter interaction lengths imposed by the propagation losses.

Chemically functionalized high Q MRRs are of a considerable potential for real sensing application with the refractive index sensing approach on silicon chips. High refractive index sensitivities due to the high index contrast combined with high surface area nanoporous chemical coatings offers opportunities for sensitive gas detection on highly compact MRR sensors. Moreover, functionalization of the nanoporous surfaces with specific functional groups can allow selective and multiplexed gas detection. Various gas sensitive materials have been utilized for the detection in the optical domain. Nanoprous metal oxides, silicates, metal-organic-frameworks, organic dyes and polymer films are among these materials. However, most of these materials have not been so far well studied for gas detection on highly portable, energy efficient and mass producible integrated sensing platforms. Particularly, for gas sensing with silicon microring resonators, materials with measurable refractive index changes in the NIR spectrum are of a prior choice. Optical transparency and film homogeneity are other important considerations for selecting gas sensitive chemical films. In this respect, nanoporous silicates with specific functional groups become among the materials of interest for selective and sensitive gas detection on silicon chips.

Sensor reversibility and response time are the two useful parameters to be considered in the selection process of gas sensitive materials. Particularly, rapid sensor response is a crucial aspect for real time sensing applications in various industrial and bio-medical areas. Hence, gas sensitive coatings responsive in less than a couple of minutes are usually required. Such a rapid response is achievable for most nanoporous gas sensitive materials due to enhanced gas diffusion and surface accessibility. On the other hand, sensor reversibility can be relevant in some sensing applications. Materials with relatively moderate/weaker binding affinity and yet selective response to a target gas are needed for such applications. However, in some other applications, disposable sensors are preferred to avoid sample contamination risks. In this case, reversibility becomes less relevant and such sensors can take advantage of highly selective response often offered by materials with strong binding affinities to specific gaseous molecules.

Effective index changes on silicon waveguide sensors due to the adsorption of gas molecules can be associated with different physical phenomena. Capillary condensation, physical or chemical adsorption, change in carrier density, and thermo-optic effect due to heat of adsorption are the potential mechanisms

that can play a role in the refractive index change. For practically reasonable material and device parameters, theoretical estimates indicate that capillary condensation of vapor molecules and physical/chemical adsorption induced density enhancement of gas molecules are more relevant mechanisms especially for nanoporous coatings.

References

[**1**] B. Lins, F. Pflaum, R. Engelbrecht and B. Schmauss.*Absorption line strengths of* $^{15}NH_3$ *in the near infrared spectral region.* Applied Physics B: Lasers and Optics, 102:293-301, 2011.

[**2**] K. Liu, W. Jing, G. Peng, J. Zhang, Y. Wang, T. Liu, D. Jia, H. Zhang, and Y. Zhang*Wavelength Sweep of Intracavity Fiber Laser for Low Concentration Gas Detection* . IEEE Photonics Technology Letters, 20(18):1515 - 1517, 2008.

[**3**] R. Siebert and Jorg Muller. *Infrared integrated optical evanescent field sensor for gas analysis Part II. Fabrication.* Sensors and Actuators A, 119:584-592, 2005.

[**4**] P. Werle and F. Slemr. *Signal-to-noise ratio analysis in laser absorption spectrometers using optical multipass cells.* Applied Optics, 30(4):430-434, 1991.

[**5**] A. Densmore, D.-X. Xu, P. Waldron, S. Janz, P. Cheben, J. Lapointe, A. Delâge, B. Lamontagne,J. H. Schmid, and E. Post. *A Silicon-on-Insulator Photonic Wire Based Evanescent Field Sensor.* IEEE Photonics Technology Letters, 18(23):2520 - 2522, 2006.

[**6**] N. Yebo, D. Taillaert, J. Roels, D. Lahem, M. Debliquy, D. van Thourhout and R. Baets. *Silicon-on-Insulator (SOI) Ring Resonator Based Integrated Optical Hydrogen Sensor.* IEEE Photonics Technology Letters, 21:960-962, 2009.

[**7**] K. De Vos, T. Claes, Y. D. Koninck, S. Popelka, E. Schacht, R. Baets and P. Bienstman. *Multiplexed antibody detection with an array of silicon-on-insulator microring resonators.* IEEE Photonics Journal, 9:225-235, 2009.

[**8**] N. Jokerst, S. Palit, L. Luan, S. Dhar and T. Tayler. *Chip scale integrated microresonator sensing systems.* ECS transactions, Journal of Biophotonics, 2:212-220, 2009.

[**9**] Y. Sun and X. Fan. *Analysis of ring resonator chemical vapor sensor development.*Optics Express, 16:10254-102682, 2008.

[**10**] A. Yariv. *Critical Coupling and Its Control in Optical Waveguide-Ring Resonator Systems.* IEEE Photonics Technology Letters, 14(4):483-485, 2002.

[**11**] L. Chrostowskia, S. Grista, J. Flueckigera, W. Shia, X. Wanga, E. Ouelletb, H. Yuna, M. Webba, B. Niea, Z. Lianga, K. C. Cheunga, S. A. Schmidtc, D. M. Ratnerc, and Nicolas A. F. Jaegera. *Silicon photonic resonator sensors and devices.* Proceedings of SPIE (invited), 8236:823620-1, 2012.

[**12**] C. Chao and L.J Guo. *Design and Optimization of Microring Resonators.* Journal of Lightwave Technology, 24(3):1395-1402, 2006.

[**13**] J. Hu, X. Sun, A. Agarwal, and L. C. Kimerling. *Design guidelines for optical resonator biochemical sensors.* Journal of Optical Society of America B, 26(5):1032-1041, 2009.

[**14**] A. Yimit, K. Itoh, and M. Murabayashi. *Detection of ammonia in the ppt range based on a composite optical waveguide pHsensor.* Sensors and Actuators B 88:239-245, 2003.

[**15**] J. F. Fernandez-Sanchez, T. Nezel, R. Steiger, U. E. Spichiger-Keller. *Novel optical NO_2 selective sensor based on phthalocyaninato-iron(II) incorporated into a nanostructured matrix.* Sensors and Actuators B, 113: 630-638, 2006.

[**16**] E. D. Gaspera, M. Guglielmi, A. Martucci, L. Giancaterini, and C. Cantalini. *Enhanced optical and electrical gas sensing response of sol-gel based NiO ?Au and ZnO-Au nanostructured thin films.* Sensors and Actuators B, 1164: 54-63, 2012.

[**17**] S. Achmann, G. Hagen, J. Kita, I. M. Malkowsky, C. Kiener and R. Moos. *Metal-organic framework for sensing applications in the gas phase.* Sensors, 9: 1574-1589, 2009.

[**18**] D. N. Dybtsev, H. Chun, S. H. Yoon, D. Kim and K. Kim. *Microporous Manganese Formate: A simple metal-organic porous material with high framework stability and highly selective gas sorption properties.* Journal of American Chemical Society, 126:32-33, 2004.

[**19**] K. Kato and R. M. Strongin. *Chemomechanical polymers as sensors and actuators for biological and medicinal applications.* Sensors 7:1578-1611, 2007.

[**20**] KS. P. Sree, J. Dendooven, D. Smeets, D. Deduytsche, A. Aerts, K. Vanstreels, M. R. Baklanov, J. W. Seo, K. Temst, A. Vantomme, C. Detavernier, and J. A. Martens. *Spacious and mechanically flexible mesoporous silica thin film composed of an open network of interlinked nanoslabs.*Journal of Material Chemistry, 21:7692 - 7699, 2011.

[**21**] N. A. Yebo, P. Lommens, Z. Hens, and R. Baets. *An integrated optic ethanol vapor sensor based on a silicon-on-insulator microring resonator coated with a porous ZnO film.* Optics Express 18:11859 - 11866, 2010.

[**22**] D. Buso, G. Busato, M. Guglielmi, A Martucci, V. Gello, G. Mattei, P. Mazzoldi and M. L. Post. *Selective optical detection of H2 and CO with SiO2 sol- gel films containing NiO and Au nanoparticles.* Nanotechnology, 18: 475505, 2007.

[**23**] P. H Rogers and S. Semancik. *Development of optimization procedures for application-specific chemical sensing.* Sensors and Actuators B, 163:8-19, 2012.

[**24**] T. Sathitwitayakul , M.V. Kuznetsov, I. P. Parkin, and R. Binions.*The gas sensing properties of some complex metal oxides prepared by self-propagating high-temperature synthesis.*Material Letters, 75 :36-38, 2012.

[**25**] W. Cao and Y. Dua.*Optical fiber-based evanescent ammonia sensor.*Sensors and Actuators B, 110:252?259, 2005.

[**26**] B. J. Melde, B. J. Johnson and P. T. Charles.*Mesoporous silicate materials in sensing.* Sensors, 8: 5202-5228, 2008.

[**27**] T. Yokoi, H. Yoshitake and T. Tatsumi.*Synthesis of amino-functionalized MCM-41 via direct co-condensation and post-synthesis grafting methods using mono -, di- and tri- amino-organoalkoxysilanes.* Journal of Material Chemistry, 14:951-957, 2004.

[**28**] S. P. Sree, J. Dendooven, T. I. Korányi, G. Vanbutsele, K. Houthoofd, D. Deduytsche, C. Detavernier and J. A. Martens.*Aluminium atomic layer deposition applied to mesoporous zeolites for acid catalytic activity enhancement.* Catalysis Science and Technology. 1:218-221, 2011.

[**29**] X.Tang, J. Provenzano, Z. XU, J. Dong, H. Duanb and H. Xiao.*Acidic ZSM-5 zeolite-coated long period fiber grating for optical sensing of Ammonia.* Journal of Material Chemistry, 21:181, 2011.

[**30**] Y-C. Chang, H. Bai, S-N. Li and C-N. Kuo.*Bromocresol Green / Mesoporous Silica Adsorbent for Ammonia Gas Sensing via an Optical Sensing Instrument.* Sensors, 11:4060-4072, 2011.

[**31**] S. Tao, L. Xu and J. C. Fanguy.*Optical fiber ammonia sensing probes using reagent immobilized porous silica coating as transducers.* Sensors and Actuators B: Chemical, 115(1):158-163, 2006.

[**32**] M. R. Baklanov, K. P. Mogilnikov, V.G. Polovinkin, F.N. Dultsev.*Determination of pore size distribution in thin films by ellipsometric porosimetry.* Journal of Vacuum Science and Technology B 18:1385-1391, 2000.

[**33**] E. Feigenbaum, K. Diest and H. A. Atwater.*Unity-Order Index Change in Transparent Conducting Oxides at Visible Frequencies.* Nano Letters, 10:2111-2116, 2010.

[**34**] A. S. Negi, S. C. Anand.*A text book of physical chemistry.* Nano New Age International, 1985, p 723.

[**35**] A. Vorckel, M. Monster, W. Henschel, P. H Bolivar and H. Kurz. *Asymmetrically coupled silicon-on-insulator microring resonators for compact add-drop multiplexers* . IEEE Photonics Technology Letters, 15(7):921-923, 2003.

[**36**] K. S. Sing, D. H. Everett, R. A. W. Haul, L. Moscou, R. A. Pierotti, J. Rouquerol, T. Siemieniewska. *Reporting Physisorption Data for Gas/Solid Systems.* Pure & Applied Chemistry, 57:603-619, 1985.

4 Experimental settings

In this chapter, experimental settings used in this work for gas sensing measurements are discussed. Home built optical and gas handling setups are employed for characterizing the sensor prototypes.

4.1 Vapor generation and gas handling setup

Figure 4.1 schematically shows vapor handling system used to generate different vapor concentrations of volatile compounds. A homemade Teflon bubbler contains a liquid volatile compound of interest at a chosen operating temperature. The vapors are generated by bubbling the liquid with nitrogen or air. In most of the experiments, nitrogen is used as both a carrier and diluting gas. The carrier gas is passed through the bubbler and the saturated vapor is carried out of the bubbler to the gas sensing chamber. To maintain the bubbler at a fixed temperature and hence attain a target saturated vapor pressure, a refrigerated circulator water bath (Thermo Scientific DC10- K15)is used. The output flow rate of the vapor, F_{vapor} is given by the bubbler equation[1].

$$F_{vapor} = \left(\frac{P_{vapor}}{P_o - P_{vapor}} \right) F_c \tag{4.1}$$

where F_c is the carrier flow rate, P_{vapor} (mmHg) is the vapor pressure of the compound, and P_o is the outlet pressure in the bubbler headspace. The va-

por pressure, P_{vapor} at a given bubbler temperature is calculated with Antoine equation[1]:

$$\log P_v = A - \frac{B}{C+T} \tag{4.2}$$

where P_v is the vapor pressure, T is the temperature and A, B and C are compound specific empirical constants. The output of the bubbler is diluted with nitrogen to achieve a required level of vapor concentration. Flow meters are used to control the dilution level. The diluted vapor is carried to a gas chamber which contains the sensing chip for characterization. The gas chamber is connected to an exhaust for a continuous gas flow. The resulting vapor concentration, C_{vapor}(in parts per million) in the chamber is calculated by[1] :

$$C_{vapor}(ppm) = \frac{10^6 F_{vapor}}{F_d + F_c + F_{vapor}} \tag{4.3}$$

where F_d, and F_c are the dilution and the carrier flow rates respectively. Ethanol and xylene vapors studied in this thesis were generated using this bubbler technique. For experiments involving room temperature gases instead of volatile compounds, certified gas cylinders (Paraxair inc.) are used in place of the bubbling technique. NH_3, CO_2, CO are some of these gases used in the sensing experiments. High chemical resistance, high purity and low permeability PVDF (Polyvinylidene Flouride) tubing are are used in the gas flow system of the setup.

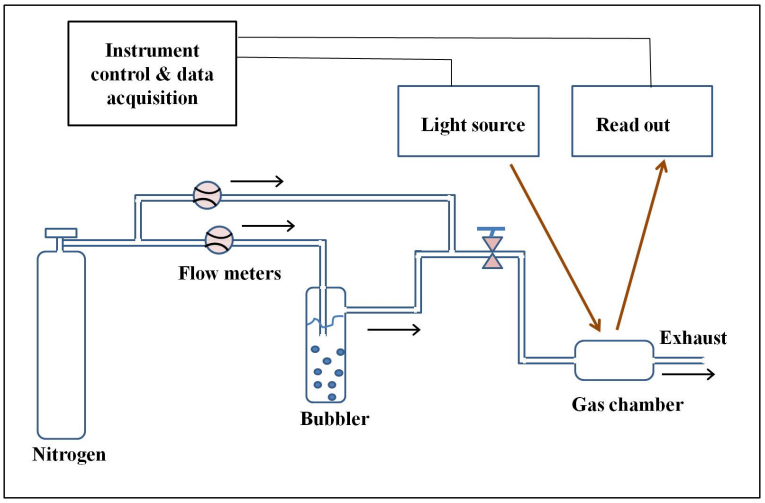

Figure 4.1: Schematic layout of the overall gas sensing setup.

4.2 Optical setup for gas sensor characterization

One of the practical issues in gas sensing experiments is efficient optical coupling to compact sensor chips while maintaining a confined gas environment around these chips. Two vertical-coupling setups are used to achieve this goal.

4.2.1 Fiber-to-infrared camera optical setup

The first optical setup is used in conjunction with a gas chamber which holds the sensor chip in it. The top side of the chamber is sealed with a transparent glass window through which light is vertically coupled in and out of the chip. The vertical spacing between the sample surface and the glass window is kept at about 2mm. The photograph shown in figure 4.2 shows the setup. An optical fiber positioned at 10° from the vertical couples light into the chip through the glass window. The output light is collected by an IR camera (Xenics-Xeva). IR camera read-out offers the advantage of simultaneous interrogation of multiple sensors on a chip.

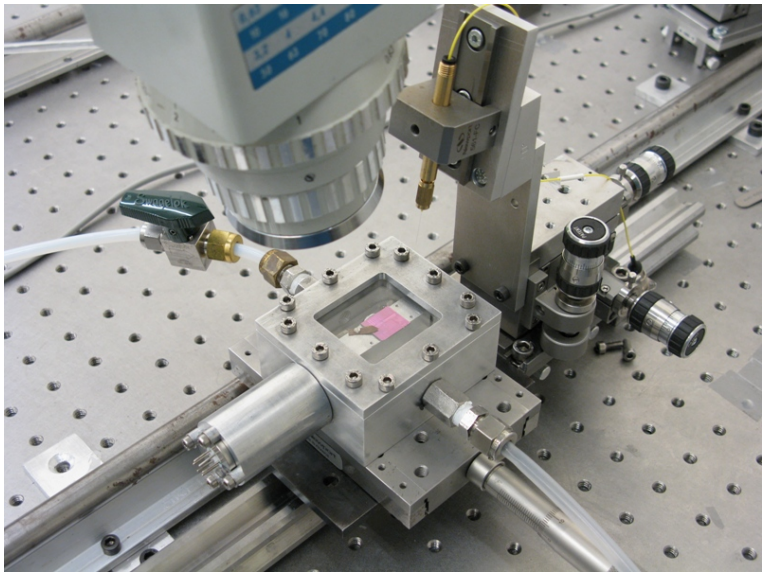

Figure 4.2: Vertical gas sensing setup with an IR camera readout.

4.3 Fiber-to-fiber optical setup

While the IR-camera setup is suitable for most gas sensing experiments conducted in this study, it has some limitations for noise sensitive measurements.

A large area on the chip is illuminated due to the relatively distant coupling through the glass window. Hence, significant scattering and reflection from the sample surface and the glass window introduces noise to the camera measurement. This could be unacceptable for sensor configurations involving measurements of small intensity changes such as absorption spectroscopy. A fiber-to-fiber vertical setup offers a better performance in this regard. A small gas cell glued on the sensing chip is used to achieve compatibility with the fiber-to-fiber setup. The gas cell, made of glass, is 9mm wide, 10mm long and about 5mm high. A UV curable glue (Norad -NEA121)is used to fix the cell on the silicon photonic chips. First the glue is spin coated on a clean substrate and transferred to the cell by press-stamping. Finally, the cell is aligned on the sensor chip and exposed to 100W UV light(Omnicure s1000) for 3min. The input and output grating couplers are left outside the gas cell for close coupling and read-out with optical fibers. Figure 4.3 shows the photograph of the fiber-to-fiber vertical gas sensing setup.

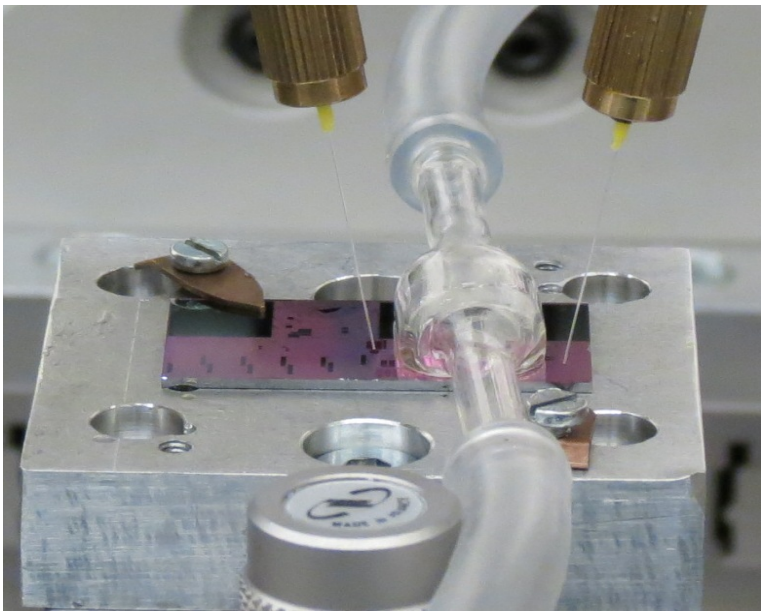

Figure 4.3: Vertical gas sensing setup directly coupled to input and output fibers.

4.4 Measurement instruments

Tunable laser
A high tuning resolution laser (Santec TSL-510) was used as a light source in most of the sensing experiments conducted in this thesis. The laser wavelength can be tuned with an accuracy of +/-5pm. This laser has a 130nm tunable range between 1500-1630nm and provides a maximum power of 10mW. Input powers used in most sensing experiments were typically below 2mW with the exception of gas spectroscopy experiments employed on long spiral waveguides.

Infrared camera
An infrared camera read-out was predominantly used in this thesis for the characterization of sensors based on microring resonators. The camera read-out allows a relatively convenient interrogation of a sensor contained within a sealed gas chamber. Moreover, the output from multiple sensors can be read-out simultaneously with this scheme. The digital Xenics-Xeva camera used here is sensitive in 0.9-1.7μm spectral band and has a frame rate of 50Hz.

Optical power meter
Optical power meters were used in several occasions to monitor power from the sensor chips. Preliminary tests on the optical chips prior to gas sensing were often conducted on a vertical fiber-to-fiber setup with a power meter read-out. Moreover, preliminary experiments on waveguide based gas spectroscopy discussed in chapter 9 were carried out using the fiber-to-fiber setup with a power meter unit. A Lightwave multimeter (Agilent 8153A) was used in these experiment.This meter has a power measurement range of 0.01pW -1W, and a data acquisition time of about 20ms/data point.

Heater
A cartridge heater(Redring -120-228) is embedded within the gas chamber discussed in section 4.2.1. The heater is connected to a temperature sensor and a digital temperature controller(Ormon Industrial). The heater allows sensor characterization at different temperatures. In this thesis this hating was mainly used for desorption of some sensors prior to the following experiments. The heater can be operated from room temperature to 120 °C.

4.5 Sensor characterization procedure

Prior to loading a sensor sample, the gas chamber is purged with a continuous gas flow of nitrogen for about 20-30 minutes. In experiments where thermal desorption is necessary, the sample bed is maintained at a higher tempera-

tures upto 120 °C by applying external voltage to an embedded cartridge heater. This evacuation step ensures that the chamber and the tubings are cleaned from residual gas traces from earlier experiments. Typically, a flow rate of 2-3 l/min was used for this evacuation step. The nitrogen flow is maintained after loading the sample, and the sensor output is monitored until a stable transmission spectrum is attained. For instance, for a microring resonator based sensor, the stability of the resonance wavelength is checked with continuous wavelength scan over a period of 10-20 minutes under nitrogen flow at room temperature. A steady state resonance within an accuracy of +/-10 pm is typically achieved with this procedure. This steady state condition is taken as a reference to the following experiments under gas exposure. The response of a sensor to different gas concentrations is measured with respect to the reference condition by varying the analyte (gas) flow while keeping a constant flow of the carrier gas(nitrogen). The response and recovery of a sensor is studied by manually turning on and off the gas flow while the laser is scanned continuously across the resonance wavelength of the sensor ring. The data handling software used in this thesis scans the laser with a rate of about 0.2 nm/sec. Typically the laser is swept over 2-4 nm span across the resonance. The laser is potentially tunable with scan rates as high as 100 nm/sec. Future optimization on data control and acquisition system would be beneficiary to achieve lower noise and more faster read-out. Commercial sensors for NH_3 and CO are kept in the vicinity of the test setup to monitor any possible gas related risks and hence ensure the safety of the measurement area.

References

[**1**] Y. Wang, Z. Zhou, Z. Yang, X. Chen, D. Xu and Y. Zhang. *Gas sensors based on deposited single-walled carbon nanotube networks for DMMP detection*. Nanotechnolgy, 20:345502(8pp), 2009.

5

Experimental study of metal oxide and polymer film coated silicon microring resonators for gas sensing

A few classes of materials have been frequently used for gas detection on different sensing platforms. Metal oxides are among these materials extensively studied and employed for gas detection with electrical sensing technologies [1-3]. Nevertheless, the potential and the limitations of metal oxides for optical gas sensing have been rarely investigated. On the other hand, stable, optically transparent and homogeneous organic materials are attractive for refractive index based optical chemical sensing. Some polymer materials have typically high affinity for organic vapors (VOCs), and at the same time, have properties suitable for optical applications. In this chapter, experimental studies on a metal oxide material, ZnO, and a polymer, Polydimethylsiloxane(PDMS), for integrated silicon photonic gas detection are presented. ZnO nanoparticles synthesized through colloidal chemistry are used as gas sensitive porous films on silicon microring resonators. High sensitivities for ethanol and xylene vapors, and CO gas are shown taking advantage of strong chemical affinity and high surface area offered by the ZnO nanoparticle films. Moreover, the potential of PDMS for reversible and fast detection of VOCs on silicon photonics chips is demonstrated. Critical performance measures including sensor selectivity, re-

versibility and response time are also discussed.

5.1 Ethanol vapor detection with a porous ZnO film coated silicon - on- insulator microring resonator

5.1.1 Introduction

A trend in current sensor development is miniaturization to obtain inexpensive and compact gas sensors that are robust and safe, have low power consumption and enable multiplexing of sensor arrays and remote sensing [4-6]. Furthermore, miniaturization opens a way to a chip level implementation, integration with other vital functionalities, and mass fabrication.

Gas sensors developed for miniaturization use various detection principles, like electrochemical, catalytic or optical detection [4, 6]. A widely used sensor concept is electrochemical sensing using the change of resistance of metal oxide semiconductors (MOS) upon gas adsorption [1-3]. However, MOS sensors often require operation at elevated temperature to achieve higher sensitivities. Therefore, high power consumption can be an issue with such sensors [7]. In addition, the sparking risks associated with the electrical contacts further make these sensors potentially unsafe for operation in explosive environments. Optical gas sensors have the potential to solve these problems. They can be operated at room temperature and often require no electrical connections[1]. So far, optical sensing has been dominantly achieved by means of optical fibers [5]. This, however, is an approach that does not readily lend itself for miniaturization and integration.

Silicon on Insulator (SOI) was recently proved to be a viable technology for a wide range of integrated optical applications [10-15]. Here, optical gas sensing by coating an SOI microring resonator (MRR) with a porous film of ZnO nanocrystals is explored. Using transducer chemical coatings on optical circuits is not uncommon in optical sensing [4, 5] since they strongly reduce the interaction length as compared to a direct spectroscopic gas analysis. Moreover, a proper choice of both the sensitive optical component and the chemical coating can lead to a significant enhancement in the sensor response. Chemical coatings made from metal oxides as used here have been extensively studied for electrical gas sensing applications [6-9], but not so much for optical gas sensing. Using a ZnO coated MRR, the detection of 100 ppm ethanol in air is demonstrated at room temperature and detection limit below 25 ppm is predicted. This result demonstrates the promise of a reasonably sensitive, compact and inexpensive optical gas sensors based on SOI technology.

5.1.2 Sensor structure and sensitivity estimates

Figure 5.1 a), b) and c)depict an SEM image of a 5 μm radius MRR, a schematic structure of a Si nanowire coated with a ZnO sensitive film, and a simulated profile of TE mode field propagating through the nanowire respectively.

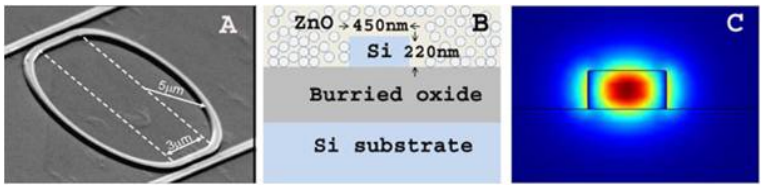

Figure 5.1: (a) A scanning electron microscope (SEM) image of an SOI MRR of 5ţm radius. (b) Cross section view of the SOI ethanol sensor structure. (c) TE mode electric field profile of a 450nm wide and 220nm high SOI waveguide with ZnO cladding , simulated with COMSOL Multiphysics.

The sensitivity and the detection limit of MRR based sensors depend on the quality factor, Q, and the confinement factor, Γ, of the MRR. High Q ring resonators have longer effective lengths due to the reduced propagation losses. This increases the effective interaction length with the surrounding leading to a raise in sensitivity. Moreover the minimum measurable or resolvable resonance shift, which determines the detection limit, is improved for high Q MRRs. The other important factor, Γ, measures the magnitude of the evanescent field extending outside the waveguides for the interaction with the surrounding[12]. The SOI MRRs used in this work have Q values higher than 25000. The effective interaction length, L_{eff} of a MRR depends on Q and Γ,where higher quality and confinement factors raise L_{eff} (eq.(5.1)) [14].

$$L_{eff} = \frac{\Gamma Q \lambda}{2\pi n_g} \tag{5.1}$$

To detect the concentration of gas molecules in an environment, MRRs can be functionalized by sensitive chemical coatings. The physical changes in such sensitive coatings can modulate the MRR resonance λ_{res} in different ways. For example, λ_{res} is affected by a change in refractive index of the coating through evanescent field interaction, or by a temperature increase of the MRR caused by a chemical reaction initiated in the coating [11, 13]. In fact, films of an adequate sensitivity are required to achieve detectable resonance shifts at low gas concentrations. In this respect, porous films offer a large surface area for gas adsorption, resulting in higher sensitivities [21].

In this work, the MRRs are coated with films of 3.5 nm ZnO nanocrystals for optical sensing of ethanol vapor. ZnO is an attractive material in this respect

due to its affinity to volatiles, low toxicity, convenience for doping, and low cost [8]. Moreover, ZnO is transparent in the near infrared around 1550 nm, enabling applications based on evanescent field interactions in SOI. Finally, literature results indicate that ZnO nanocrystalline films show a good electrical sensitivity to alcohols at lower operating temperatures [8, 9].

Figure 5.1(b) shows an impression of the cross section of the basic sensor structure of a MRR coated by a film of stacked nanocrystals. As these films are inherently porous, adsorption of ethanol by the ZnO nanocrystals may induce a MRR resonance wavelength shift due to evanescent field interaction. Using the Lorentz-Lorenz equation for a composite (porous) medium[19], we can estimate the refractive index of the ZnO coating. Assuming a porosity of 40% and a refractive index n_{ZnO} of 1.93, we obtain a value of 1.483. The resulting simulated electric field profile of the sensor structure, i.e., a 450 nm wide and 220 nm high SOI waveguide coated with the ZnO film, is shown in figure 5.1(c). Following this field profile, a confinement factor of 0.23 is calculated in the porous coating at 1530 nm. For a MRR evanescent wave sensor, the changes in mode effective index and the coating refractive index are directly related through [15]:

$$\frac{\Delta\lambda}{\lambda} = \frac{\Delta n_{eff}}{n_g} = \frac{\Gamma \Delta n_{coating}}{n_g} \tag{5.2}$$

Accordingly, a ZnO coating refractive index change lower than 1.4 x 10^{-4}, corresponding to a resonance shift less than 100pm, can be detected with a MRR sensor structure having this confinement factor and a Q value of 15,000. If we attribute the change in refractive index of the ZnO nanocrystal film upon adsorption to the partial filling of the pores by ethanol molecules, an estimate of the resonance wavelength shift can be obtained using once more the Lorentz-Lorenz equation. With a layer porosity of 40 % and assuming that 10 % of the pores are filled with ethanol (n=1.35), a refractive index change of the film of about 0.0172 is obtained, corresponding to a change of 4 x 10^{-3}. This leads to a MRR resonance shift of 1.2 nm at 1530 nm, which should be readily detectable. A group index of 4.96 calculated from the 15 nm free spectral range of the ZnO coated MRR is used in this estimation [17]. Importantly, the small changes in n_{eff} ensure that the wavelength shift measured is directly proportional to the volume of ethanol absorbed by the coating.

5.1.3 Sample Fabrication and Preparation

The MRRs with grating couplers have been fabricated with standard CMOS fabrication facilities. In practice, 193 nm deep UV photolithography in combination with dry etching is used to fabricate high Q (> 25000) resonators. The fabrication details are well documented in ref. [18,22].

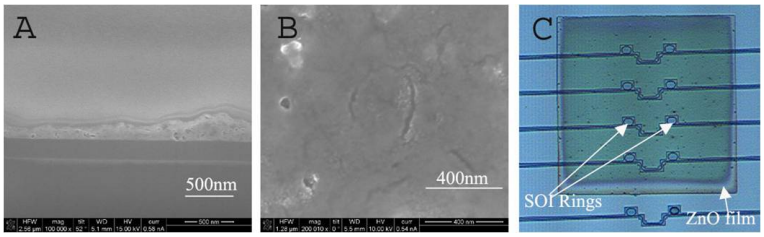

Figure 5.2: (a) SEM cross section view of a drop casted ZnO film on an SOI sample. (b) SEM image showing the top view of the ZnO film. (c) Optical microscope image of a ZnO nanparticle coating on SOI ring resonators.

The ZnO nanoparticles are synthesized following a low temperature synthesis technique [23, 24]. A 15 mL solution of 0.1 M, 99.99 % pure zinc acetate in dimethyl sulfoxide is vigorously stirred at room temperature and 5 mL of a 0.5 M solution of tetramethylammonium hydroxide (98 % pure) in ethanol is added drop-wise over a time span of 10-15 min. The resulting ZnO nanoparticles are precipitated by adding 40 mL of ethyl acetate. After centrifugation (2000 rpm/2min), the supernatant containing most of the unreacted precursor salts is removed and the remaining nanoparticles are resuspended in 20 mL of ethanol. Afterwards, they are washed a second time by adding 40 mL of a 1:1 mixture of ethyl acetate and heptane and again resuspended in 20 mL of ethanol to obtain a transparent and colorless suspension.

To facilitate the local deposition of ZnO nanocrystal films, negative photoresist (AZ 2070 from Micro chemicals) patterns are prepared on the SOI chip. This is done by 365 nm Ultra Violet (UV) photolithographic process. The patterned sample is finally baked at 140 °C for 2 min to make the photoresist resistant to the ethanolic suspension [24].To prepare sufficiently thick ZnO nanoparticle films, the nanoparticle suspension is drop cast on this patterned sample and allowed to dry in air for 15 min. Finally, lift-off of the photoresist is achieved by means of a 1-methylpyrrolidine solution at 80 °C, leaving porous local coatings around the ring resonators. Figure 2 shows the SEM and optical image of a roughly 200 nm thick ZnO film on MRRs. In spite of the non uniformity in film thickness and irregularities in morphology, the optical quality of these nanocrystal films is adequate enough for the work envisaged here. This is due to the fact that the film is thick enough such that the evanescent field does not interact with the rough surface. If required, the coating procedure can be adapted in future to make better quality films. After coating the ZnO film, the sample is heated at 100 °C for 2 min in order to make sure that all the ethanol (solvent) residue is removed.

5.1.4 Experimental results

The experimental setup discussed in section 4.2.1(chapter 4) is used for sensor characterization. The ZnO coated SOI chip is placed in a gas chamber whose top side is sealed with a transparent glass window such that light can be coupled vertically through it. A coupling fiber from a tunable laser (Santec TSL -510) is aligned to the input grating couplers at 10 degrees from the vertical. The light from the output gratings is collected with an IR camera (XenIcs Xeva - 511). Homemade software is used to control the laser and the camera, and to record the data. Different concentrations of ethanol vapor are obtained by bubbling a small volume of liquid ethanol with nitrogen. The vapor concentrations at different temperatures are estimated using the Antoine equation [25]. The bubbler is kept at low temperature (0 °C) in order to lower the ethanol vapor pressure. The resulting saturated vapor is diluted with nitrogen at different flow rates to adjust the ethanol concentration and the mixture is then allowed to flow through the chamber.

The SOI MRRS used here have measured Q values of ~ 26000 and 15000 before and after coating. Probably, this reduction in quality factor is related to scattering losses due to the imperfections of the drop cast ZnO nanocrystal film. However, a Q value of 15000 still corresponds to a MRR resonance bandwidth (full width half max) of approximately 100 pm, which is narrow enough to run our sensitivity measurements. Figure 5.3 represents the measured results of the

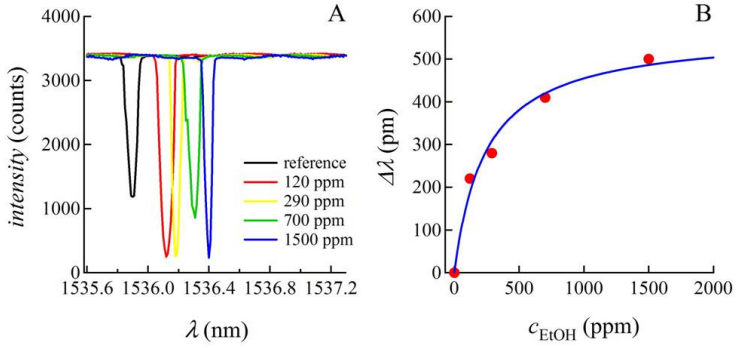

Figure 5.3: a). Measured transmission spectrum of the sensor as a function of ethanol vapor concentration. (b). The corresponding measured resonance shift at different vapor concentrations; the solid curve represents the theoretical fit based on Langmuir isotherm.

ethanol sensing experiments. Figure 5.3(a) shows the measured transmission at the through port of a MRR for different ethanol concentrations c_{EtoH} in nitrogen. One sees that exposure to ethanol leads to a redshift of the resonance wave-

length. This corresponds to an increase of the effective refractive index upon accumulation of ethanol in the ZnO film. Exposure to 1500 ppm of ethanol leads to a shift of 500 pm, a number that is in reasonable agreement with the initial rough estimate of 1.2 nm. Moreover, one sees that even at 120 ppm of ethanol, a pronounced shift of the resonance wavelength by 220 pm is measured. The corresponding sensitivity curve is shown in Fig. 5.3(b), where the markers indicate experimental datapoints and the trend line is a fit to a Langmuir isotherm. Assuming that the wavelength shift $\Delta\lambda$ is proportional to the volume of adsorbed ethanol, and writing the partial pressure p_{EtoH} of ethanol as $c_{EtoH}/10^6$ bar, this isotherm reads as:

$$\Delta\lambda = \Delta\lambda_{max}\frac{Kp_{EtoH}}{1+Kp_{EtOH}} = \Delta\lambda_{max}\frac{Kc_{EtoH}}{10^6+Kc_{EtOH}} \tag{5.3}$$

From the fit, we obtain an equilibrium constant K of about 4 x 10^3, corresponding to a free energy of adsorption of -20 kJ/mol, and a maximum wavelength shift of $\sim$ 560 pm. The good correspondence with the Langmuir model suggests the microporous nature of the ZnO film made from a colloidal suspension of 3 nm diameter particles. As discussed in section 3.3, Langmuir-like adsorption isotherm is typically observed in microporous materials. At the time of these experiments, 100 ppm was the lowest concentration we could achieve due to the limitations of cooling and the flow capabilities. However, using the Langmuir isotherm to interpolate the curve between 0 and 100 ppm, and considering the 100 pm resonance bandwidth of the ring, we estimate that a measurable shift of 50 pm is obtained at an ethanol concentration of 25 ppm. The sensor response with time at 300 ppm ethanol is shown in Fig. (5.4), where the markers indicate data points and the trend lines fits to exponentials. We find that the sensor reaches 90 % of its near-steady response within 15 seconds, while 80 % recovery with respect to the pre-ethanol exposure resonance wavelength is achieved within 6 seconds with adequate nitrogen flow (2 l/min) in the chamber. The fact that only a partial recovery of the sensor is achieved, as noticed on the figure, is likely due to a strong binding of ethanol on the ZnO surface.

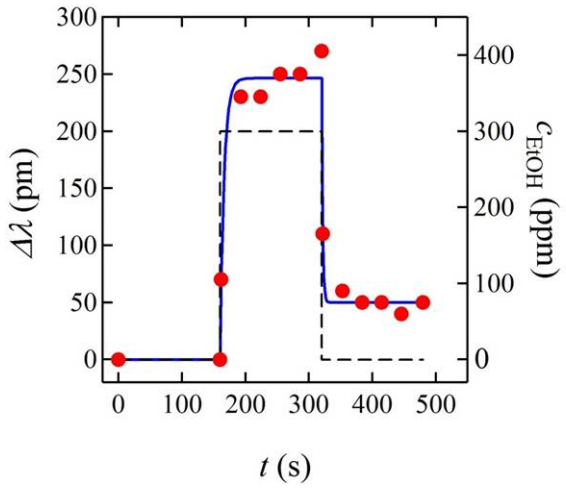

Figure 5.4: Sensor response with time for one on-off cycle at 300ppm ethanol vapor concentration. The solid lines are exponential fits at the rising (ON) and falling (OFF) edges of the response. The dotted line shows the switching between 0 (ON) and 300 ppm (OFF) ethanol.

5.2 Sensitivity of ZnO functionalized microring resonators for carbon monoxide gas

In this section, an experimental study on the sensitivity of ZnO functionalized silicon MRR for carbon monoxide is presented.

5.2.1 Sensor fabrication

The ZnO nanoparticle film is prepared following the procedure detailed in section 5.1.3. The thickness of the film studied here is approximately 110 nm. In this experiment, low concentrations are obtained by diluting 1000 ppm CO (Paraxair) with nitrogen carrier gas. The carrier gas flow is kept at about 2 l/min while the CO gas flow is varied.

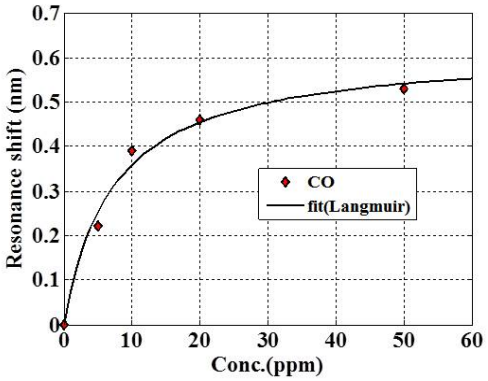

Figure 5.5: Measured resonance shift of ZnO coated MRR as a function of CO concentration .

5.2.2 Experimental results

Figure 5.5 shows measured resonance shifts when the sensor is exposed to CO in 0- 50 ppm range. The data is fitted to the Langmuir adsorption isotherm (R^2 = 0.992). The equilibrium constant and the maximum wavelength shift extracted from the Langmuir fit are 13.7 x 10^3 and 620 pm respectively. Over 3 times higher equilibrium constant obtained for CO as compared to ethanol (section 5.1) indicates a stronger affinity of the ZnO surface to CO. In general, this experimental result demonstrates that high refractive index sensitivities are achievable from metal oxide functionalized MRRs in response to interactions with gaseous molecules. The estimated linear sensitivity is ~ 40 pm/ppm. For a

measurement system able to resolve a 10 pm shift, the corresponding detection limit is approximately 0.2 ppm.

With a crude assumption that about 90 % of the pores are occupied by the gas molecules at the saturation pressure, the corresponding refractive index change can be estimated from the sensitivity curve in figure 5.5. For approximately 600 pm shift observed at the saturation, the refractive index within the pores estimated with Lorentz -Lorenz relation is about 83 % of that of a liquid CO. A 40 % porous film is assumed and a refractive index of CO $n_{CO} \sim 1.23$ at 78 K reported in the literature is taken in this estimation [26]. A partial recovery after exposure to CO is also observed in this experiment indicating typically strong binding of molecules on the ZnO surface.

5.3 Reversibility and selectivity of ZnO based sensors

Sensor reversibility is an important performance measure in some sensing applications. The experimental results discussed so far have shown that the ZnO films exhibit high affinity to gaseous and vapor molecules. This could be attributed to a high chemical reactivity of the ZnO surface resulting in strong binding of the gas molecules. Consequently, relatively slower gas desorption, and hence, recovery can be expected of this material. As indicated in 5.4, partial and relatively slow reversibility is typically observed. However, sensor recovery is of a minor importance in some sensing applications such as medical diagnostics where sample contamination needs to be avoided. Hence, irrespective of reversibility, low-cost silicon photonic sensors are of a potential role as disposable gas detection tools as long as other performance requirements are satisfied.

On the other hand, this experimental study has offered insights that metal oxide surfaces can be too reactive as to the level it can be difficult to distinguish the effect of one gas from another. This can pose difficulty for effective tuning of the surface with functional materials for selective gas detection. Attempts have been made to dope ZnO with transition metals Cu and Co, and an organic material, hemin. These functionalizations were intended to enhance selective responses for gases such as ammonia and nitric oxide. However, due to the high background sensitivity of the ZnO surface, no conclusive observations on the functionalization effects could be achieved so far.

5.4 Volatile organic compound sensitivity of PDMS and ZnO films

5.4.1 Introduction

Volatile organic compounds (VOCs) are released in gaseous form from a variety of solids and liquids of common industrial and household use. Some VOC emitting products include paints, cleaning supplies, building materials, copiers and printing machines, and pesticides. Typically, the concentrations of many VOCs are higher indoors than outdoors. VOCs are a wide variety of chemical compounds, of which some can have serious short and long term health impacts. Examples of VOCs include acetone, alcohols , ethylbenzene, xylene , and heptane. Health risks due to long term VOC exposure can be associated with potential carcinogenic, and neurotoxic effects of some these compounds. The harmful effects of most VOCs may be observed long after the primary exposure. On this account, monitoring of indoor VOCs levels is often required to ensure occupational safety in industries and workplaces where the risk of exposure to these compounds is high. Permissible exposure limits(PEL) for most VOCs are in the range of 50- 1000ppm [27].

In this section, experimental results on the potential VOC detection capabilities of functionalized silicon photonic chips are presented. As an extension to the ethanol vapor sensitivity detailed in section 5.1, the performance of the ZnO coated silicon microring resonator is discussed for volatile organic compound detection. On the other hand, polymer films such as siloxane containing chemicals, are attractive materials for optical VOC sensing applications[28-30]. PDMS is a commonly used hydrophobic rubbery material for VOC extraction from aqueous solutions and vapor phase mixtures[29,30]. It has been extensively employed in gas chromatography and solid-phase microextraction (SPME)[30]. It is a porous polymer with a good physical stability and processing properties suitable for the fabrication of ultra-thin films and membranes of high affinity for a range of organic VOCs including acetone, toluene, benzene, xylene, and chloroform[28-30]. Experimental comparison of the ZnO nanoparticle film and polydimethylsiloxane (PDMS) coated MRRs is made for potential VOC detection. Xylene is used to characterize the performance of the two sensors. This industrially relevant VOC has a permissible exposure limit of about 150 ppm[27].

5.4.2 Sensor fabrication and experimental settings

A PDMS base polymer with its curing agent (Dow Corning) is used to fabricate thin films on SOI MRRs. The uncured base polymer is mixed with the curing agent in a 10:1 ratio by weight and diluted in dichloromethane. For fabricating

approximately 150nm thick films, the polymer mixture is diluted with 1:1000 dilution ratio by weight. The resulting solution is spin coated on an SOI sample at 2000 rpm for 50 seconds. Finally, the sample is cured at 150 degrees for 10 minute.

The ZnO nanoparticle suspension is synthesized following the steps detailed in section 5.1.3 with some modifications to increase the nanoparticle concentration. Increasing the concentration allows fabrication of sufficiently thick films using a spin coating technique instead of drop casting discussed in section 5.1.3. As will be demonstrated in the forth coming sections, spin coated films can provide improved sensing performance in contrast to drop cast ones. In a typical synthesis, 0.5 M zinc acetate (which is 5 times higher than used for the drop-cast films) in 5 mL of dimethyl sulfoxide is vigorously stirred at room temperature and 8 mL of a 0.5 M solution of tetramethylammonium hydroxide in ethanol is added drop-wise and the two solutions are mixed for about 50-60 min. The resulting ZnO nanoparticles are precipitated by adding ethyl acetate. After centrifugation (2000 rpm/2min), the supernatant containing most of the unreacted precursor salts is removed and the remaining nanoparticles are re-suspended in 13 mL of ethanol. Afterwards, the suspension is washed a second time by precipitating with heptane and it is resuspended in 13 mL of ethanol. The ZnO nanoparticle concentration obtained with this procedure is around 180 - 200μ M. Films as thick as 150 nm are fabricated by spin coating multiple layers of this solution. Typically, 4 - 6 coating steps are applied. A spin coating speed of 2000rpm and an acceleration of 1400 rpm for 15 seconds is used for each coating step. About 10 seconds drying time is maintained between consecutive coatings. Different xylene vapor concentrations used in this study are generated by a bubbler setup described in section 4.1 (chapter 4). To lower the vapor pressure and hence operate at low xylene concentrations in 50- 400ppm range, the bubbler is kept at -8°C. The PDMS and ZnO coated MRRs are exposed to different concentrations of xylene and the response and recovery trends are studied.

5.4.3 Experimental results and discussions

Figure 5.6 shows experimentally obtained resonance shifts for 150nm thick PDMS film on silicon MRR. The sensor shows a linear sensitivity in the 0.1- 1% xylene concentration range. From the trend in figure 5.6, the estimated detection limit is lower than 500ppm. More remarkably, fast response and complete sensor recovery is achieved at different xylene concentrations in the above mentioned range. The response and recovery of the sensor with time is shown in figure 5.7. The sensor reaches its equilibrium response in less than 20 seconds and almost 100 % recovery is achieved in 40 - 60 seconds. Similar experiments

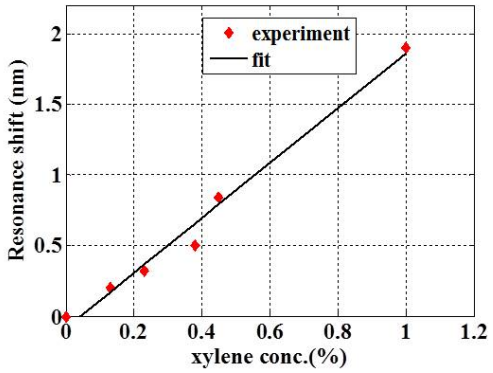

Figure 5.6: Measured resonance shift of PDMS coated MRR as a function of xylene vapor concentration.

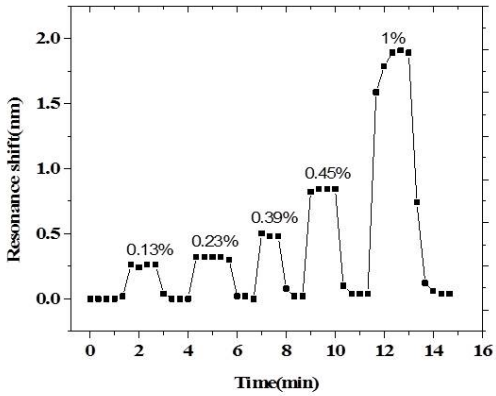

Figure 5.7: Response and recovery of a PDMS coated MRR as a function of time for 0.1-1 % xylene vapor .

have been conducted on a spin coated ZnO nanoparticle film on a silicon MRR. The results are shown in figure 5.8. In contrast to the PDMS coating, much higher sensitivity is attained from the ZnO film. A detection limit below 1ppm xylene is predicted from this result. The equilibrium response is reached in a similar time scale (20 seconds) as the PDMS film. However, only a partial recovery is observed confirming with typical ZnO characteristics. Only about 60 % recovery is reached after purging with nitrogen for about 13 minutes.

On the other hand, it is worth noting that the spin coated ZnO film has demonstrated far better performance as compared to the drop cast film studied in

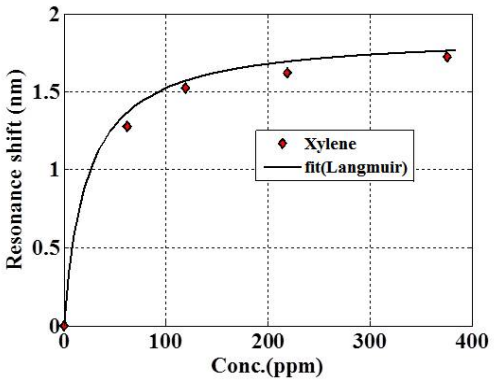

Figure 5.8: Sensitivity of ZnO nanparticle film coated MRR for xylene vapor in 50 -400ppm concentration range.

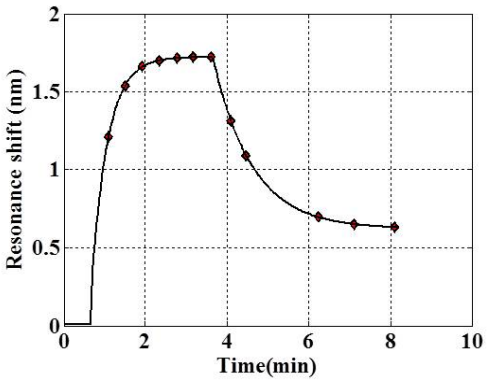

Figure 5.9: Response and recovery with time of ZnO coated MRR at ~ 380ppm xylene .

section 5.1 (ethanol sensor). Comparing the response time for drop cast (figure 5.4) and spin coated films (figure 5.9) it is observed that the spin coated film reaches equilibrium in a short time. On the contrary, gradual response build up was noticed from the drop cast film after the sensor has reached about 90 % (figure 5.4) of its equilibrium response for ethanol. The improvement in the sensor performance can be attributed to the film uniformity which allows fast and uniform access to the porous film surface. Consequently, increased sensitivity and faster response can be attained. Besides homogeneity, the film thickness is an important parameter in determining the sensitivity and the response time. In this sensor, an optimized thickness of ~ 120nm film is used as compared to ~

230nm film used for ethanol vapor sensing. As shown in figure 3.6 (chapter 3), the refractive index sensitivity of the silicon nanowire becomes less dependent on the film thickness as the film gets thicker than 150nm since the refractive index change in upper part of the film is no longer interacting with the evanescent field. Depending on the film homogeneity, the extra portion can hinder efficient gas diffusion to the interaction region, hence, lowering the sensitivity as well as slowing down the sensor response.

Despite the fact that the ZnO coating shows a superior VOC sensitivity, polymer coatings such as PDMS may be more preferable for practical applications. The highly reversible nature of the PDMS film allows low cost and long-life sensor implementation on silicon chips. Moreover, fast response and recovery demonstrated by these sensors offers opportunities for real-time VOC monitoring. In some applications such as in early warning systems for a class of hazardous VOCs, it may not be necessary that each VOC is selectively identified. Polymer functionalized silicon photonic sensors can have a valuable future role in such applications as cost effective and compact VOC detectors. Improvements in the detection limit and the sensor selectivity can potentially be achieved by employing polymer materials optimized for a given VOC sensing application. A commercially available general purpose PDMS polymer is used in this work. Future investigations may also address optimal optical designs for enhanced detection such as TM ring resonators.

5.5 Summary

In this chapter, the application of ZnO nanocrystal and PDMS films for silicon photonic gas sensing is presented. High sensitivities for volatile organic compounds, ethanol and xylene, as well as for CO gas have been experimentally demonstrated from ZnO functionalized MRRs. Sensitivities down to sub ppm gas concentrations are achieved. Typical response times for these sensors are in the range of 20-40 seconds. On the other hand, this study has provided an insight that metal oxide films as demonstrated here can be strongly responsive to a range of gaseous compounds, hence, being less suited for selective gas detection. Partial sensor recovery is another point typically observed for ZnO films. Consequently, such devices can be more suited for disposable sensing applications. It is also noticed that spin coated ZnO nanoparticle films of appropriate thickness exhibit speedy equilibrium response as well as higher sensitivities as compared to drop cast films. This could be attributed to enhanced gas diffusion as a result of film homogeneity and fairly optimal thickness.

Polymer materials, such as PDMS, are characterized by high affinities towards industrially and environmentally relevant organic vapors. PDMS coated MRRs have demonstrated attractive performance features for potential VOC sensing. Based on an experimental data obtained for ~ 150nm thick PDMS coating, a detection limit of ~ 500ppm is estimated for xylene vapor. Moreover, a remarkable reversibility and fast response is observed with this sensor. The response and recovery times are approximately 20 and 40 seconds, respectively. This result demonstrates the potential role of polymer functionalized silicon MRRs for low cost an real time VOC detection. Such sensors can be used to detect a given class of VOCs for early warning, for instance, in industrial work places. The relatively higher detection limit demonstrated here can potentially be improved by choosing proper coating materials optimized for a specific sensing application.

In conclusion, these experimental studies have demonstrated the feasibility of sensitive and fast gas detection on silicon photonic platform. Further improvements in performance features such as gas specificity can be achieved with chemical films tailored for a targeted sensing application.

References

[**1**] S. M. Kanan, O. M. El-Kadri, I. A. Abu- Yousef, M. C. Kanan. *Semiconducting Metal Oxide Based Sensors for Selective Pollutant Gas Detection.* Sensors, 9:8158-8196 , 2009.

[**2**] T. Sathitwitayakul, M.V. Kuznetsov, I. P. Parkin, and R. Binions. *The gas sensing properties of some complex metal oxides prepared by self-propagating high-temperature synthesis.* Material Letters, 75 :36-38, 2012.

[**3**] X. Wang, N. Miura, and N. Yamazoe. *Study of WO3-based sensing material for NH3 and NO detection.* Sensors and Actuators B, 66: 74-76, 2000.

[**4**] A. Airoudj, D. Debarnot, B, Beche, F. Poncin-Epaillard. *Design and Sensing Properties of Integrated Optical Gas Sensors Based on a Multilayer Structure.* Journal of Analytical Chemistry, 80:9188-9194, 2008.

[**5**] M. El-Sherif, L. Bansal, J. Yuan. *Fiber Optic Sensors for Detection of Toxic and Biological Threats.* Sensors 7:3100-3118, 2007.

[**6**] B. Timmer, W. Olthuis, A. van den Berg. *Ammonia sensors and their applications - a review.* Sensors and Actuators B, 107:666-677, 2005.

[**7**] I. Syhan, A. Helig, T. Becker, G. Muller, I. Elmi, S. Zampolli, M. Padilla, S. M. Marco. *Discontinuously operated Metal Oxide Gas Sensors for Flexible Tag Microlab Applications.* IEEE Sensors Journal, 8:176-181, 2008.

[**8**] X.L. Cheng, H. Zhao, L. H. Huo, S. Gao, J. G. Zhao. *ZnO nanoparticulate thin film: preparation, characterization and gas-sensing properties.* Sensors and Actuators, 102:248-252, 2004.

[**9**] A. Forleo, L. Francioso, S. Capone, P. Siciliano, P. Lommens, Z. Hens. *Synthesis And Gas Sensing Properties of ZnO Quantum dots.* Sensors and Actuators B, 146:111-115, 2010.

[**10**] P. Dumon, W. Boagerts, A. Tchelnokov, J-M. Fedili, R. Baets. *Silicon Nanophotonics.*Future Fab International 25:29-36, 2008.

[**11**] N. Jokerst, S. Palit, L. Luan, S. Dhar, T. Tayler. *Chip scale integrated microresonator sensing systems.*Journal of Biophotonics, 2:212-220, 2009.

[**12**] Y. Sun and X. Fan. *Analysis of ring resonator chemical vapor sensor development.*Optics Express, 16: 10254-102682, 2008.

[**13**] N. Yebo, D. Taillaert, J. Roels, D. Lahem, M. Debliquy, D. van Thourhout, R. Baets. *Silicon-on-Insulator (SOI) Ring Resonator Based Integrated Optical Hydrogen Sensor.* IEEE Photonics Technology Letters, 21: 960-962, 2009.

[**14**] A. Nikowsiki, L. Chen, M. Lipson. *Cavity-enahanced on-chip absorption spectroscopy using microring resonators.*Optics Express, 16: 10254-102682, 2008.

[**15**] J.T. Robinson, L. Chen, M. Lipson. *On-chip gas detection in silicon optical microcavities.*Optics Express, 16: 14296-4301, 2008.

[**16**] T. Claes, J. G. Morela, K. De Vos, E. Schacht, R. Baets, P. Bienstman. *Label-Free Biosensing With a Slot -Waveguide -Based Ring Resonator in Silicon on Insulator.*IEEE Photonics Journal 17:197-204, 2009.

[**17**] F.Y. Gardes, A. Brimont, P. Sanchis, G. Rasigade, D. Marris-Morni, L. O-Faolain, F. Dong, J.M Fedeli, P. Dumon, L. Vivien, T.F. Krauss, G.T. Reed, J. Marti. *High-speed modulation of a compact silicon ring resonator based on a reverse-biased pn diode.*Optics Express 17:21986-21991, 2009.

[**18**] P. Dumon, W. Boagerts, V. Wiaux, J. Wouters, S. Beckx, J. Van Campenhout, D. Taillaert, B. Luyssaert, P. Bientsman, D. Van Thourhout, R. Baets. *Low-loss SOI Photonic Wires And Ring Resonators Fabricated With Deep UV Lithography.*IEEE Photonics Technology Letters 16:1328-1330, 2004.

[**19**] B. J. Melde, B. J. Johnson, P.T Charles. *Mesoporous Silicate Materials in Sensing.*Sensors 8: 5202-5228, 2008.

[**20**] J. Kobler and T. Bein. *Porous Thin Films of Functionalized Mesoporous Silica Nanoparticles.* ACS Nano 2, 2324-2330, 2008.

[**21**] M. R. Baklanov, K. P. Mogilnikov, V.G. Polovinkin, F.N. Dultsev. *Determination of pore size distribution in thin films by ellipsometric porosimetry.* Journal Vacuum Science Technology B, 18:1385-1391, 2000.

[**22**] S. K. Selvage, P. Jaenen, W. Bogaerts, D Van Thourhout, P. Dumon, R. Baets. *Fabrication of Photonic Wire and Crystal Circuits in Silicon-on-Insulator using 193nm Optical Lithography.*Journal Lightwave Technology, 27:4076-4083, 2009.

[**23**] D.A Schwartz, N.S. Norberg, Q. P. Nguyen, J. M. Parker, D.R. Gamelin. *Magnetic Quantum Dots: Synthesis, Spectroscopy, and Magnetism of Co2+- and Ni2+-Doped ZnO Nanocrystals.* Journal American Chemical Society, 125:13205, 2003.

[**24**] P. Lommens, D. Van Thourhout, P. F. Smet, D. Poelman, Z. Hens. *Electrophoretic deposition of ZnO nanoparticles: from micropatterns to substrate coverage.*Nanotechnology, 19:245301, 2008.

[**25**] Y. Wang, Z. Zhou, Z. Jang, X. Chen, D. Xu and J. Zhang. *Gas sensors based on deposited single-walled carbon nanotube networks for DMMP detection.* Nanotechnology 20:345502, 2009.

[**26**] R. E. Gagnon, P. H. Gammon, H. Kiefte, and M. J. Clouter. *Determination of the refractive index of liquid carbon monoxide.*Applied Optics, 18(8): 1237-1239, 1979.

[**27**] Web address: http://www.osha.gov/

[**28**] L.I.B Silva, T. A. P Rocha-Santos and A.C Duarte. *Sensing of volatile organic compounds in indoor atmosphere and confined areas of industrial environments.*Global NEST Journal, 10(2):217-225, 2008.

[**29**] M. Peng, L. M. Vane, S. X. Liu. *Recent advances in VOCs removal from water by pervaporation.*Journal of Hazardous Materials B98:69-90, 2003.

[**30**] G. P. Perez and R. M. Crooks. *Pore-Bridging Poly(dimethylsiloxane) Membranes as Selective Interfaces for Vapor-Phase Chemical Sensing.*Journal of Analytical Chemistry, 76:4137-4142, 2004.

6

Selective and reversible ammonia gas detection with nanoporous film functionalized silicon photonic micro-ring resonator

6.1 Introduction

An attractive approach to achieve enhanced sensitivities from MRR based sensors is through application of high surface area coatings [1]. Materials with nano size pores, often termed as micro-porous (diameters smaller than 2 nm) and meso-porous (diameters from 2 to 50 nm), coated on optical MRRs offer significantly high surface area on pore walls for adsorption of gas molecules. As a result of the increase of adsorption capacity, very low detection limits could be attained. For specific gas detection, the surface of the porous coating can be functionalized chemically either directly during synthesis or via post-synthesis modification.

Ammonia detection draws a considerable interest with regard to environmental, industrial and medical perspectives. Ammonia levels in farming areas and industrial workspaces often need to be controlled to ensure occupational

health. Allowed exposure limit in such environments is about 20 ppm. On the other hand, breath ammonia has been recognized as a bio-marker for physiological disorders in humans [2]. For instance, a high correlation between blood urea nitrogen (BUN) and breath ammonia level in kidney patients has been reported [2]. The BUN test is currently the standard technique for monitoring kidney patients under dialysis treatment. However, this technique involves an invasive and lengthy laboratory procedure. As a consequence, there has been a growing interest for breath ammonia detection as a fast, real time and non-invasive alternative tool for medical diagnosis and health monitoring [2-5].

Different sensor technologies are available for NH_3 detection in various application areas. NH_3 sensors based on metal oxide semiconductors (MOS) have been frequently reported [6, 7]. Despite the potential for miniaturization and high sensitivities down to 10's of ppb levels, poor selectivity has been a common issue with metal oxide sensors [6, 8]. In addition, most MOS sensors need to be operated at higher temperatures up to 300 °C or higher, hence extra power consumption can also be an issue [7,8]. Sensors based on conducting polymers have also been demonstrated for sensitive and selective detection of NH_3 [3, 4]. Yet, the performance of such sensors has been limited by noticeably slow reversibility after exposure to NH_3 molecules [3, 4].

Optical and mass spectroscopic techniques exist for NH_3 detection [9-12]. Those techniques provide more reliable and selective measurements. However, the high complexity and large size of spectroscopic sensors obstruct their miniaturization, portability and manufacturing at low cost. Commonly, these sensors are bench - top instruments, thus, being less suitable for portable applications [9-12]. More recently, photoacoustic ammonia sensor based on a quantum cascade laser has also been demonstrated for breath ammonia detection [4]. Nevertheless, this device still remains complex due to the requirement for an expensive light source and phase sensitive (lock-in) instrumentation. With the potential to selectively detect sub ppm - ppb concentrations using chemically functionalized MRRs, silicon nano-photonic gas sensors can take advantage of their miniature feature and potentially low cost CMOS fabrication for portable sensing applications [13-18].

In this work, selective detection of gaseous ammonia with MRRs coated with acidic nanoporous aluminosilicate films is demonstrated. The early stage NH_3 sensor presented here shows fast, reversible, and selective response with respect to a potential interfering gas, CO_2. Two alternative approaches are used to functionalize the silicon MRRs with NH_3 selective acidic nanoporous aluminosilicate films. In the first route, an aluminosilicate microporous film inspired by the synthesis of zeolites was applied [19,20]. In the second approach, a mesoporous silica film is deposited and functionalized with aluminum using Atomic Layer Deposition (ALD). Fast and reversible response to NH_3 is achieved and

selectivity over CO_2 is obtained with both types of films. Literature on selective gas sensors on a photonic chip is very limited. To our knowledge, this is a first demonstration of fast, reversible and selective ammonia sensing on a silicon photonic chip using a porous functional coating. The potential of this sensor for a cheap, compact, portable and integrated breath ammonia monitoring instrument is discussed.

6.2 Sensor basics

The micro-ring resonators studied here are coated with porous aluminosilicate films for NH3 detection. The combination of aluminum and silicon in an oxide framework gives rise to Brønsted acid sites [21]. Since NH_3 is a base, it is expected to be strongly adsorbed on these films while acidic gases such as CO_2 will be less favored. Preferential adsorption of NH_3 molecules will lead to an effective refractive index change of the coated ring resonator. Figures 6.1(a) and (b) show a schematic cross section and a scanning electron microscope image of approximately 100 nm thick mesoporous silica film on a 5 μm radius silicon microring resonator, respectively.

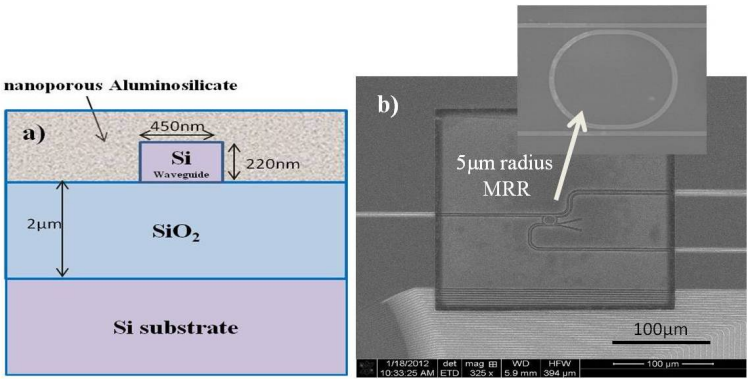

Figure 6.1: a) schematic representation of an SOI microring resonator cross section coated with a porous gas sensitive film (not drawn to scale) (b) Scanning Electron Micrograph of a 5 μm radius MRR coated by a mesoporous silica film (thickness ~ 100 nm);Inset:magnified view of the coated MRR.

6.3 Sensor design and fabrication

6.3.1 Design and fabrication of SOI MRRs

The silicon microring resonators used here for gas detection have a radius of 5 μm, and have been designed for operation in the telecom wavelength range near 1550 nm. The fabrication was done in a standard CMOS fabrication facility as detailed in [13, 16]. In order to localize gas sensitive coatings around the MRRs, the chips were photo-resist patterned. After the coating step, lift-off is used to remove the photoresist.

6.3.2 Mesoporous silica film deposition

The synthesis of mesoporous silica thin films was adapted from [22] which were inspired by the synthesis of Zeotile-4 ordered mesoporous silica material [23]. Zeotile-4 is a 3D ordered, powder silica material presenting multiple mesoporosity obtained as a result of secondary structuring of pre-fabricated silicalite nanoslabs using surfactant template [23]. While the powder material has a 3D ordered structure, the adaptations made in the synthesis presents to make smooth and homogeneous film resulted in an unordered mesoporous structure with accessible porosity [22]. In a typical film synthesis, first colloidal suspension of structured silica species (nanoslabs) was prepared by hydrolysis of tetraethylorthosilicate (TEOS) in aqueous tetrapropylammonium hydroxide (TPAOH) solution. After hydrolysis, water was added and the suspension is kept on stirring for 24 h. This nanoslab suspension was mixed with HCl and then combined with an acidified triblock copolymer solution. The resulting mixture was diluted with absolute ethanol and spincoated on photo resist patterned SOI samples. Then the films were hydrothermally annealed at 90 °C by keeping them in a closed autoclave containing slight amount of water. After drying, the photoresist was removed by a lift-off process and the films are calcined at 350 °C. Mesoporous silica films thus obtained were characterized with ellipsometeric porosimetry (EP) [22]. Figure 6.2 shows adsorption-desorption isotherm and pore size distribution obtained from EP measurements using toluene as the probe molecule. The shape of the isotherms with a clear hysteresis loop between the adsorption and desorption branches at higher partial pressures indicates the presence of mesopores. The high uptake of toluene which results in an increase in refractive index is a direct consequence of the high porosity of the mesoporous films. A typical film with thickness of ca. 150 nm showed a total porosity above 80 % with pores of ca.12-15 nm.

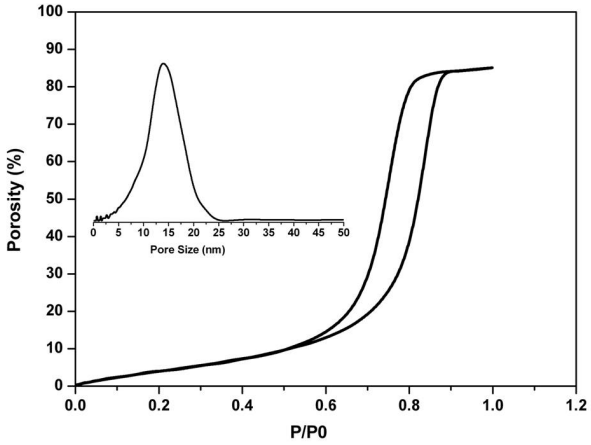

Figure 6.2: Toluene adsorption-desorption isotherms measured by Ellipsometric Porosimetry (EP) and mesopore size distribution (inset) of a calcined silica film which is representative of the mesoporous silica coating over the MRR prepared for further functionalization with Al ALD

6.3.3 Microporous aluminosilicate film preparation

The preparation of microporous films starts with the synthesis of nanoslabs doped with aluminum through the hydrolysis and polycondensation of TEOS in aqueous TPAOH solution. To introduce Al into the silicate structure, the TPAOH solution is first mixed with appropriate amount of aluminum metal powder. The amount of Al taken was such that the resulting material was expected to have a Si:Al atomic ratio of 100:1. The resulting clear solution was diluted with absolute ethanol and spincoated on photoresist patterned SOI samples. Finally, after the lift-off, the films are calcined at 350°C. The EP measurements (figure 6.3) show an adsorption-desorption isotherm presenting very strong uptake of toluene at very low partial pressures due to the capillary condensation of toluene in micropores. The absence of hysteresis revealed that the films were purely microporous. The pore size distribution calculated from the adsorption branch was centered at 1.2 nm. The microporous films with 100 nm thickness showed a porosity of ca.45% which is quite high for a microporous film specimen.

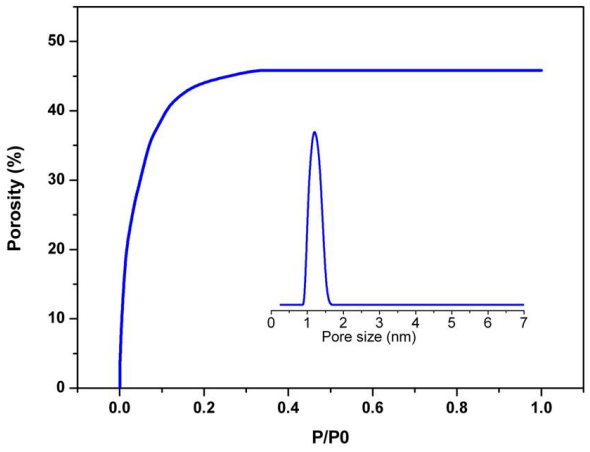

Figure 6.3: Toluene adsorption-desorption isotherms measured by Ellipsometric Porosimetry (EP) and (inset)mesopore size distribution of a calcined silica film which is representative of the mesoporous silica coating over the MRR prepared for further functionalization with Al ALD

6.3.4 Aluminum deposition on walls of mesoporous silica films using ALD

Atomic layer deposition of aluminum (Al-ALD) was used to introduce acid sites into the mesoporous films of section 3.2 [24-26]. ALD is a self-limiting thin film growth technique in which a substrate is exposed to chemical precursors and water in an alternating way [24]. The films in this work were treated in a home-built ALD reactor and subjected to 10 ALD cycles. Each ALD cycle involved two subsequent self-terminating half reactions. In the first half reaction, the sample is exposed to trimethylaluminum, TMA [$Al(CH_3)_3$, 97% purity, Sigma-Aldrich] vapor for 10 seconds, followed by 15 seconds evacuation of the reaction chamber. The second half reaction consists of a 10 second water vapor pulse followed by 15 seconds of evacuation under vacuum. The depositions were done at a temperature of 200 °C with TMA/H_2O pressures of 0.3 Pa. Before Al-ALD treatment the mesoporous film was evacuated in-situ at the ALD temperature. Following the ALD coating of the mesoporous silica the sample was exposed to ambient air prior to the sensing experiments.

6.4 Sensing experiments

An optical setup consisting of a small gas chamber, a tunable laser and an infrared camera is used for the sensing experiments [1, 16]. Before measuring the sensor response to NH_3 and CO_2, reference signals are recorded using pure carrier gas (nitrogen) flowing in the test chamber. Nitrogen is used as a carrier gas to dilute and introduce different concentrations of NH_3 and CO_2 gases into the test chamber. The sensitivity of the sensors to CO_2, an interfering gas in applications such as breath analysis [2, 12], was investigated in parallel so as to evaluate the selective response toward NH_3. The recovery of a sensor after exposure to a test gas is evaluated with just carrier gas flowing in the chamber.

The resonance shifts of the MRR with microporous aluminosilicate coating upon introducing a probe gas into the chamber at different concentration are shown in figure 6.4 (a). A well distinguishable sensitivity to NH_3 over CO_2 is observed in 0-800 ppm concentration range. The response to NH_3 fits well (R^2 = 0.9946) to Langmuir adsorption isotherm with a linear response extending to 200 ppm [1]. The good agreement with the Langmuir isotherm confirms the typical pseudo-Langmuir (Type-I) adsorption profile of microporous materials as discussed in section 3.3.3. The Langmuir equilibrium constant and the maximum wavelength shift calculated with this fit are ~ 13.5 x 10^3, and ~ 620 pm, respectively. In the studied concentration range, the response to CO_2 is low and saturates at only ~ 30 pm. The error bars represent 7-10% standard deviation observed over three measurements taken on the same sample. Interestingly, at a given NH_3 concentration, an equilibrium response is reached in less than 30 seconds while over 95% recovery is reached within 60 - 90 seconds. The response and recovery of the NH_3 sensor with respect to time fitted to exponentials is shown in figure 6.4 (b). A slight change of the base signal was observed after the first exposure while the responses to later NH_3 exposures almost fully recovered.

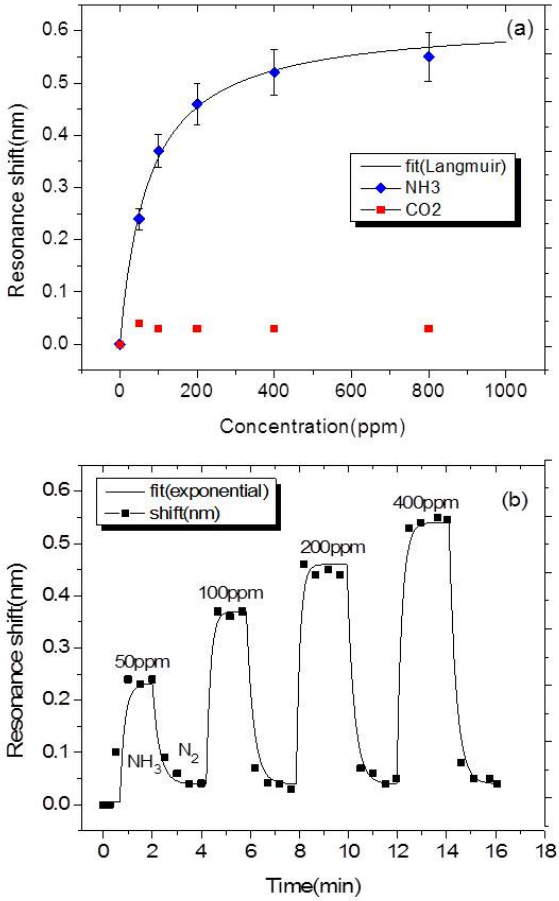

Figure 6.4: a) response from a microporous acidic film coated MRR (a) resonance shift with respect to NH_3 and CO_2 concentrations (b) response and recovery with time at NH_3 concentrations of 50,100,200 and 400 ppm introduced for two minutes.

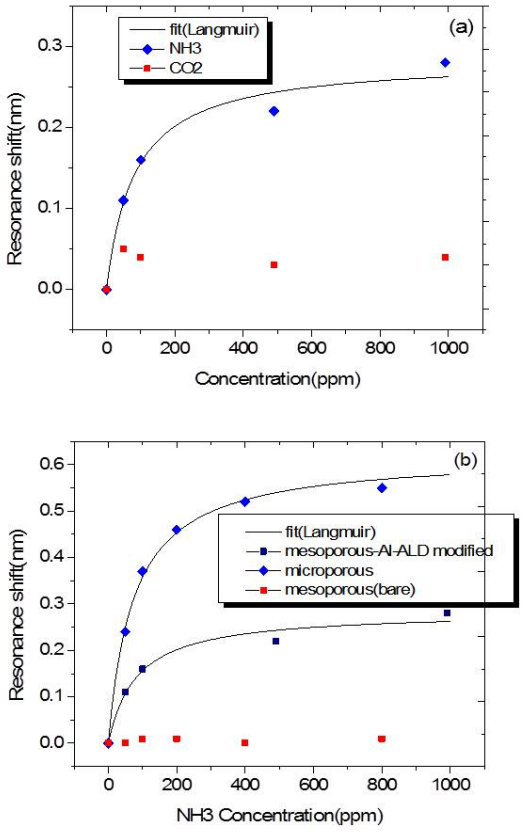

Figure 6.5: a) measured response from ALD modified mesoporous silica coated MRR upon saturation with NH_3 and CO_2 gases, (b) comparison of NH_3 sensitivity of microporous aluminosilicate film, and mesoporous silica film with and without Al-ALD.

As with the microporous coating, a selective response to NH_3 is also obtained using an MRR with mesoporous coating. The corresponding responses to NH_3 and CO_2 gases are shown in figure 6.5 (a). In contrast to the microporous film, the Al-ALD treated mesoporous coating showed a lower sensitivity to NH_3. This can have various reasons, such as a difference in exposed surface area, differences in acidity or hydration level. Further investigations will be needed to identify the critical physico-chemical parameters. The synthesis of porous coatings using the nanoslab approach and the variability of the Al-ALD process will enable fine tuning of the film response. Figure 6.5(b) summarizes the NH_3 sensitivities measured from the microporous aluminosilicate

film, mesoporous silica Al-ALD film, and non-functionalized mesoporous silica film. The bare mesoporous silica coating lacking aluminum showed almost no response to NH_3. The introduction of aluminum atoms in silicates via direct synthesis in the microporous films or via Al-ALD is responsible for acid sites generation and ammonia adsorption. In agreement with an earlier demonstration [25] our work confirms that acidity is essential for ammonia sensitivity.

The MRRs with nano-porous coating used here have resonance peaks of around 50pm FWHM corresponding to a quality factor of about 30,000. Taking into account this narrow resonance, the sensitivity trend shown in figure 6.4 (a), and the CO_2 interference level, a detection limit of about 5ppm is estimated. In this work such a low detection limit has been achieved using the microporous film. For applications such as breath NH_3 monitoring where 0.2 - 2 ppm levels need to be detected, the sensitivity of our sensors could be enhanced by optimizing the porous films with respect to porosity, Al content and hydrophilicity.

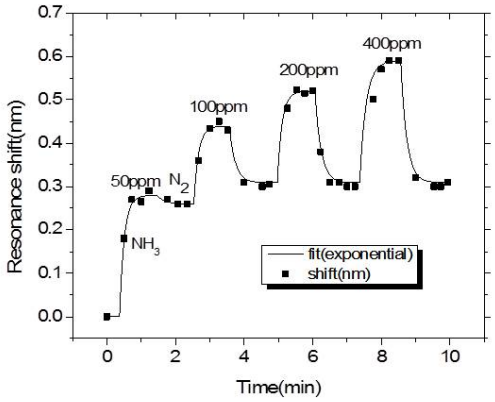

Figure 6.6: Response and recovery with time of a microporous aluminosilicate film after heating at 100 °C for 20min and cooling to room temperature in N_2 environment.

Besides the selective behavior, fast and reversible response observed in our sensors makes them attractive for various real time applications. Due to a strong binding between NH_3 and surface acid sites, earlier demonstrations based on acidic films were typically limited by very slow recovery [3,27]. To understand the possible physical mechanism behind comparably fast reversibility of our sensors, additional experimental studies were conducted. Noting that our sensor chips were stored in ambient environment before characterization, surface adsorbed water molecules could be present on the films. In all of the experiments discussed above, the samples have been tested without any pretreat-

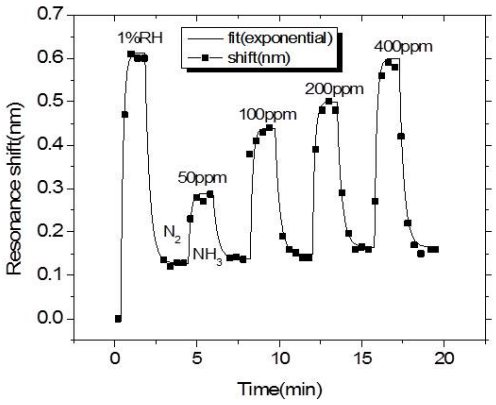

Figure 6.7: NH_3 sensitivity and recovery with time of a microporous aluminosilicate film coated sensor after thermal desorption followed by a short pre-humidification step with 1% RH.

ment except that the test chamber was purged with nitrogen flow before and after loading a sample. The presence of pre-adsorbed humidity could lead to relatively less strong binding of NH_3 on the acid sites.

In order to remove possible humidity content from the film, the sensor is kept inside the test chamber under nitrogen flow and preheated at 100°C. Then the sensor is characterized after cooling down to room temperature. As shown in figure 6.6, degradation in the sensor reversibility is observed especially during initial ammonia exposures. The removal of residual humidity from the film can allow NH_3 molecules to directly adsorb on the acidic sites, hence leading to stronger binding. The gradual reversibility pickup is likely due to a predominantly physical nature of later NH_3 adsorptions.

To confirm the effect of pre-adsorbed humidity on the sensor reversibility, a direct experimental evaluation has been run by exposing a dry sensor to humidity before applying NH_3. The following experimental steps have been used. First, NH_3 adsorbed during an earlier test was desorbed by heating at 200 °C for 10min in ambient condition. Afterwards, the sample is brought inside the test chamber and heated at 100 °C for 10 min under N_2 atmosphere to remove any humidity picked up during sample loading. After cooling to room temperature, the sensor is applied a brief exposure of 1% relative humidity (RH) for 5 min. Finally, the sensor was tested at different NH_3 concentrations. The measured response is shown in figure 6.7. More importantly, the sensor regained its reversible behavior after the pre-humidifcation procedure. Hence, it is indicated that a slight level of pre-humidification plays an important role in enhancing

sensor reversibility while maintaining selective response to NH_3 with respect to acidic gases such as CO_2. This behavior can be attributed to less strong and still selective NH_3 adsorption on protonated water molecules bound on the surface acid sites.

It is also noticed from these experiments that the sensors exhibit high sensitivity towards humidity. While strong interference from humidity is a common issue with most gas sensors, it can practically be solved by techniques such as employing external humidity filters on the gas route [4] or by tailoring the surface hydrophobicity. Future steps in this study would focus on sensitivity enhancement and evaluations against other potentially interfering breath gases.

6.5 Summary

In the previous chapter, the potential of rapid and sensitive gas detection on silicon photonic chips has been demonstrated. It was further indicated that specifically tailored materials can lead to selective gas detection. Developing on these results and the accompanying insights , selective gas detection capabilities of specifically functionalized silicon MRRs is demonstrated in this chapter. Alumino-silicate films obtained through a synthesis based technique as well as ALD are incorporated on silicon MRRs. Owing to Al atoms introduced into the silica framework, these films exhibit acidic surfaces suitable for preferential adsorption of gaseous bases such as NH_3. Sensitive, reversible and fast response to NH_3 and high selectivity with respect to CO_2 is achieved with these sensors. Equilibrium response is attained in less than 30 seconds and over 95% recovery is reached within 90 seconds. A detection limit of 5ppm is estimated for a microporous acidic films obtained via synthesis. A further improvement of the sensitivity could be achieved by optimizing the porosity and the surface properties of the porous alumino-silicate films. On the other hand , it is indicated that preadsorbed water vapor is responsible for relatively weaker adsorption of NH_3 on the acidic films which led to a reversible sensor response. This work demonstrates the high potential of on-chip optical gas sensors for ultra portable, low cost and real time gas detection in a wide range of applications including medical breath analysis.

References

[**1**] N. A. Yebo, P. Lommens, Z. Hens and R. Baets. *An integrated optic ethanol vapor sensor based on a silicon-on-insulator microring resonator coated with a porous ZnO film.*Optics Express, 18:11859-11866, 2010.

[**2**] L. R. Narasimhan, W. Goodman and C. K. N. Patel. *Correlation of breath ammonia with blood urea nitrogen and creatinine during hemodialyis.* PNAS, 98: 4617-4621, 2001.

[**3**] P. Heiduschka, M. Preschel, M. Rosch, and W. Gopel. *Regeneration of an electropolymerised polypyrrole layer for the amperometric detection of ammonia.* Biosensors Bioelectronics, 12(12): 1227-1231, 1997.

[**4**] A. D. Aguilar, E. S. Forzani, L. A. Nagahara, I. Amlani, R. Tsui and N. J. Tao. *A breath ammonia sensor based on conducting polymer nanojunctions.* IEEE Sensors Journal, 8: 269-273, 2008.

[**5**] R. Lewicki, A. A. Kosterev, D. M. Thomazy, T. H. Risby, S. Solga, T. B. Schwartz, and F. K. Tittel. *Real time ammonia detection in exhaled human breath using a distributed feedback quantum cascade laser based sensor.*Quantum Sensing and Nanophotonic Devices VIII, Proceedings of SPIE, 7945, 79450K, 2011.

[**6**] X. Wang, N. Miura and N. Yamazoe. *Study of WO3-based sensing material for NH3 and NO detection.*Sensors and Actuators B, 66:74-76, 2000.

[**7**] F. Winquist, A. Spetz and I. Lundstrom. *Determination of ammonia in air and aqueous samples with a gas-sensitive semiconductor capacitor.*Analytica Chimica Acta, 164:127-138,1984.

[**8**] P. H Rogers and S. Semancik. *Development of optimization procedures for application-specific chemical sensing.*Sens and Actuators B 163: 8-19,2012.

[**9**] A. B. Kanu and H. H. Hill Jr.. *Ion mobility spectrometry detection for gas chromatography.*Journal of Chromatography, 1177:12-27, 2008.

[**10**] V. Ruzsanyi, J. I. Baumbach , S. Sielemann, P. Litterst, M. Westhoff and L. Freitag. *Detection of human metabolites using multi-capillary columns coupled to ion mobility spectrometers.*Journal of Chromatography A, 1084: 145-151, 2005.

[**11**] C. Wang and A.B. Surampudi. *An acetone breath analyzer using cavity ringdown spectroscopy: an initial test with human subjects under various situations.*Measurement Science and Technology, 19: 1-10, 2008.

[**12**] J. Manne, O. Sukhorukov, W. Jäger and J. Tulip. *Pulsed quantum cascade laser-based cavity ring-down spectroscopy for ammonia detection in breath.*Applied Optics, 45:9230-9237, 2006.

[**13**] S. K. Selvaraja, P. Jaenen, W. Bogaerts, D. V. Thourhout, P. Dumon and R. Baets. *Fabrication of photonic wire and crystal circuits in silicon-on-insulator using 193nm optical lithography.*Journal of Lightwave Technology, 27:4076-4083, 2009.

[**14**] B. Jalali and S. Fathpour. *Silicon photonics.*Journal of Lightwave Technology, 24:4600-4615, 2006.

[**15**] K. De Vos, T. Claes, Y. D. Koninck, S. Popelka, E. Schacht, R. Baets, and P. Bienstman. *Multiplexed antibody detection with an array of silicon-on-insulator microring resonators.*IEEE Photonics Journal, 9: 225-235, 2009.

[**16**] N. A. Yebo, D. Taillaert, J. Roels, D. Lahem, M. Debliquy, D. Van Thourhout and R. Baets. *Silicon-on-insulator (SOI) ring resonator based integrated optical hydrogen sensor.*IEEE Photonics Technology Letters, 21: 960-962, 2009.

[**17**] A. Ramachandran , S. Wang, J. Clarke, S. J. Ja, D. Goad, L.Wald, E. M. Flood, E. knobbe, J.V. Hryniewicz, S. T. Chu, D. Gill, W. Chen, O. King and B.E. Little. *A universal biosensing platform based on optical micro-ring resonators.*Biosensors and Bioelectronics, 23: 939-944, 2007.

[**18**] R. Orghici, P. Lützow, J. Burgmeier, J. Koch, H. Heidrich, W. Schade, N. Welschoff and S. Waldvogel.*A microring resonator sensor for sensitive detection of 1,3,5-Trinitrotoluene (TNT).*Sensors, 10: 6788-6795, 2010.

[**19**] S. Eslava, M.R. Baklanov, C. E. A. Kirschhock, F. Iacopi, S. Aldea, K. Maex and J. A. Martens. *Characterization of a molecular sieve coating using ellipsometric porosimetry.*Langmuir, 23: 12811-12816, 2007.

[**20**] A. M. Doyle, G. Rupprechter, N. Pfander, R. Shlogl, C. E. A. Kirschhock, J. A. Martens and H. J. Freund.*Ultra-thin zeolite films prepared by spin-coating silicalite-1 precursor solutions.* Chemical Physics Letters, 382:404-409, 2003.

[**21**] G. J. Kramer, R. A. Van Santen, C. A. Emeis and A. K. Nowak . *Understanding the acid behavior of zeolites from theory and experiments.* Nature 363:529 - 531 ,1993.

[**22**] S. P. Sree, J. Dendooven, D. Smeets, D. Deduytsche, A. Aerts, K. Vanstreels, M. R. Baklanov, J. W. Seo, K. Temst, A. Vantomme, C. Detavernier and J. A.

Martens. *Spacious and mechanically flexible mesoporous silica thin film composed of an open network of interlinked nanoslabs.* Journal of Material Chemistry, 21: 7692-7699, 2011.

[**23**] C. E. A. Kirschhock, V. Buschmann, S. Kremer, R. Ravishankar, C. J. Y. Houssin, B. L. Mojet, R. A. van Santen, P. J. Grobet, P. A. Jacobs and J. A. Martens. *Zeosil Nanoslabs: Building Blocks in nPr4N+- Mediated Synthesis of MFI Zeolite.* Chemie International Edition, 40:2637-2640, 2001.

[**24**] S. M. George. *Atomic Layer Deposition.* Chemical Review, 110: 111-131, 2010.

[**25**] S. P. Sree, J. Dendooven, T. I. Korányi, G. Vanbutsele, K. Houthoofd, D. Deduytsche, C. Detavernier and J. A. Martens. *Aluminium atomic layer deposition applied to mesoporous zeolites for acid catalytic activity enhancement.* Catalysis Science and Technology, 1:218-221, 2011.

[**26**] C. Detavernier, J. Dendooven , S. P. Sree, K. F. Ludwig and J. A. Martens. *Tailoring nanoporous materials by atomic layer deposition.* Chemical Society Review, 40:5242-5253, 2011.

[**27**] X.Tang, J. Provenzano, Z. XU, J. Dong, H. Duanb and H. Xiao.*Acidic ZSM-5 zeolite-coated long period fiber grating for optical sensing of Ammonia.* Journal of Material Chemistry, 21:181, 2011.

7

On chip interrogation of microring resonator gas sensors

7.1 Introduction

Today, integrated spectrometer devices are essential components in wavelength division multiplexing applications. Besides their dominant use in these data communication areas, on-chip wavelength resolving devices can have outreaching benefits in diverse optical applications. In this chapter, the potential role of on-chip spectrometers as inexpensive read-out components for silicon photonic bio/chemical sensors is discussed. A brief overview of integrated spectrometers followed by the basic operation principles is presented in the first few sections. Later on, state of the art implementations of these devices for off-chip and on-chip sensor interrogation are overviewed. Finally, the design and experimental study of an arrayed waveguide grating spectrometer for the interrogation of a silicon microring resonator based gas sensor is presented.

The two types of planar waveguide spectrometers which have gained interest in the WDM communication networks are arrayed waveguide gratings (AWGs) and echelle gratings. Even if planar spectrometers, especially AWGs, have been popular and widely used in telecom applications, the utilization of these devices for other applications has been limited. One of the main setbacks has been the limited wavelength resolution offered by the current inte-

grated spectrometers. On the other hand, compact and monolithic on-chip spectrometers capable of providing high-resolutions suitable for sensing applications such as Raman, infra-red spectroscopy and wavelength shift monitoring are of a considerable potential to advance the field of integrated optical sensors. Such spectrometers, integrated with compact sensing units, can have a considerable role in bio-medical and environmental applications as low cost and portable detection tools.

7.2 State of the art on chip spectrometers

As mentioned earlier, AWGs and echelle gratings (also called planar concave gratings (PCGs)) largely lend themselves for on-chip spectrometery. Particularly, AWGs have dominated the planar spectrometer market mainly due to the relative ease of fabrication [1]. In contrast, echelle gratings have been limited by critical fabrication requirements for high quality vertical grating facets. The losses in this device can be beyond acceptable levels for practical applications if this fabrication precision is not met. However, recently progresses in the fabrication of PCG devices have been made and performance improvements have been demonstrated [2,3]. Both AWGs and PCGs can be used for various applications to resolve a broad spectrum into distinct wavelength channels.

AWG (de-)multiplexers are implemented using planar waveguides as both imaging and dispersive elements. These devices image an optical field at the input waveguide onto an array of output waveguides such that different wavelength components of the input field are collected at different output waveguides. Planar concave gratings, on the other hand, play a role of a diffraction grating on a chip. An input light diverges through a slab waveguide region and illuminates the grating. Light of distinct wavelength components is diffracted backward and is focused on a region where the output waveguides are situated. The images of these two devices are depicted in figures 7.1 and 7.2. The basic principles behind the two devices are similar. Both devices combine focusing functions with dispersion. Both AWGs and PCGs use slab regions to focus or refocus light in and out of the dispersive units. In PCGs, the grating teeth provide phase delays where as in AWGs the phase delay is achieved by array waveguides of incremental delay length which split the input light.

Low index contrast material systems, particularly, the silica-on-silicon platform have been most widely used for the implementation of planar spectrometers[4]. The popularity of these systems has been mainly due to the convenience for efficient coupling with optical fibers and the low insertion loss. However, the size of these devices is prohibitively large since bigger waveguide structures are required to sufficiently confine the propagating light and ensure low loss performance[4]. More recently, semiconductor material systems exhibiting high

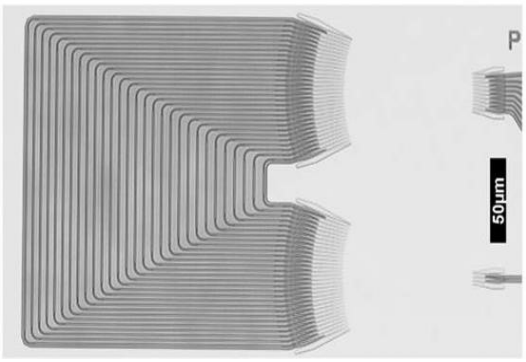

Figure 7.1: A microsope of image of an SOI Arrayed waveguide grating.

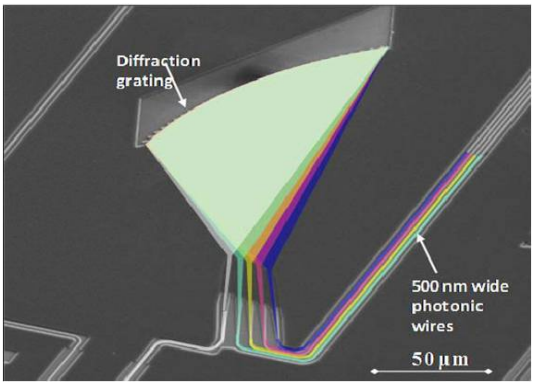

Figure 7.2: An SEM image of an SOI planar concave grating. The colorful art portrays the wavelength spiliting property of the device.

index contrast between the core and cladding material have drawn an increasing interest for on chip spectrometer implementation. Silicon on insulator, and InP material systems are the two examples of such material platforms[4-7]. Particularly, the silicon on insulator structures offer an immense potential for high integration and cost effective fabrication exploiting the well established CMOS fabrication.

AWG and PCG spectrometers have been demonstrated on SOI platform. Highly compact AWGs with wavelength resolutions ranging from 0.8nm - 3.2nm, and with insertion loss as low as 1.1 dB and cross talk level of -25dB have been demonstrated. An approximate footprint of only 0.07 mm^2 has been utilized to implement these devices with 8 channels [7]. High resolution and large channel count AWG has also been reported [5]. This AWG has 50 channels and 0.2nm channel spacing. However, the device footprint and the insertion

loss are yet to be improved for this particular device demonstration.

Fabrication progress on SOI PCG spectrometers has also been made in the recent years. Highly compact SOI PCG spectrometer fabricated with CMOS tools has been reported [1]. This device has 4 channels spaced by 20nm and takes a footprint of about 0.04mm^2. By employing second order Bragg reflectors on the grating facets, significant improvement in the insertion loss is achieved. The measured insertion loss is 1.9dB and a cross talk level better than -25dB is achieved from the same device. A 12 channel echelle grating with 8nm channel spacing and a 5.5nm flat passband has also been demonstrated recently[2]. The reported on-chip loss for this device is 1.7dB and the cross talk is better than 25dB. In this demonstration, sensitivity to facet verticality is reduced by arranging the ouput waveguides close to the zero degree angle of the echelle grating. More recently, an 8 channel PCG with 3.2nm channel spacing is demonstrated on 0.05mm^2 footprint. The channel to channel isolation of this device is 19dB [3].

In general, while both the PCG and AWG spectrometer configurations on SOI platform promise high future potentials, the current state appears to indicate that AWG spectrometers can be of a more immediate use for higher channel count and narrow channel spacing applications.

Other classes of configurations proposed for on chip spectrometer implementation are based on microresonators. Z. Xia et. al. recently demonstrated a possible implementation of high resolution on-chip spectrometer using a large scale array of microdonut SOI resonators[8].The spectrometer shows a linewidth of $\sim$ 0.6nm with an operating bandwidth of $\sim$ 50nm. This high resolution and bandwidth is achieved in a compact size using miniaturized microdonut resonators (radius $\sim 2\mu$m) with a high quality factor, single-mode operation, and a large free spectral range. As compared to dispersive spectrometers typically limited by the trade-off between size and resolution, microresonators are proposed to provide high resolution on small footprints. However the fabrication of arrays of microresonators with high perfection to meet specified operating wavelengths and precise detuning from each other has been a major challenge. This demonstration indicated that, an added freedom to adjust the inner and outer diameters of microdonut resonators could provide a better control over the resonance behavior. A total number of 84 microdonut resonators are used to cover the operation bandwidth without excessive overlap among the neighboring resonances.

In addition, an on-chip spectrometer device using combined functionalities of a microring resonator and a planar diffraction grating was proposed on SOI platform[9]. In this configuration, a ring resonator is used to pre-filter the input light such that the diffraction grating output will have narrower passband. Using this technique, a 100 channel spectrometer with a 0.1nm channel spacing

is demonstrated on 2mm^2 footprint. The channel density is increased by time-serialization of the measurements. A heater is used to align the FSR of the ring with the diffraction grating transmission peaks. Time serialization is achieved also by thermo-optically tuning the ring resonance. However , the insertion loss for this device reaches up to −23dB. In addition, the active tuning used in this approach can introduce extra device complexity.

7.3 Sensor interrogation with on-chip spectrometers

The interrogation of refractive index sensors in wavelength domain provides a number of advantages with respect to intensity interrogation. First, it readily lends itself for multiplexing of sensor arrays. Secondly, it provides immunity from intensity noise whereby providing opportunities for highly sensitive detection. More specifically, SOI micro resonator sensors operated in refractive index sensing configuration offer superior sensitivities to the surrounding. These devices have increasingly become appealing for trace gas and biomolecule detection. However, current wavelength interrogation based sensing systems are typically characterized by bulky and costly instrumentation [10-12]. An external tunable laser source or the combination of a broadband source and a high - resolution spectrometer are usually employed. As a result, the size and cost benefits of on chip sensors are overshadowed by these external units.

Despite a few efforts made so far, more progress and novel solutions are highly required to realize cost effective and portable ring resonator sensors. Operating with fixed wavelength laser and monitoring the intensity variation with the wavelength shift can be one alternative. However, this imposes several stringent requirements on the laser specification as well as on the overall operating conditions. A laser source with a narrow bandwidth and high stability would be required to comply with this approach. Such an interrogation scheme can significantly limit the dynamic range of the sensor. Moreover, effects such as temperature fluctuations can easily misalign the ring resonance from the laser wavelength.

Recently, an on-chip interrogation of a ring resonator sensor with a cascaded reference-sensor configuration has been proposed[13]. In this scheme, a broadband light source instead of an expensive tunable laser source is used. The FSRs of the two rings are designed such that a periodic envelope of much larger FSR than that of the two rings is created due to a vernier effect. The peak intensity of the envelope changes as the sensor ring resonance shifts. The change in the overlap between the source spectrum and this envelope is used as a measure to the wavelength shift. In this demonstration, the ratio of the sensor and the

reference signal is taken to cancel out the noise due to intensity fluctuations. The authors theoretically estimate that a sensitivity in the order of 2 x 10^4 dB /RIU can be achieved with this approach for TM mode SOI rings. This corresponds to a detection limit of about 5 x 10^{-7} RIU when the FSRs of the two rings are well aligned. However, for such a sensitive operation, the mis-alignment between the two FSRs is required to stay below 1% or the performance will be lower. The other requirement is that the envelope spectrum is well in the vicinity of the source spectrum so that the shift can be tracked with the overlap between the two spectra. This requirement for a fabrication precision can be a practical challenge in such an interrogation technique. A narrow linear dynamic range might also be another limiting issue.

An alternative approach can be the use of on chip spectrometers such as PCGs and AWGs for the interrogation of ring resonator sensors. These spectrometers employed with cheap broadband light sources, such as superluminescent LEDs, can significantly cut down the size and cost of current microring resonator based sensors. Particularly, viable application of AWGs for the wavelength shift interrogation has been demonstrated. It has been demonstrated that a thermally tuned arrayed waveguide grating can measure a wavelength shift from a Fiber Bragg Grating sensor [14]. In this approach, the AWG spectral response is thermally tuned such that it is aligned with the FBG response. Since the AWG spectral shift is known for a given applied heating, it can be used as an indirect measure for the FBG response shift. A 32 channel, a 0.8nm channel spacing AWG was used in this demonstration. Active tuning involved in this technique can be a limiting factor as it adds to the device complexity, energy consumption and response time.

In another approach, it is proposed that an AWG can be used as both a demultiplexer to multi-FBGs and an array of edge filter to interrogate wavelength shifts from these FBGs in a distributed sensor system[15]. This scheme uses a pair of AWG channels to measure wavelength shifts from each FBG in the distributed system. The FBG spectral peak overlaps with two AWG adjacent channels. The intensity ratio between the two channels changes with the FBG response shift and it is used as a read-out mechanism.

More recently, a high resolution AWG based wavelength interrogation device fabricated on a silicon on insulator platform has been demonstrated[16] . This AWG is designed with 50 channels and a 0.18nm channel spacing. Taking advantage of the high index contrast waveguide platform, the device is implemented on relatively small footprint. The spectrometer is used for an interrogation of a tilted fiber Bragg grating(TFBG) refractometer. It is demonstrated that this device can simultaneously monitor two widely spaced TFBG resonances with high resolution of about 1.2pm.

However, the application of planar AWG spectrometers so far has been lim-

ited to the interrogation of fiber based sensors. On the other hand, provided their integrated nature, these spectrometers lend themselves for direct implementation with on-chip optical sensor devices. In this work, an arrayed waveguide grating spectrometer is demonstrated as an alternative approach for the interrogation of silicon microring gas sensors. An interrogation technique utilizing an intensity ratio measurement of two neighboring adjacent channels is adopted. This approach is attractive as it provides immunity from noise due to source intensity fluctuation. It further offers possibilities for interrogation of multiple ring resonator sensors since a pair of AWG channels can monitor each sensor.

7.4 AWG basics and design for wavelength interrogation

7.4.1 Basics

An AWG, schematically shown in figure 7.3 consists of an array of waveguides with incremental phase delay between the waveguides . At the input and output sides, star couplers bridge the array waveguides with the input and output waveguides. The wavelength dependent phase difference between the aperture on the grating line is controlled by a length difference between the arrayed waveguides. Focusing of the field propagating in the array waveguides is achieved if the optical path length difference between consecutive waveguides is equal to the integral multiple of the wavelength as given by (7.1)

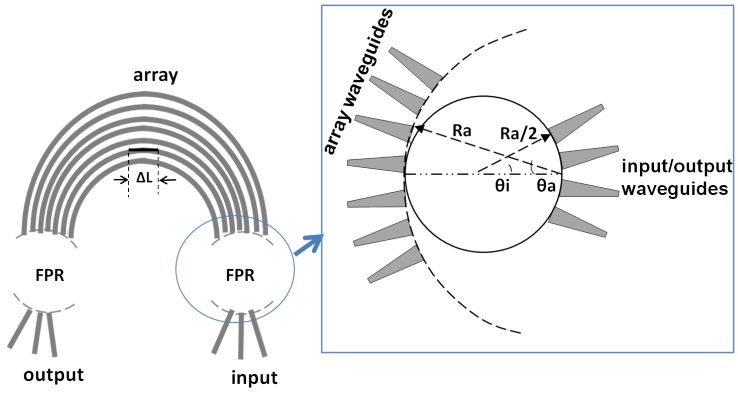

Figure 7.3: A schematic representaiton of an AWG structure.The inset shows a Rowland mounting configuration of the array and input/output waveguides .

$$\Delta L = m \cdot \frac{\lambda_c}{n_{eff}} \tag{7.1}$$

Where ΔL is the delay length, λ_c is the central wavelength , n_{eff} is the effective index of an array waveguide, and m is an integer called an array order. Under this condition, the array waveguide functions as a lens with image and object planes at a distance R_a of the array apertures. The focal line which defines the image plane follows a circle with radius $R_a/2$ and the input and output waveguides are mounted on this line at the respective side of the array waveguide. This geometry is called land mounting.

The phase difference phase difference between array waveguides due to the length increment ΔL can be given by :

$$\Delta\phi = \frac{2\pi f n_{eff}}{c}\Delta L \tag{7.2}$$

The delay length, ΔL along with the propagation length difference in the star couplers, defines the wavelength of maximum transmission between a pair of input/output ports.

Assuming the input and output ports in a diagonal configuration ($\theta_o = -\theta_i$),the angular dispersion at the output ports in terms of the propagating light frequency is given by

$$D_\theta = \frac{d\theta_o}{df} = -\frac{n_g \Delta L}{f n_{FPR} R_a \Delta\alpha} \tag{7.3}$$

Where θ_o is the output angle, f is the frequency, n_g is the group index, R_a is the radius of the grating line, $\Delta\alpha$ is the angular pitch of the grating arms, and n_{FPR} is the effective index in the slab(free propagation) region.

For Rowland mounting shown in the figure 7.3(inset), the linear dispersion on the grating line can be deduced from the above equation and is given by

$$D_l = -\frac{n_g \Delta L}{f n_{FPR} \Delta\alpha} \tag{7.4}$$

The free spectral range of an AWG device is given by

$$\Delta f_{fsr} = \frac{c}{n_g \Delta L} = \frac{f_c}{m}\frac{n_{eff}}{n_g} \tag{7.5}$$

Where $f_c$is the frequency of the central channel. Since the input field is sampled periodically, the resulting field at the output focal line is periodic. This angular period or spatial FSR is given by

$$\Delta\theta_{fsr} = \frac{\lambda}{n_{FPR} R_a \Delta\theta} = |D_\theta \Delta f_{fsr}| \tag{7.6}$$

7.4.2 Basic performance measures

Insertion loss and loss non-uniformity

An optical field undergoes attenuation as it propagates through an arrayed waveguide grating due to different loss mechanisms. The junction between the arrayed waveguides and the free propagation regions contributes to a large part of the loss incurred by the field. To minimize this loss, adiabatic operation in the fan-in and fan-out regions is required. Particularly for high index contrast SOI waveguides, a two step etch is used to comply with this requirement. To reduce the loss non-uniformity across the frequency channels, the FSR can be increased a little bit. Insertion loss as low as 1-2dB has been already demonstrated to be achievable for SOI AWGs [7]

Cross talk

One of the most useful performance measures of an AWG device is the inter-channel crosstalk. It is a measure of unwanted contribution from one channel to another, particularly a neighboring one. The truncation of the input field due to a limited array aperture is one of the main source of cross talk. The mode overlap between adjacent channels is another contributor to the cross talk. For high index contrast waveguides characterized by high mode confinement, this effect can be lower and narrow spacing between the array waveguides is possible. However, in practice, other mechanisms play significant role in determining the cross talk level. One of the main mechanism is error in the phase transfer of the array waveguides. Imperfection in the waveguide geometry and non-uniformity in the refractive index lead to inferior cross talk level. Various design tunings have been used to reduce these phase errors. For instance, expansion of the SOI waveguide width along some sections on the array waveguide have been applied to improve the cross talk level caused by sidewall roughness and non-uniformity. Cross talk levels better than 25dB have been achieved for SOI AWGs[7]

Channel overlap

Channel overlap is another important parameter for wavelength interrogation application. In conventional WDM applications, a distinctly resolved AWG channel response is typically required. Unlike WDM applications, AWG based wavelength shift interrogation may necessitate rather strong channel overlap. Particularly, for a wavelength interrogation scheme based on intensity ratio measurement, the overlap between adjacent AWG output channels plays an important role. Figures 7.4, 7.5, and 7.6 demonstrate that sufficient overlap is necessary to ensure sensitive wavelength shift interrogation in a broader dynamic range. However, the overlap should be achieved while maintaining optimally sharp channel response such that small resonance shifts can be re-

solved. The cross talk should also be minimized to avoid inconsistent intensity ratio measurements.

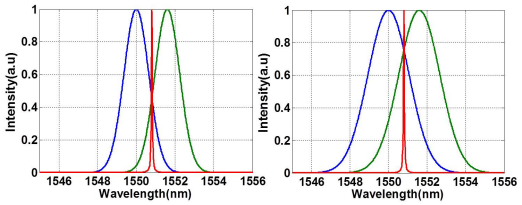

Figure 7.4: A depiction of a microring resonance of 0.05nm FWHM centered half way between two adjacent AWG channels with Gaussian response of 2.5nm FWHM (left),1.5nm FWHM(right).

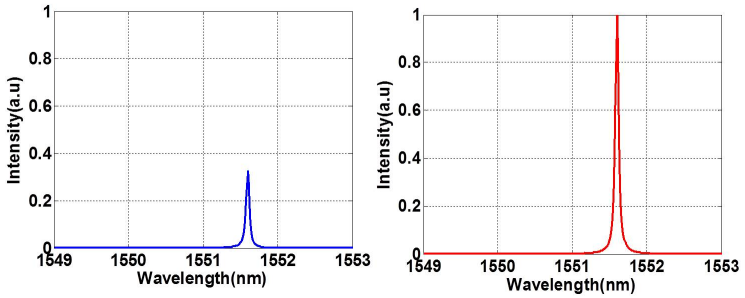

Figure 7.5: Relative intensities at adjacent channels when the resonance is red shifted by 0.8nm for Gaussian AWG response of 2.5nmFWHM

7.5 A microring resonator gas sensor interrogation with an on chip arrayed waveguide grating

In this work, we use an AWG to interrogate a MRR based ethanol vapor sensor [12]. The ring is coated with a porous ZnO nanoparticle film. Ethanol vapor concentrations ranging from 100ppm to 1000ppm are readily monitored with this sensor-interrogator system by measuring the intensity ratios between adjacent AWG channels. To our knowledge, in previous demonstrations, either silica-based AWGs or larger footprint high resolution SOI AWGs were used. Moreover, the application of such interrogators for on-chip sensors such as ring resonators has not been yet demonstrated. By monitoring the intensity ratios between two adjacent channels of a high resolution, 0.18nm channel spacing SOI AWG, it has been demonstrated that very small wavelength shifts from an FBG sensor can be

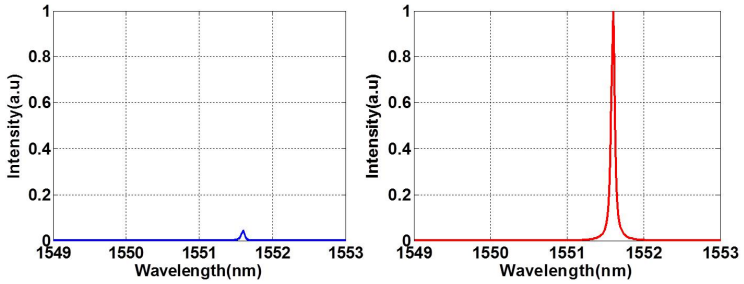

Figure 7.6: Relative intensities at adjacent channels when the resonance is red shifted by 0.8nm for Gaussian AWG response of 1.5nmFWHM

interrogated [16]. However, such a high resolution comes at the cost of a large device size (8mm x 8mm), and the reported insertion loss is very high. In addition, for very sensitive sensors, where large resonance shifts can be achieved at low analyte concentrations, moderate channel resolutions offer a better dynamic range for interrogation with intensity ratios. In this work, we demonstrate that a 1.6nm channel spacing AWG with broad spectral response can be used to interrogate very sensitive MRR based gas sensors. The AWG used in this work takes a footprint of 500 μm x 200 μm and is fabricated on a chip which also contains the MRR sensor.

7.5.1 Sensor interrogation basics

In an AWG-interrogated MRR sensor configuration, the drop port of the microring resonator is connected to an AWG input port. The AWG is designed such that its adjacent output channels overlap significantly, so the MRR resonance will consequently be detected at any two of such overlapping channels. Ultimately, the variations in the intensity ratio between the adjacent channels can indicate the MRR resonance shift due to the surrounding effects.

Approximating the MRR resonance and the AWG channel response by Lorentzian and Gaussian profiles, respectively, (7.7) can be used to estimate the variations in intensity ratios between the kth and (k+1)th channels with the resonance shift [15, 16]. For instance, provided a 0.05nm FWHM resonance peak and a 200GHz AWG, figure 7.7 shows how the intensity ratio evolves across three neighboring AWG channels centered at 1550nm, 1551.6nm and 1553.2nm, as a function of the resonance wavelength. The solid and dotted curves show values calculated for Gaussian channel profiles with FWHM of 2nm and 1.5nm, respectively. Most importantly, figure 7.7 demonstrates that a sufficient channel overlap is crucial in order to achieve well-resolvable power ratio changes corresponding to small resonance shifts. This criterion is more critical for a

MRR with a very narrow resonance peak, and the effect becomes apparent as the resonance shifts further towards the center of a channel.

$$\frac{I_k}{I_{k+1}} = \frac{\int_0^\infty T_{MRR}(\lambda) \cdot T_{AWG}(k,\lambda) d\lambda}{\int_0^\infty T_{MRR}(\lambda) \cdot T_{AWG}(k+1,\lambda) d\lambda} \tag{7.7}$$

where $T_{MRR}(\lambda)$, $T_{AWG}(k,\lambda)$, $T_{AWG}(k+1,\lambda)$, represent the transmissions from the MRR drop port, k^{th} AWG channel and $(k+1)^{th}$ AWG channel respectively at an arbitrary wavelength, λ.

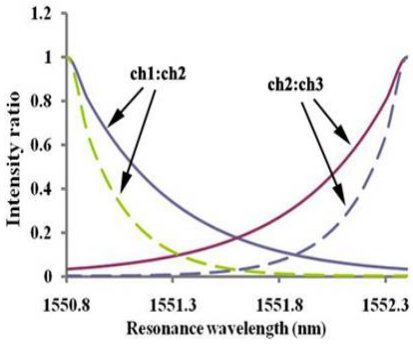

Figure 7.7: Given three neighboring AWG channels centered at 1550nm, 1551.6nm and 1553.2nm, theoretical estimates of intensity ratios between adjacent channels as a function of the MRR resonance wavelength for Gaussian profiles of 1.5nm FWHM (dotted lines), and 2nm FWHM (solid lines)

7.5.2 Design and fabrication

Different techniques such as MMI-coupled AWGs have been reported to provide a broad as well as flat channel response. For instance, the combined effect of broad and two-fold image of the input light produced by an MMI input waveguide has been utilized to obtain the above mentioned response [17]. For wavelength shift interrogation, fairly sharp response instead of a flat one is required while maintaining an adequate channel overlap. In such an application, the MMI can be replaced by a simple broad waveguide to obtain broader channel profiles. In an AWG spectrometer, the waveguide mode size at the input and output Rowland circles plays a similar role as the slit width of a bulk spectrometer[5]. In this work, a 16 channel, 200GHz (1.6nm channel spacing), AWG is designed such that the output from a 5μm radius MRR drop port overlaps with any two adjacent channels. Very compact and low insertion loss SOI such AWGs

were demonstrated in the past [7]. For this particular sensor interrogation application, an adiabatically tapered input waveguide with start width of 0.45μm and a broader end width of 4μm is chosen in order to broaden the channel response, and hence, enhance the overlap between adjacent channels. The start width of the tapered output waveguides is 2μm.

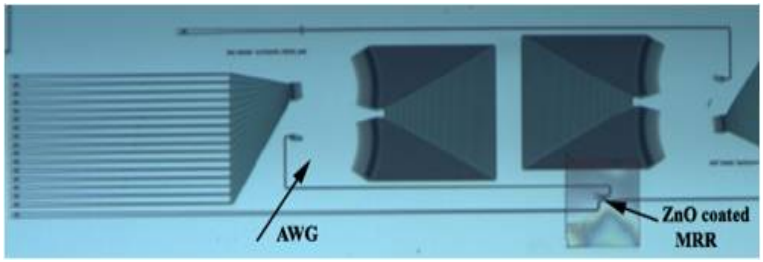

Figure 7.8: An optical microscope image of the AWG interrogated ethanol vapor sensor with ZnO porous film on the MRR. The AWG used for the spectral response characterization is partially shown in the image.

The device is fabricated in a CMOS fab using 193nm deep UV lithography as detailed in [7]. To add gas sensitive functionality to the device, about 240nm thick porous ZnO film is locally coated on the MRR. The ZnO film is prepared from colloidal nanoparticles suspended in ethanol. The porous nature of the film offers a large surface area for gas adsorption. The detailed nanoparticle synthesis and sensitive film preparation procedures are presented in [12]. Figure 7.8 shows an optical microscope image of the fabricated AWG interrogated ethanol vapor sensor. For the purpose of preliminary studies on the AWG channel response, an additional AWG is fabricated on the same chip without a ring attached to it.

7.5.3 Experiments

The spectral response from an AWG with a 4μm input waveguide measured with an SLED and a spectrum analyzer is shown in figure 7.9. The transmission is normalized to that of a 450nm wide photonic waveguide on the same chip. The insertion loss for the central channels is about -3dB, and the nearest neighbor cross talk is around -17dB, which is of a typical order for such compact SOI AWGs. Notably, a strong overlap between neighboring channels is achieved. The 3dB bandwidth of a channel response is approximately 2.3nm with over 0.9nm overlap with channels at either side.

In the eventual sensing system, the broadband source and the detectors will be co-integrated with the sensing chip. However, for the present experiment the sensing chip is mounted on a temperature stabilized sample bed in a small

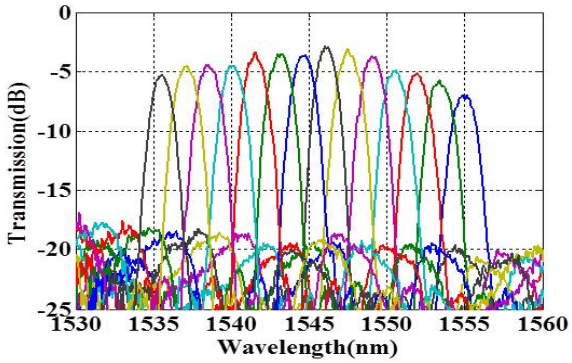

Figure 7.9: Normalized transmission spectrum of an AWG with 4ţm wide input waveguide

gas chamber and the light source and the detector were kept outside. Vertical coupling through gratings is used to couple light in and out of the sensor. The top side of the gas chamber is covered with a glass window to facilitate the coupling. While a single mode fiber is used for in-coupling, the output light is collected by an Infrared Camera. Further details on the setup are presented in chapter(setupchapter). The measurement accuracy of this setup is highly influenced by the noise due to the light which is scattered from the sample surface and reaches the camera. Due to the typically low power spectral density of a broadband source, we have chosen to use a tunable laser source of about 3mW to couple sufficient light through the glass cover. Operating at such low powers reduces the noise on the camera measurement and allowed us to characterize the device in a gas environment. Figure 7.10 illustrates how the intensity across adjacent channels changes with changing gas concentration at room temperature. The noisy features are due to the distant coupling through the glass window, and the scattered light from the sample surface.

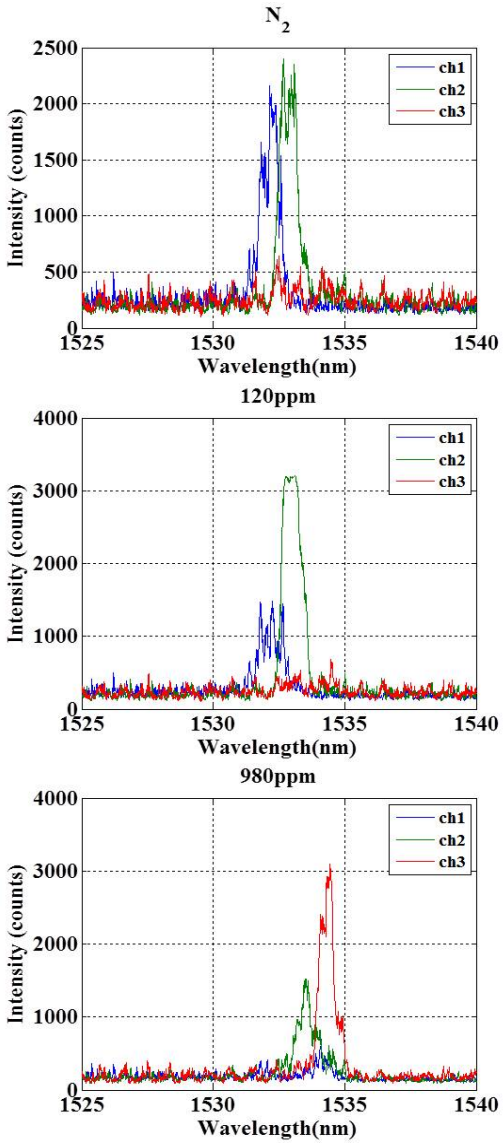

Figure 7.10: Illustrations of intensity changes measured from three neighboring channels at 0ppm(pure nitrogen), 120ppm and 960ppm ethanol vapor concentrations.

The output intensities from three consecutive AWG channels are simultaneously monitored before and after exposure to 120ppm, 240ppm, 480ppm and 960ppm ethanol vapor concentrations. The average intensity measured from each channel is then used to calculate the fractional intensity between adjacent channels at a given gas concentration. To better visualize the relation between the resonance wavelength and the intensity ratios, the resonance shifts at these vapor concentrations are recorded from the MRR through-port. Figure 7.11 depicts the average channel intensities as a function of vapor concentration, and figure 7.12) shows the intensity ratios calculated at the corresponding measured resonance shifts. The solid lines in figure 7.12 are exponential fit to the ratios between two adjacent channels.

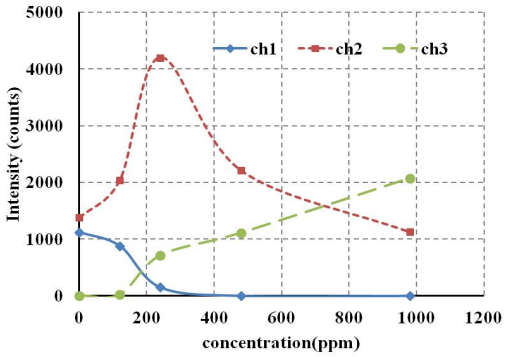

Figure 7.11: Average intensities measured from three channels at different ethanol vapor concentrations

As observed in figure 7.12, fairly smooth transition from a pair of adjacent channels to the next pair is readily achieved signifying a good overlap between neighboring channels. The FWHM of the resonance measured at the MRR through port is less than 50pm. While this on-chip sensor-interrogator system is suitable for highly sensitive gas sensors as demonstrated in this work, it can also be used to detect small resonance shifts. From the trend shown in figure 7.12, resonance shifts ranging from 50pm - 800pm should be readily interrogated with the ratio between just two channels.

In order to further ensure compact and low cost implementation of such a sensor, integrated approaches should replace external temperature stabilization mechanisms. A reference ring fabricated in series with the sensor can be used to monitor temperature driven wavelength drifts. Accordingly, the resonance wavelength of the reference ring can be designed to overlap with the AWG channels that are not used by the sensor. Alternatively, athermal AWG operation can be achieved by using a cladding material of a negative thermo-optic

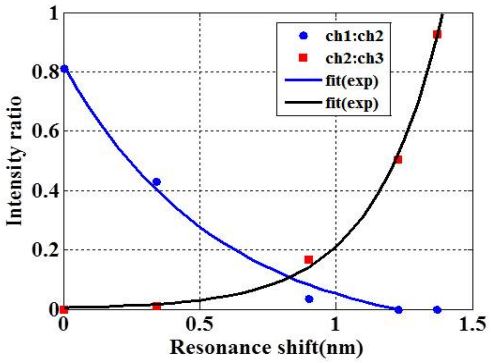

Figure 7.12: calculated intensity ratios as a function of resonance shifts corresponding to vapor concentrations shown in fig 7.11 with an exponential fit to ch2:ch3 (solid line)

coefficient to cover the region outside the sensing window.

7.6 Summary

It is demonstrated that a compact on-chip AWG spectrometer can be used to interrogate resonance shifts from MRR sensors. An SOI MRR ethanol vapor sensor is interrogated by a 200GHz AWG designed to have strongly overlapping output channels. Such an on-chip interrogation system presents itself as an attractive solution to the current interrogation challenges, and opens opportunities for low cost and compact implementation of MRR based sensors

[**1**] J. Brouckaert, W. Bogaerts, S. Selvaraja, P. Dumon, R. Baets and D. Van Thourhout. *Planar Concave Grating Demultiplexer With High Reflective Bragg Reflector Facets* . IEEE Photonics Technology Letters, 20(4): 309 - 311, 2008.

[**2**] Dazeng Feng, W. Qian, H. Liang, C-C. Kung, J. Fong, B.J. Luff and M. Asghari *Fabrication Insensitive Echelle Grating in Silicon-on-Insulator Platform* .IEEE Photonics Technology Letters, 23(5): 284 - 286, 2011.

[**3**] W .M. J. Green, B. J. Offrein and Y. A. Vlasov. *Silicon-on-Insulator Echelle Grating WDM Demultiplexers With Two Stigmatic Points* . IEEE Photonics Technology Letters, 23(21): 1743 - 1745, 2009.

[**4**] X. J. M. Leijtens, B. Kuhlow and M. K. Smit . *Arrayed Waveguide Gratings.*Springer Series in Optical Sciences, 123: 125 -187, 2006.

[**5**] P. Cheben, J. H. Schmid, A. Delâge, A. Densmore, S. Janz, B. Lamontagne, J. Lapointe, E. Post, P. Waldron and D.-X. Xu. *A high-resolution silicon-on-insulator arrayed waveguide grating microspectrometer with submicrometer aperture waveguides.* Optics Express, 15(5):2299-306, 2007 .

[**6**] P. Dumon, W. Bogaerts, D. Van Thourhout, D. Taillaert, R. Baets, J. Wouters, S. Beckx and P. Jaenen . *Compact wavelength router based on a Silicon-on-insulator arrayed waveguide grating pigtailed to a fiber array.*Optics Express, 14(2):664-669 ,2006.

[**7**] W. Boagerts, S.K. Selvaraja, P. Dumon, J. Brouckaert, K. De Vos , D. Van Thourhout and R. Baets. *Silicon-on-Insulator Spectral Filters Fabricated With CMOS Technology* . IEEE Journal of Selected Topics in Quantum Electronics, 16(1):33 - 44, 2010.

[**8**] Z. Xia, A. A. Eftekhar, M. Soltani, B. Momeni, Q. Li, M. Chamanzar, S. Yegnanarayanan and A. Adibi. *High resolution on-chip spectroscopy based on miniaturized microdonut resonators* . Optics Express, 19(13): 12356-12364, 2011.

[**9**] B. B. C. Kyotoku, L. Chen and M. Lipson . *Sub-nm resolution cavity enhanced microspectrometer.* Optics Express,18(1): 102-107, 2010.

[**10**] M. Iqbal, M.A. Gleeson, B. Spaugh, F. Tybor, W.G. Gunn, M. Hochberg, T. Baehr-Jones, R.C. Bailey, L.C. Gunn . *Label-Free Biosensor Arrays Based on Silicon Ring Resonators and High-Speed Optical Scanning Instrumentation.* IEEE Journal of Selected Topics in Quantum Electronics, 16:654-661, 2010.

[**11**] A. Ramachandran, S. Wang, J. Clark, S.J. Ja, D. Goad, E. Knobbe,J.V. Hryniewicz1, S.T. Chu1, W. Chen1, O. King1, B.E. Little1 *A universal biosensing platform based on optical micro-ring resonators.* Biosensors and Bioelectronics , 23:939-944, 2007.

[**12**] N. A. Yebo, P. Lommens,Z. Hens,and R. Baets. *An integrated optic ethanol vapor sensor based on a silicon-on-insulator microring resonator coated with a porous ZnO film.* Optics Express, 18:11859 -11866, 2010.

[**13**] L. Jin, M. Li and J-J. He. *Optical waveguide double-ring sensor using intensity interrogation with a low-cost broadband source.* Optics Letters, 36:1128-1130, 2011.

[**14**] G. Z. Xiao, P. Zhao, F. G. Sun, Z. G. Lu, Z. Zhang and C. P. Grover. *Interrogating fiber Bragg grating sensors by thermally scanning a demultiplexer based on arrayed waveguide gratings.* Optics Letters, 29(19): 2222-2224, 2004.

[**15**] P. Cheben, E. Post, S. Janz, J. Albert, A. Laronche, J. H. Schmid, D -X. Xu, B. Lamontagne, J. Lapointe, A. Delâge, and A. Densmore. *Tilted fiber Bragg grating sensor interrogation system using a high-resolution silicon-on-insulator arrayed waveguide grating.* Optics Letters, 33:2647-2649, 2008.

[**16**] Q. Fang, F. Li and Y. Liu. *Compact SOI arrayed waveguide grating demultiplexer with broad spectral response.* Optics Communications, 258 :155-158, 2005.

8

Conclusions

An increasing dynamics in the environmental and the health sectors as well developments in various industrial applications have recently shown that a paradigm shift in current detection technologies is inevitable. In this respect, novel gas detection tools are anticipated to have a major contribution in advancing today's health care, environmental control, industrial process control, and threat detection. The bio-medical sensing market, in particular, is expected to rise due to the increasingly aging population, more spending in the heath care, growing shift towards point-of-care diagnostics and monitoring, and increasing incidents of chronic diseases. The detection of exhaled gaseous compounds is expected to have a key role in patient diagnosis and continuous health monitoring. In addition, dissolved gas sensors are of a high demand for water resource conservation and quality control. The food industry and the motor vehicles industry are other drives for better gas sensing technologies.

Different gas detection technologies exist today. However, the majority of these technologies in one way or another lack the capabilities most medical and environmental applications necessitate. For instance, ensuring global health care demands that the detection tools are accessible to the general public irrespective of economic or geographic boundaries. This would require the sensing tools to be affordable, energy efficient, robust, prompt and portable. However, the widely used sensors for health care are typically expensive, invasive and far less portable, hence, becoming less suitable for point-of-care deployment. On

the other hand, mass-produced and low cost sensing solutions are of an ideal role in large scale industrial applications such as the food packaging and the automotive sectors. Traditional bulk gas sensors typically suffer from large size, complexity and high cost. On the other hand, cheap and compact sensors such as those based on metal oxide semiconductors are typically characterized by limitations such as poor selectivity. In this regard, mass produced chip-scale silicon photonic gas sensors can immensely take advantage of cost, size and energy related befits over the traditional technologies, hence, promising a rapid contribution to the field. Silicon photonics offers these potential benefits taking advantage of the well-established multi-billion CMOS fabrication technologies as well owing to ultra-small feature sizes achievable with the HIC platform. More importantly, a high environmental sensitivity of silicon photonic structures makes this platform an ideal candidate for sensing applications.

In general, apart from biomolecule detection in the liquid phase, the research on silicon photonic sensors for medical, environmental and industrial gas sensing applications has been very limited so far. In this doctoral research the potential of this technology for on-chip gas detection is studied and the key capabilities for low cost, sensitive, selective, and rapid gas sensing are demonstrated.

A refractive index sensing approach based on mircroring ring resonators has been primarily explored in this research. High refractive index sensitivity, sensor multiplexing and ultra-compactness are some of the attractive features of MRRs. The refractive index sensing technique typically involves chemical transduction mechanisms for selective and sensitive gas detection. Nanoporous materials, in particular, have been of a central research interest in this work. Exploiting a considerably high surface area offered by these materials, enhanced gas sensitivities have been demonstrated. The nanoporous surface further lends itself for the incorporation of functional groups for selective gas detection. Efficient diffusion of gas molecules facilitated with the porous structures is another valuable feature offered by these materials for rapid sensor response. In this respect, MRRs functionalized with nanoprous ZnO, silica and polymer films have been studied for efficient gas detection.

High sensitivities for volatile organic compounds, namely ethanol and xylene, as well as for gaseous CO have been experimentally demonstrated from nanocrystalline ZnO functionalized MRRs. Sensitivities down to sub ppm gas concentrations are achieved. Typical response times for these sensors are in the range of 20-40 secs. On the other hand, this study has provided an insight that metal oxide films, such as ZnO, as demonstrated here can be strongly responsive to a range of gaseous compounds, hence, being less suited for selective gas detection. Partial sensor recovery is another point typically observed for ZnO films. Consequently, such devices can be more suited for disposable sensing

applications.

On the other hand, Polymer materials, such as PDMS, are characterized by high affinities towards industrially and environmentally relevant organic vapors. PDMS coated MRRs have demonstrated attractive performance features for potential VOC sensing. Xylene vapor is detected using this sensor prototype with a detection limit of of ~ 500ppm. Moreover, a remarkable reversibility and rapid response is measured from this sensor. The response and recovery times are approximately 20 and 40 secs, respectively. This result demonstrates the potential role of polymer functionalized silicon MRRs as re-usable, low cost and real time VOC detection tools. Such sensors can be used to detect a given class of VOCs for early warning, for instance, in industrial workplaces.

More interestingly, it is demonstrated that specifically tailored materials can lead to selective gas detection on silicon photonic chips. Alumino-silicate films obtained through a synthesis based technique as well as atomic layer deposition(ALD) are incorporated on silicon MRRs. Owing to Al atoms introduced into the silica framework, these films exhibit acidic surfaces suitable for preferential adsorption of gaseous bases such as NH_3. Sensitive, reversible and fast response to NH_3 and high selectivity with respect to CO_2 is achieved with these sensors. Equilibrium response is attained in less than 30 sec and over 95% recovery is reached within 90 sec. A detection limit of 5ppm is estimated for microporous acidic films obtained via synthesis. A further improvement of the sensitivity could be achieved by optimizing the porosity and surface properties of the porous alumino-silicate films. Such a selective NH_3 sensor can have a future application as medical breath analysis tool for diagnosis and continuous monitoring of renal patients.

On the other hand, wavelength interrogated SOI MRR sensors offer superior sensitivities to the surrounding, allow multiplexing of sensor arrays, and provide immunity to noise with respect to the intensity interrogation schemes. However, current wavelength interrogation based sensing systems are typically characterized by bulky and costly instrumentation. Despite a few efforts made so far, more progress and novel solutions are highly required to realize cost effective and portable ring resonator sensors. In this regard, a potentially low cost and compact MRR sensor interrogation approach based on an on-chip AWG spectrometer is experimentally demonstrated in this work. This spectrometer employed with cheap broadband light sources, such as superluminescent LEDs, can significantly cut down the size and cost of the current microring resonator based sensors. An SOI MRR ethanol vapor sensor is interrogated by a 200 GHz AWG designed to have strongly overlapping output channels. It is demonstrated that resonance shifts ranging from 50pm- 800pm can readily be interrogated by measuring the ratio between two overlapping adjacent AWG channels.

In conclusion, it is demonstrated in this research that on-chip optical gas

sensors promise a considerable potential for ultra portable, low cost and real time gas detection in a wide range of applications including medical breath analysis. With ongoing developments on gas selective films and efficient sensor spotting techniques, several multiplexed sensor arrays can be implemented for multi-gas detection on silicon photonic chips. These sensors can have a significant contribution for applications involving complex gas analysis such as industrial process control and cancer detection.

9

Future perspectives

9.1 Silicon photonics for on-chip gas spectroscopy

In chapter 3 (section 3.1), waveguide absorption spectroscopy has been introduced as an alternative on-chip gas sensing approach. It has also been noted that a limited interaction length and an overall system noise on silicon photonic chips are the major issues to be addressed for a spectroscopic gas detection. Practical optical spectroscopy is commonly characterized by noise contributed by various system components. Both fundamental (e.g. shot noise, thermal noise, 1/f noise) and technical (e.g. laser excess noise, interference fringes) noise affect the performance of spectroscopic sensors[1,2]. On the other hand, laser based absorption spectroscopy is fundamentally capable of a superior shot noise limited performance owing to the high photon flux. A noise to signal ratio in the order of 10^{-8} is theoretically possible with laser diode spectroscopy[1]. However, practical absorption spectroscopy systems offer far less performance due to the dominant noise from environmental fluctuations, interference fringes and laser excess noise. As a result, various advanced techniques are usually employed to maintain low noise levels as well as to achieve sufficient interaction with the gas molecules. Modulation spectroscopy, balanced detection and cavity enhanced absorption are among the widely used techniques[1-3].

Particularly for on-chip spectroscopic systems, the waveguide propagation

loss, interference fringes and environmental fluctuations such as temperature and mechanical vibrations can have a significant impact on the overall system performance. Considering gaseous NH_3 which has an absorption cross section of $\sim 3.10^{-21}$ cm^2/molecule[4] near 1532nm, absorbance levels expected to be measured with an SOI waveguide system can be estimated. Taking a typical waveguide propagation loss of 2.5dB/cm, and a confinement factor of 0.23 for a 450nm wide silicon nanowire, the optimum waveguide length at 1000ppm NH_3 is estimated to be $\sim$ 1.7cm(equation 3.2). The theoretical absorbance corresponding to this interaction length is about 3.10^{-5}. However, in practice, the noise due to reflections and scattering from the waveguide interfaces can significantly exceed this absorbance level. An attractive approach to attain less stringent requirement on the system noise level can be a technique to enhance the density of gas molecules near the evanescent interaction region. A gas preconcentrating layers on the waveguide surface can be considered for this purpose. Preliminary experimental observations with respect to noise and gas density enhancement on silicon photonic chips are presented below. Based on these observations, some insights are provided for future improvements and feasible implementation of on-chip gas spectroscopy.

9.1.1 Gas absorption tests on SOI waveguides

One of the practical issues for gas absorption measurements on optical chips is achieving mechanical stability of the setup. In addition, efficient fiber-to-chip coupling has to be achieved while minimizing unwanted reflections and scatterings from the chip surface. For this purpose, a miniature gas cell is glued on the sensor chips in a way that the input/output gratings are left outside the cell for a direct coupling with optical fibers. Moreover, the fibers are glued on the gratings to minimize mechanical vibrations and hence reduce the intensity noise. With this configuration, lower than 1% noise between consecutive transmission measurements is observed to be achievable.

Figure 9.1 shows two consecutive transmission measurements and the ratio between the two(in natural log scale) taken from a 1.5cm long spiral waveguide. The observed noise level is within 5%.

This relatively high noise level can mainly be attributed to interference fringes caused by reflections and scattering from various waveguide interfaces. Due to several corners and bends in the spiral structures, strong and complex fringes are more apparent as compared to straight waveguides. Because of the high sensitivity of SOI waveguide structures to environmental effects such as temperature, slight surrounding changes can shift these fringes. As a result, spurious absorption-like features can be observed while comparing with reference measurements. Hence, waveguide designs and layouts with minimal

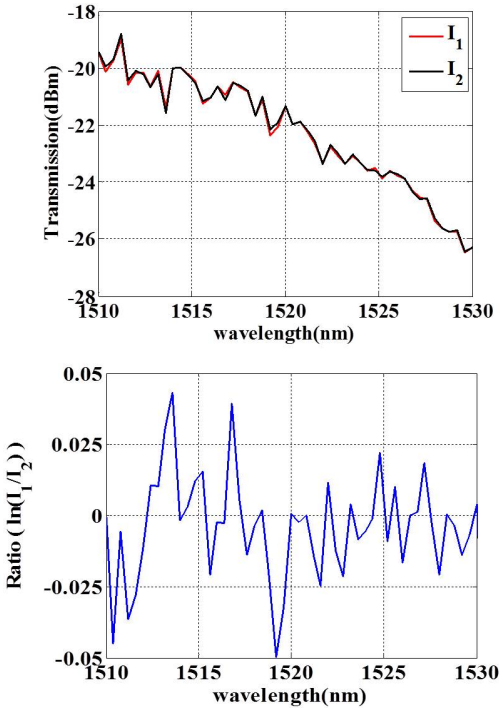

Figure 9.1: (top)Two consecutive transmission spectrum measured from 1.5cm long SOI spiral waveguide . (bottom) the ratio of the two measurements in natural log scale

interference effects are of a high importance. Preliminary experimental results from straight waveguide structures further confirm this requirement.

Figure 9.2 shows consecutive transmission spectra measured from a straight 50μm long and 450nm wide SOI waveguide. The fringe modulation depth is only 3% as compared to 20-45 % measured from a spiral waveguide. Distinct fringe pattern is observed and the disparity between two consecutive measurements is below 0.8%. Moreover, the Fourier transform (figure 9.3) of the transmission spectrum reveals distinct fringe frequencies which could potentially be filtered out with digital techniques. The potential for digital filtering can allow absorption extraction from a single measurement. Accordingly, reference measurements may not be required and the noise due to fringe shift can become less relevant in the overall absorption analysis.

While properly designed waveguide structures, as discussed here, can significantly lower the system noise, parallel enhancement of the interaction between the evanescent light and the gas molecules is equally relevant for the

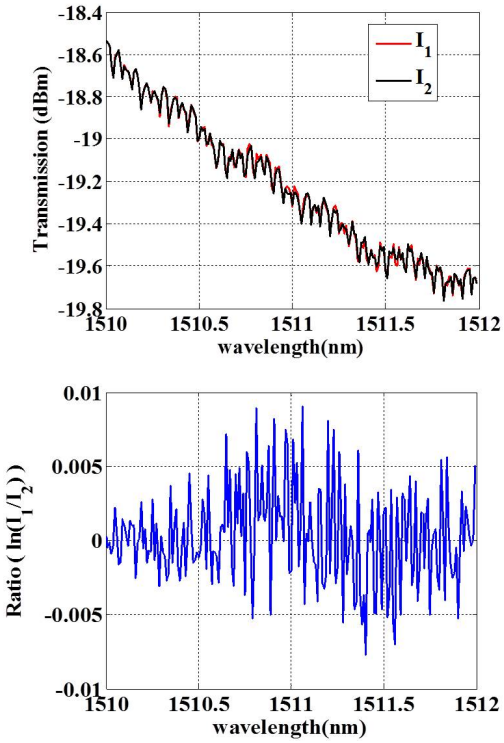

Figure 9.2: (top)Two consecutive transmission spectrum measured from 50μm long straight SOI waveguide on 12mm layout. (bottom) ratio of the two measurements in natural log scale

detection of low gas concentrations. In chapter 4 (section 4.2), it is demonstrated that an increased density of gas molecules can be attained through an adsorption process on nanoporous films. This density enhancement can be potentially exploited to compensate for limited waveguide lengths realizable on SOI chips. Estimates based on experimental resonance shifts from porous ZnO coated MRR indicated that the pore refractive index upon adsorption of gas molecules can readily approach that of the liquid phase. For instance, the pore refractive index (at RT) of ZnO films saturated with CO molecules is estimated to be about 80% of the liquid CO (at 78K) (section 5.2.3). Typically, the liquid phase density can be up to three orders higher than the gaseous phase for most compounds[5]. Hence, considering a 60% porous film, roughly 100 - 500 times gas density enhancement per volume is expected to be achievable. Some preliminary experimental studies have been run to study the potential of gas pre-concentration for on-chip gas spectroscopy. A 1cm long spiral wave-

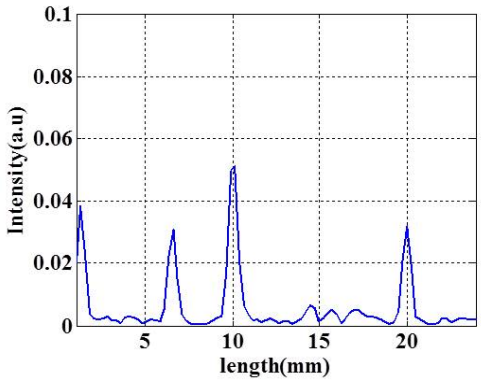

Figure 9.3: Fourier transform of the transmission spectrum shown in figure 9.2 plotted on length scale

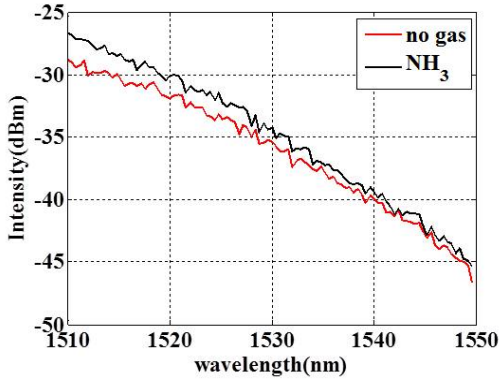

Figure 9.4: Transmission spectra measured from 150nm thick ZnO coated 1cm long spiral waveguide before and after to NH_3

guide is coated with ~150nm thick ZnO nanoparticle film and the transmission spectra are measured before and upon exposure to 2 % ammonia gas. Figure 9.4 shows this result. On the contrary to the ideal expectations, increase in the transmitted power is observed when the coated waveguide is exposed to ammonia. For this particular experiment the measured intensity increase is 30-50%. This can be attributable to the fact that high index contrast SOI structures are highly sensitive to the waveguide surface roughness[6]. Adsorption of the gas molecules may improve the surface homogeneity, thus, reducing the propagation losses. On the other hand, the change in the refractive index of the film may sufficiently alter the index contrast whereby decreasing the scattering losses. In

future, different techniques can be devised to circumvent this issue, and hence, exploit the gas pre-concentration potential of porous films. Firstly, ensuring the surface homogeneity of both the coating and the waveguide structures is a key. In addition, the relative change in intensity (before and after gas adsorption) can be disregarded if the gas absorption features can be extracted from a single measurement without the need for reference measurements. Digital signal processing techniques can play an important role in this regard.

9.2 Gas sensing with chemically functionalized SOI structures

In this doctoral research it is demonstrated that the refractive index sensing approach can have a near future role for practical gas sensing with integrated silicon photonic chips. Nonetheless, the research effort on integrated optical gas sensing remains limited. We believe that a considerable gas detection potential demonstrated in this work will attract increased interest from the scientific and industrial community. Future research may focus on various technological aspects critical for feasible gas detection on silicon chips. Progress on dedicated chemical routes for specific and sensitive gas detection will be crucial in bringing silicon photonic sensors into near future application in biomedical and environmental areas. It is shown that high surface area coatings can lead to sensitivity levels adequate for various real applications. The feasibility of selective gas detection with functionalized porous surfaces has also been demonstrated. Continuing research on surface tunable and versatile nanoporous platform would be highly valuable for more robust multi-gas sensing with silicon photonic chips. On the other hand, a major interference on nanoporous film functionalized silicon photonic refractive index sensors may come from condensing compounds such as water vapor. Research on tailored surfaces as well as various chemical filtering techniques will have a significant importance in this regard.

Other alternative approaches, such as those based on color changing chemical films, can also be considered for selective gas detection. In contrast to adsorption induced refractive index changes, absorption(color) changes on these materials can be chemically specific and may not be affected by non-specific vapor condensation. Hence, novel materials exhibiting gas induced absorption changes in the NIR would be of a significant scientific contribution for gas detection with silicon waveguide structures.

Apart from the chemistry, more sensitive photonic structures can further enhance the performance of silicon photonic gas sensing. TM mode waveguide structures and Vernier ring configurations are among those could be closely in-

vestigated for highly sensitive on-chip gas detection. Compact optical sources and on-chip interrogation units are, on the other hand, critical for low cost and ultra-portable sensor implementation. Continuing research efforts are, thus, anticipated on the development of these units.

Moreover, progress on efficient sensor spotting(coating) techniques are necessary for multiplexed gas sensing on a chip. In this respect, promising techniques such as inkjet printing can be of a valuable future research focus.

References

[**1**] K. L. Haller, P. C. Hobbs. *Double-beam laser absorption spectroscopy: shot noise-limited performance at baseband with a novel electronic noise canceler*. Optical Methods for Ultrasensitive Detection and Analysis, Proceedings SPIE, 1435:298-309, 1991.

[**2**] P. Werle and F. Slemr. *Signal-to-noise ratio analysis in laser absorption spectrometers using optical multipass cells*. Applied Optics, 30:430-434, 1991.

[**3**] Y. He and B. J. Orr. *Rapid measurement of cavity ringdown absorption spectra with a swept-frequency laser*. Applied Physics B, 79:941-945,2004.

[**4**] H. Jia, W. Zhao, T. Cai, W. Chen, W. Zhang and X. Gao. *Absorptiona spectroscopy of ammonia between 6526 and 6538 cm*$^{-1}$. Journal of Quantitative Spectroscopy & Radiative Transfer, 110:347-357, 2009.

[**5**] Web address: http://encyclopedia.airliquide.com/Encyclopedia.asp?GasID=2

[**6**] Y. A. Vlasov and S. J. McNab. *Losses in single-mode silicon-on-insulator strip waveguides and bends*.Optics Express, 12: 1622-1631, 2004.